Davies, P. J., McKenzie, J. A., Palmer-Julson, A., et al., 1991
Proceedings of the Ocean Drilling Program, Initial Reports, Vol. 133

5. SITE 812[1]

Shipboard Scientific Party[2]

HOLE 812A

Date occupied: 20 August 1990

Date departed: 21 August 1990

Time on hole: 22 hr

Position: 17°48.841′S, 149°36.313′E

Bottom felt (rig floor; m, drill-pipe measurement): 472.6

Distance between rig floor and sea level (m): 11.02

Water depth (drill-pipe measurement from sea level, m): 461.6

Total depth (rig floor; m): 662.5

Penetration (m): 189.9

Number of cores (including cores with no recovery): 22

Total length of cored section (m): 189.9

Total core recovered (m): 40.73

Core recovery (%): 21.4

Oldest sediment recovered:
Depth (mbsf): 189.9
Nature: dolomitized packstone
Age: middle Miocene

HOLE 812B

Date occupied: 22 August 1990

Date departed: 23 August 1990

Time on hole: 1 day, 1 hr, 55 min

Position: 17°48.842′S, 149°36.306′E

Bottom felt (rig floor; m, drill-pipe measurement): 472.6

Distance between rig floor and sea level (m): 11.02

Water depth (drill-pipe measurement from sea level, m): 461.6

Total depth (rig floor; m): 772.6

Penetration (m): 300.0

Number of cores (including cores with no recovery): 18

Total length of cored section (m): 149.2

Total length of washed section (m): 150.8

Total length of combined section (m): 300.0

Total core recovered (coring; m): 8.50

Total core recovered (washing; m): 2.27

Total core recovered (combined; m): 10.77

Core recovery (cored section, %): 5.7

Oldest sediment recovered:
Depth (mbsf): 300.0
Nature: dolomitized bioclastic rudstone
Age: middle Miocene

HOLE 812C

Date occupied: 26 August 1990

Date departed: 27 August 1990

Time on hole: 12 hr, 15 min

Position: 17°48.842′S, 149°36.331′E

Bottom felt (rig floor; m, drill-pipe measurement): 473.05

Distance between rig floor and sea level (m): 11.14

Water depth (drill-pipe measurement from sea level, m): 461.9

Total depth (rig floor; m): 610.9

Penetration (m): 137.8

Number of cores (including cores with no recovery): 16

Total length of cored section (m): 137.8

Total core recovered (m): 114.15

Core recovery (%): 82.8

Oldest sediment recovered:
Depth (mbsf): 121.4
Nature: dolomite
Age: late middle to early late Miocene

Principal results: Site 812 is located on the southern margin of the Queensland Plateau between the Flinders Reef and Tregrosse Reef. It represents the lagoonal-bank end-member of a three-site transect, together with Sites 813 and 814, intended to study facies distribution in response to changes in sea level across a platform-slope transition in a pure carbonate system. Drilling penetrated a 300-m-thick sequence of platform-top sediments (average carbonate content = 97%) ranging in age from middle Miocene to Pleistocene. Benthic foraminifers indicate progressive deepening of the depositional environment from a neritic setting (0–200 m) in the late Miocene to early Pliocene to an upper bathyal environment (200–600 m) during the late Pliocene and Pleistocene. Sedimentation during the middle Miocene occurred in a shallow-water, lagoonal or back-reef environment.

The sedimentation rate for the latest Pliocene and Pleistocene is slightly more than 1 cm/k.y., whereas it was less, about 0.5 cm/k.y., during the early Pliocene. The presence of a hardground or condensed horizon separating the lower Pliocene (Hole 812A) or uppermost upper Miocene (Hole 812C) from the overlying upper Pliocene sediments is consistent with the lower sedimentation rate, suggesting a significant hiatus or a period of condensed sedimentation during the early Pliocene. Shipboard paleomagnetic studies revealed a good reversal stratigraphy downward into the upper Pliocene that recorded the top of the Olduvai event (1.88 Ma) above the hardground. Below this level, the signal is normal, but should be resolvable with the shore-based study of discrete samples.

Seven seismic sequences can be identified, all of which equate well with the lithologic units defined from drilling results. Three major sedimentary units were recovered between the seafloor and 300 meters below seafloor (mbsf). The lithologic units are as follows:

Unit I: depth, 0–27.9 mbsf; age, late Pliocene to Pleistocene. Nannofossil foraminiferal oozes with pteropods that were deposited in an upper bathyal environment (200–600 m). Abundance of calcareous nannofossils in these sediments indicates predominately pelagic sedimentation.

[1] Davies, P. J., McKenzie, J. A., Palmer-Julson, A., et al., 1991. *Proc. ODP, Init. Repts.*, 133: College Station, TX (Ocean Drilling Program).

[2] Shipboard Scientific Party is as given in the list of participants preceding the contents.

Unit II: depth, 27.9–141.6 mbsf; age, late Pliocene to middle or early late Miocene. A 1.5-m-thick dolomitized limestone hardground, with a condensed upper surface, separates Unit I and Unit II.

Subunit IIA: depth, 27.9–64.3 mbsf; age, early Pliocene to late Miocene (5.26–8.2 Ma). Micritic chalks with nannofossils and foraminifers, deposited in the middle neritic outer-shelf environment (50–150 m). The nannofossil content, up to 20%, implies a mixture of fine-grained pelagic and bank-derived material, suggesting that the sediment was originally a periplatform ooze.

Subunit IIB: depth, 64.3–86.5 mbsf; age, late Miocene. Micritic chalks with foraminifers but without nannofossils. The sediments were deposited in the middle neritic outer-shelf environment (50–150 m).

Subunit IIC: depth, 86.5–105.5 mbsf; age, late Miocene. Bryozoan mollusk floatstones, deposited in the shallow neritic, inner-shelf environment (10–50 m).

Subunit IID: depth, 105.5–141.6 mbsf; age, late middle to early late Miocene. Dolomitic packstones with larger benthic foraminifers and dolostones, deposited in the shallow neritic inner-shelf environment (10–50 m).

Unit III: depth, 141.6–300.0 mbsf; age, middle Miocene(?). Unit III is separated from the overlying Unit II by a horizon that may be a solution unconformity produced by subaerial exposure.

Subunit IIIA: depth, 141.6–218.2 mbsf; age, middle Miocene(?). Dolomitized coralline algal packstones with mollusks, rhodolith rudstones with larger benthic foraminifers, and bioclastic wackestones, deposited in a shallow lagoonal, low-medium energy environment (~5 m). Cemented lithoclasts exhibit moldic porosity.

Subunit IIIB: depth, 218.2–255.7 mbsf; age, middle Miocene(?). Dolomitized bioclastic floatstones with corals and coralline algae and mollusk packstones, deposited in shallow water close to a reefal environment (5–10 m). Cemented lithoclasts exhibit moldic porosity.

Subunit IIIC: depth, 255.7–300.0 mbsf; age, middle Miocene(?). Dolomitized bioclastic peloidal packstones, foraminiferal packstones, and coralline algal rudstones, deposited in a deeper lagoonal environment (<30 m). Cemented lithoclasts exhibit moldic porosity.

Aragonite concentrations (up to 50%) were recorded at 1 mbsf and decrease downward to values between 2% and 20% at 22 mbsf. A slight increase in strontium concentrations above seawater values between 0 and 24 mbsf suggests dissolution of metastable carbonate phases. Below this level, the strontium concentrations remain constant. Whereas the chlorinity (salinity) values remain approximately constant throughout the upper 113 m, a perceptible but slight decrease in Mg^{2+} concentration occurs with a corresponding increase in Ca^{2+} concentration. These small changes may reflect *in-situ* dolomitization of the calcareous sediments. X-ray diffractograms of selected samples illustrate the occurrence of diagenetic dolomite in three intervals: at 24.5 mbsf (10% dolomitized ooze above the hardground), between 85 and 170 mbsf (10%–100% dolomitized chalk and packstone), and between 247 and 294 mbsf (10%–100% dolomitized packstone to rudstone). Smear slide descriptions indicate that dolomite is consistently present below 24.5 mbsf, beneath the top of the upper hardground.

Downhole measurements were made using the standard Schlumberger seismic stratigraphic combination tool string and the formation microscanner (FMS). In particular, interpretation of the resistivity logs shows a distinct zone between 140 and 222 mbsf in which measurements vary abruptly and indicate alternating layers of high and low porosity. The uranium log through this interval shows increased values, consistent with an expected pattern for dolomitization of different platform facies. The temperature log gave isothermal readings (~11°C) down to 225 mbsf, followed by a sharp increase to 17.6°C, which would represent a minimum temperature considering the mud-circulation operation to condition the hole prior to logging. Together, the geochemical data, downhole measurements, and lithologic descriptions suggest that seawater may be moving downward and/or laterally through the upper 225 m of the platform and may be currently dolomitizing the calcareous sediments.

The total organic carbon content of the sediments was extremely low (<0.15%). Volatile hydrocarbons, with methane concentrations of 2 ppm and no detectable ethane or propane, presented no safety problems.

BACKGROUND AND SCIENTIFIC OBJECTIVES

Sites 812, 813, and 814 are located west of Tregrosse Reef, on the southwest margin of the Queensland Plateau at ~500 m below sea level (mbsl) (see Fig. 1, "Introduction" chapter, this volume). The Queensland Plateau is the largest marginal plateau of the Australian continental margin, extending over an area of about 154,000 km^2. It is one of the largest features of its type in the world and equal in size to the Little and Large Bahama platforms. Although half of the plateau surface currently occurs at water depths of 1000 m or more, living reefs at or near present sea level occupy 15% of the surface. The origin of the reefs, and particularly their timing, composition, and diagenesis, forms an important objective of the Leg 133 drilling program.

On the Queensland Plateau, modern coral reefs occur in 15 distinct areas (Mutter, 1977). Drowned(?) reefs are more widespread, whereas buried reefs have been identified in at least 25 different locations. At present, the reefs of the plateau occur along three distinct directional axes: (1) northwest along the western margin of the plateau; (2) north-south from Moore to Herald to Malay reefs; and (3) west-east along the southern margin of the plateau and including Malay-Tregrosse-Lihou reefs (see Fig. 1, "Introduction" chapter, this volume). Many of the reefs, particularly those along the central and southern areas, appear to rise from a terrace at about 500 m. Pinchin and Hudspeth (1975) and Mutter (1977) postulate that reef growth in the area began during the Eocene, whereas Davies et al. (1989) think that reef growth began much later during the Miocene. Understanding the age and distribution of these reefs will shed substantial light upon the subsidence and climatic history of the region.

Major characteristics of the carbonate platforms comprising the Queensland Plateau are shown in Figure 1. Although it is possible that carbonate deposition may have begun as early as the Eocene, as suggested by Pinchin and Hudspeth (1975), more recent work by the Bureau of Mineral Resources (BMR) has shown that reefs along the western margin date from the middle Miocene. Reef growth throughout the platform appears to have occurred as four phases of growth, each one defining a substantial contraction from the preceding phase. In the central part of the plateau, scientists think that reef growth occurred as at least two superimposed growth phases with concomitant phases of periplatform deposition (QR1 and QR2 in Fig. 1). Samples dredged from the southern slope of the Queensland Plateau between 1000 and 1300 m consist of middle Miocene to Pliocene reefal material (Davies et al., 1989). The terrace at 450–500 m has been interpreted as representing the end of QR2 reef growth while also forming the pedestal for a third phase of reef growth (QR3) and periplatform sediments. Scientists have further suggested that this phase of reef growth grew near today's sea level and now forms a plateau at about 50 m. The most recent reef complexes (QR4), developed on the 50-m terrace, cover a much smaller area than earlier platforms. There may have been a contraction of the size of the platforms throughout their history.

The reefs of the Queensland Plateau hold the key to understanding the subsidence and climatic history of the plateau, together with the Miocene history of sea level of the area. Drilling at DSDP Site 209 revealed an Eocene to Holocene section, which defines an initially slow (20 m/m.y.) subsidence history (Davies et al., 1989) that markedly increased to about 40 m/m.y. from about 11 Ma in the middle

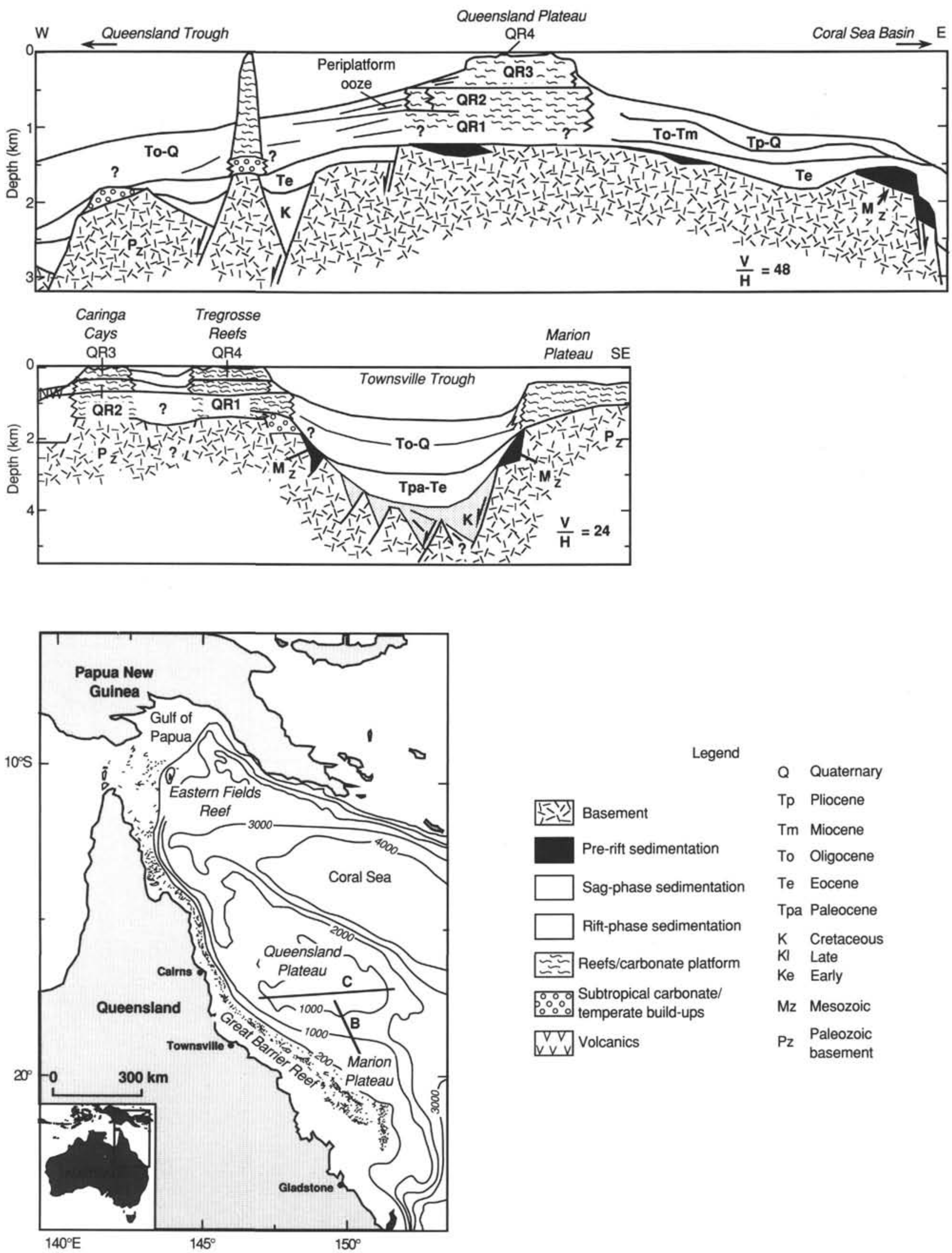

Figure 1. Schematic diagram showing the distribution of carbonate platforms on the Queensland Plateau. Location of cross-sections C and B is indicated on map.

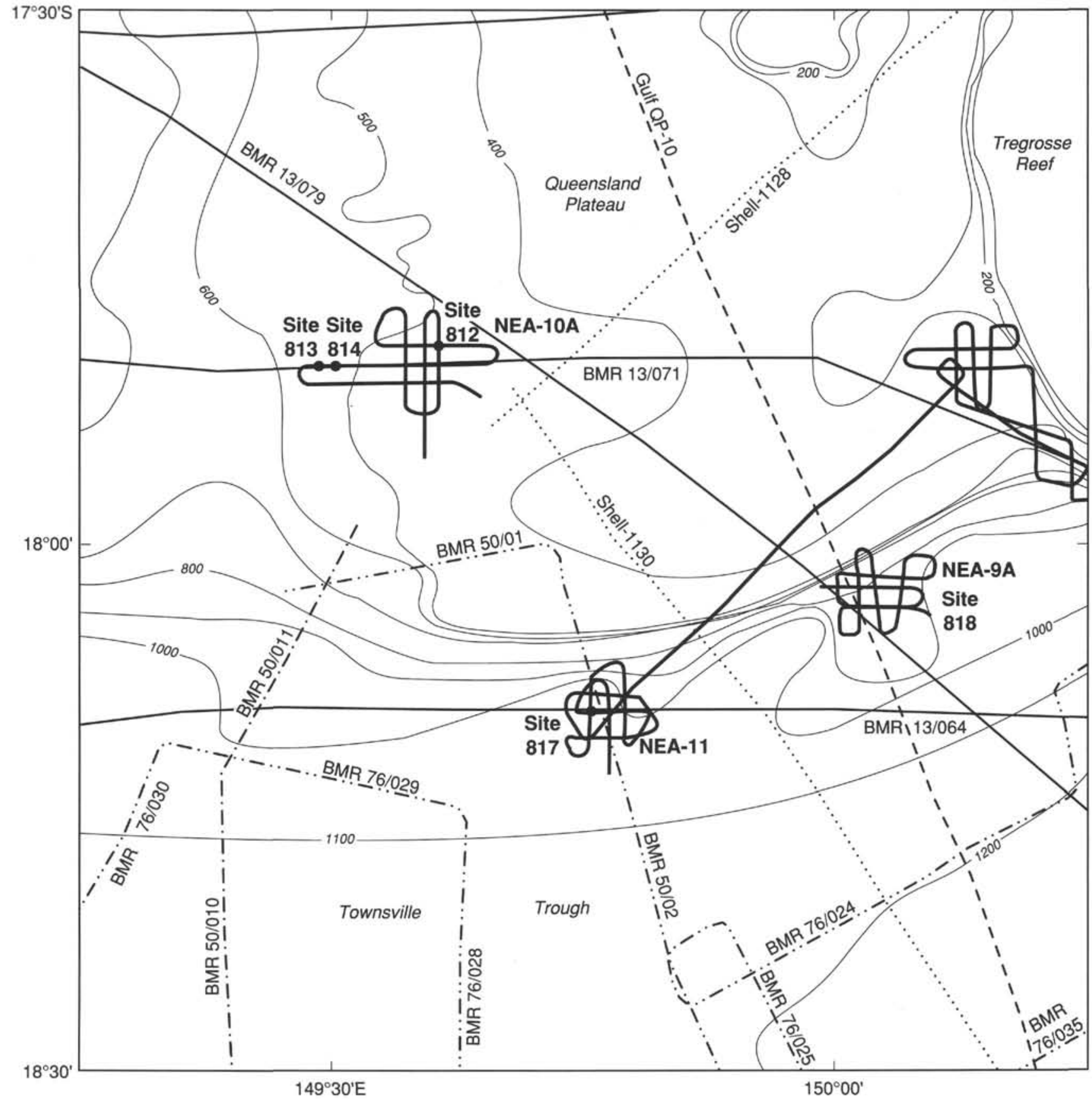

Figure 2. Track chart showing the distribution of regional seismic data in the area around Sites 812, 813, and 814. Simplified bathymetry (m) and site surveys conducted by BMR at Sites 817 and 818.

Miocene. This age thus may represent the first major contraction of the carbonate platforms of the Queensland Plateau. Later contractions may define additional subsidence pulses.

The composition of the platforms has previously been investigated to reconstruct the climatic history of the region. Davies et al., (1987, 1989) proposed that tropical carbonate platforms are underlain by temperate platforms as a consequence of the northward drift of Australia into the tropics throughout the Cenozoic. Drilling at Site 812, to determine the composition of the earliest platform, was intended to shed further light on this temperate/tropical transition.

The magnitude and periodicity of late Miocene history of sea level was of substantial interest, particularly in the seismic stratigraphic and eustatic contexts. Any evidence that defines absolute changes in time and space might impact on our understanding of the isotopic composition of the Miocene ocean.

Objectives at Site 812

Site 812 is located to the southwest of Tregrosse Reef on an older platform. A track map showing the location of the site and the site survey seismic data is shown in Figures 2 and 3 (see "Site Geophysics" section, this chapter). The pre-drilling prognosis for the site is shown in Figure 4. The objectives for Site 812 were:

1. To determine the age and facies of the periplatform and reef sequences toward the margin of the carbonate platform complex.

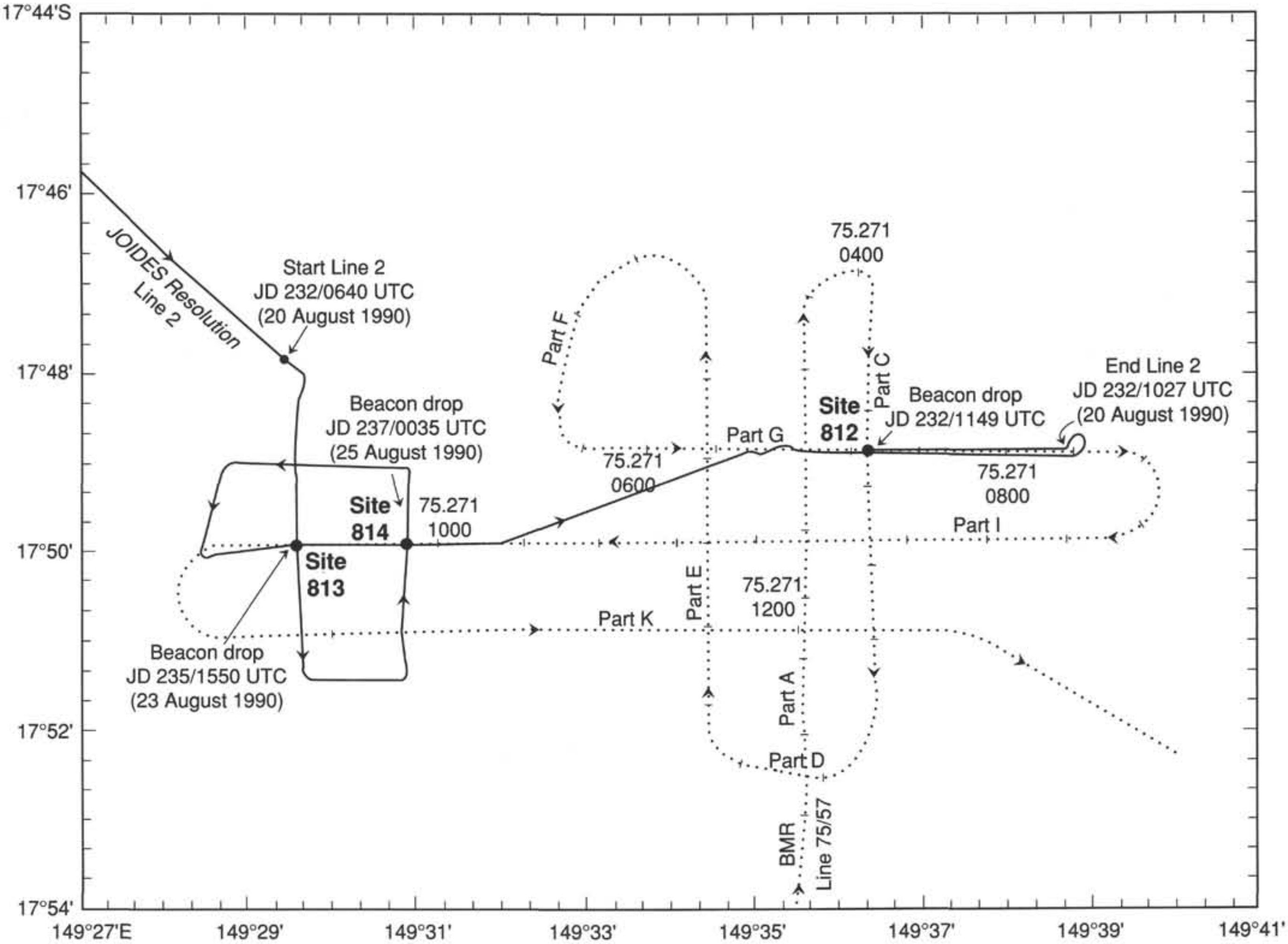

Figure 3. *JOIDES Resolution* Leg 133 site location tracks (solid line) and *Rig Seismic* 1987 site survey tracks (dotted line) around Sites 812, 813, and 814.

2. To determine the Oligocene to Holocene paleoceanographic and paleoclimatic signal in the reef and periplatform sequences.
3. To analyze the "backstepping" history of the shallow carbonate banks of the Queensland Plateau.
4. To establish the relationship between sea-level fluctuations and bank-derived carbonate facies.
5. To determine the Late Cenozoic seawater carbonate saturation history within the region.
6. To determine the diagenetic signal contained within periplatform sediments; in particular, to establish the stability regimes of high-magnesium calcite and aragonite within the platform margin environment.

OPERATIONS

Transit from Site 811 to Site 812

The transit to Site NEA-10A/1 (Hole 812A) covered 109 nmi in 9.4 hr at an average speed of 11.6 kt. During the transit we streamed the magnetometer. A 22-nmi seismic survey was run over proposed Sites NEA-10A/2, -10A/3, and -10A/1 at an average speed of 4.8 kt. The survey was conducted within an optimal global positioning system (GPS) window. The ship returned to the GPS position indicated for Hole 812A, and a Benthos shallow-water beacon was dropped at 2150L (all times reported in this section are local time, or L) on 20 August 1990. The ship was unable to hold its GPS position because of low signal level. A second beacon was deployed on a taunt wire; the diamond coring system (DCS) core winch line was put on the taunt wire winch to provide the required length for later holes, and the beacon was dropped at 0115L August 21.

Site 812

Hole 812A

Hole 812A was spudded at 0218L August 21 at 17°48.841'S and 149°36.313'E. The precision depth recorder (PDR) indicated that water depth was 460.4 m. The bit was positioned at 457.0 m and the first core was shot. Core 133-811C-1H recovered 4.89 m of sediment and therefore was accepted as a mud-line core; the mud line was determined to be at 461.6 m below sea level. Continuous APC cores (Cores 133-812A-1H through -4H) were taken from 0.0 to 27.9 mbsf, with 27.9 m of sediment cored and 26.08 m recovered (93.48% recovery). An orientation survey was taken at Core 133-812A-4H. APC coring was terminated when the APC had a partial stroke on Core 133-812A-4H that damaged the shoe and shattered the liner. Continuous XCB cores (Cores 133-812A-5X to -8H) were taken from 27.9 to 64.3 mbsf with 36.4 m cored and 1.56 m recovered (4.29% recovery). The circulation rate was held low in an

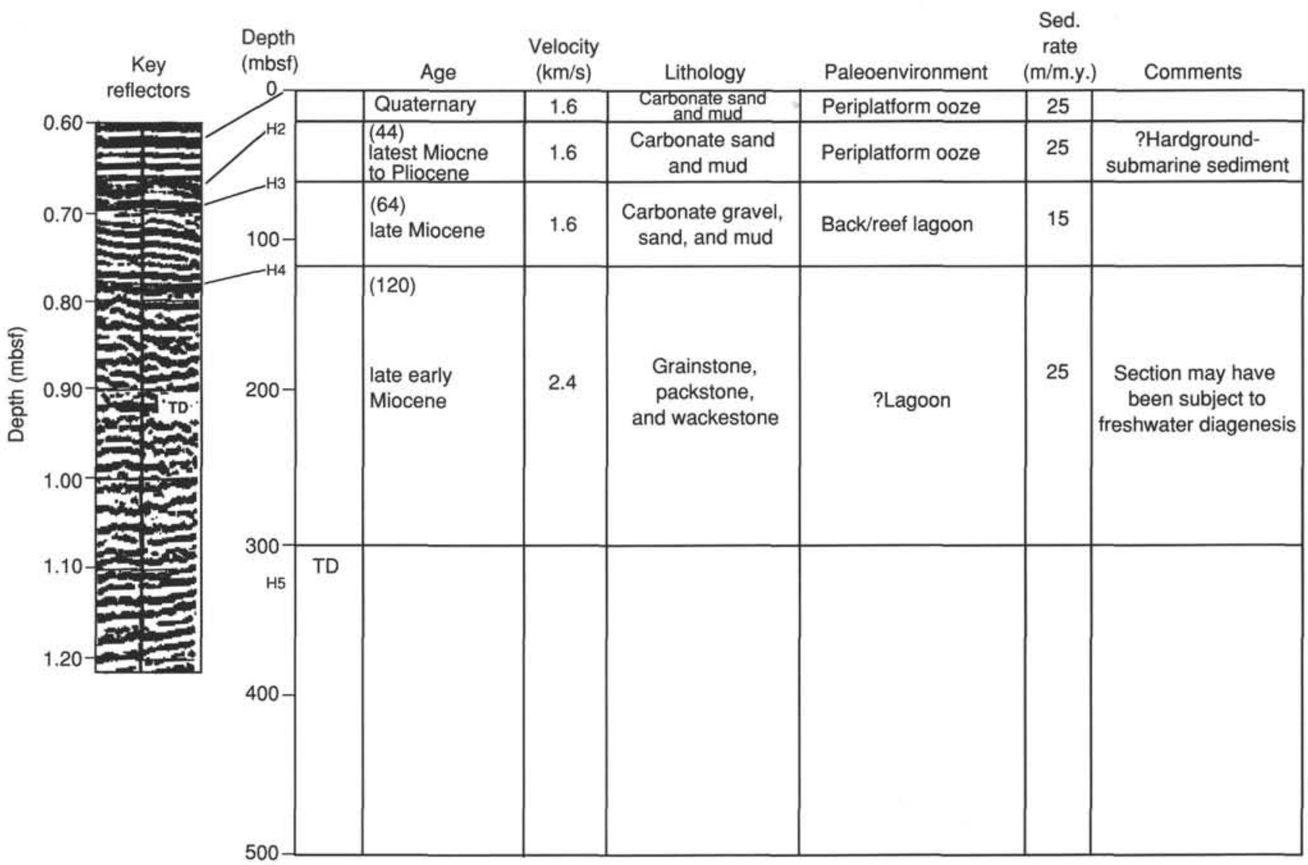

Figure 4. Pre-drilling prognosis for Site 812.

effort to improve recovery of flowing dolomitic sands, and frequent mud sweeps were required. Overpulls of 20,000–40,000 lb were common.

We attempted to use the vibrapercussive corer (VPC) for Core 133-812A-9V, but recovery was negligible (although the liner support ring had sand packed around it, indicating that some core had entered the liner).

Continuous XCB cores (Cores 133-812A-10X to -22X) were taken from 64.3 to 189.9 mbsf with 125.6 m cored and 13.09 m recovered (10.42%). The drill string repeatedly became stuck in interbedded hard dolomite and flowing dolomitic sands. The pipe stuck at 177.4 mbsf; it was worked to 270,000 lb overpull (230,000 string weight) without success. The Hydrolex jars were used for four 100,000-lb blows, and rotation and circulation were regained. A 30-bbl gel sweep was pumped and Core 133-812A-22X was cut. The string stuck again and was worked out of the hole with 250,000 lb overpull. The bit cleared the seafloor at 1950L and cleared the rotary table at 2130L 21 August.

Hole 812B

The ship was moved 15 m west to Hole 812B at 17°48.842′S and 149°36.306′E. A 9-7/8-in. ODP-rebuilt four-cone insert bit was run with the RCB bottom-hole assembly (BHA). Four additional 8-1/4-in. drill collars (DC) were picked up for added weight on bit in a 12-DC BHA. Hole 812B (NEA-10A/1) was spudded at 0208L 22 August. A 9-7/8-in. hole was drilled with a wash barrel in place from 0 to 72.4 mbsf. After a 4-1/2 hr delay for rig repairs, the RCB BHA was run back to 72.4 mbsf and Core 133-812B-1W was retrieved. A second wash barrel was dropped and the 9-7/8-in. hole was drilled from 72.4 to 150.0 mbsf. However, the pipe became stuck again; it was worked up to 410,000 lb maximum overpull (230,000 lb string weight) from 117.9 to 108.4 mbsf. The jars failed to free the pipe. We think that it may have been stuck above the BHA in a notch on one of the protruding dolomite ledges. Circulation rates had been reduced in a futile attempt to improve recovery, which probably aggravated hole-cleaning problems with fine sloughing dolomitic sands.

The hole was swept with 20 bbl of mud, rotation was restored, and the pipe was reamed back to bottom (as a precautionary measure), encountering rock rubble at the bottom of the hole. We think that the rock rubble came from dolomite ledges that were broken off as the stuck pipe was pulled up hole. The hole was swept with 20 bbl of mud and we retrieved Core 133-812B-2W, which yielded hard dolomite. Continuous rotary cores (Cores 133-812B-3R to -18R) were taken from 150.8 to 300.0 mbsf, with 149.2 m cored and 8.52 m recovered (5.71%). We credit an increase in circulation rate from 300 to 500 gal/min and a 15-bbl mud sweep in mid-core for successfully avoiding stuck pipe. A short trip made to condition the hole for logging encountered no drag and only 1 m of fill at the bottom of the hole, indicating that the hole was stable. A 20-bbl mud sweep was circulated before and after the conditioning trip. The 9-7/8-in. RCB bit was dropped with a mechanical bit release (MBR); however, the sleeve-shifting tool was also lost in the hole. The open-ended pipe was pulled to 68.8 mbsf for logging.

Logs were run as follows:

1. The induction/density/sonic/caliper/gamma ray (DITE/HLDT/SDT/MCDG/NGT) logging tool was placed into the pipe at 0805L 23 August and was out of the hole at 0955L.

2. The formation microscanner/gamma ray/temperature (FMS/NGT/TCC) logging tool entered the pipe at 1050L 23 August and was back out at 1210L.

3. The wireline packer was picked up to do two isolation packer tests; however, as the tool was being picked up, it bowed and the electrical connections failed. This problem was indicated by erratic amperage to the swash plate pump motor. The tool was picked up again at 1230L 23 August, and electrical troubleshooting continued until 1945L, when the RCB BHA cleared the seafloor at 2023H.

The drill pipe was pulled while the ship moved into the dynamic positioning (DP) mode to Hole 813A (NEA-10A/3); the MBR cleared the rotary table at 2145L 23 August.

Return to Hole 812C

Operations at Site 814 demonstrated the potential of using the XCB to penetrate thin, hard layers (where these could be accurately predicted in the section) and subsequent return to APC coring to recover the softer underlying sediments. We decided to return to Site 812 to attempt to recover the softer sediments underlying the hard layers at 40 mbsf. The transit to Hole 812C covered 5.2 nmi in 4.5 hr at an average speed of 1.2 kt. The beacon signal was regained after locating the site using GPS coordinates, and the ship was positioned 15 m west of the beacon at 17°48.842′S, 149°36.331′E. The bit was positioned at 459.9 mbsl for the first core. Core 133-812C-1H was spudded at 2150L 26 August 1990; it recovered 7.45 m of sediment, indicating a mud-line water depth of 461.9 mbsl.

Continuous APC cores (Cores 133-812C-1H through -3H) were taken from 0.0 to 26.4 mbsf, with 26.4 m cored and 26.78 m recovered (101.44%). The hard dolomite and limestone layer encountered in Holes 812A and 812B was expected in the following core, so we ran the XCB. Core 133-812C-4X was taken from 26.4 to 29.5 mbsf, with 3.1 m cored and 0.45 m recovered (14.52% recovery). The bit again entered soft nannofossil foraminifer ooze, so the APC was again picked up as planned. Cores 133-812C-5H through -13H were taken from 29.5 to 115.0 mbsf, with 85.5 m cored and 86.78 m recovered (101.5% recovery) before the APC refusal point was reached. Cores 133-812C-14X through -16X were taken from 115.0 to 137.8 mbsf, with 22.8 m cored and 0.04 m recovered (0.18% recovery). The hole was becoming tight and the pipe was worked with up to 300,000 lb overpull. A 20-bbl gel sweep was circulated and the pipe was pulled out of the hole. The bit cleared the seafloor at 0740L and was back on deck at 0900L 27 August.

The coring summary for Site 812 appears in Table 1.

SITE GEOPHYSICS

JOIDES Resolution separated from the beacon at Site 811 at 0540 hr LT (JD 231/1940 UTC) on 20 August 1990, and commenced the 9-hr transit to Sites 812, 813, and 814 (proposed sites NEA-10A/1, -10A/3, and -10A/2) at 0700L (JD 231/2100 UTC). The magnetometer was towed immediately after departure, and continuous bathymetric and magnetic data were recorded during the Line 2 transit heading southeast toward Site 814 (proposed site NEA-10A/3). The ship arrived at a position of 17°46.725′S and 149°28.114′E, about 2 nmi northwest of Site 814 at 1624L (JD 232/0624 UTC), ready to start the site location survey.

Sites 812, 813, and 814 lie in 450–550 m of water near the southern margin of the Queensland Plateau between Flinders and Tregrosse reefs (Fig. 2), and about 65 km west of the edge of the modern Tregrosse Reef bank. The sites were positioned across the buried edge of the Tregrosse bank, in a variety of depositional settings, to provide de-

Table 1. Coring summary, Site 812.

Core no.	Date (Aug. 1990)	Time (UTC)	Depth (mbsf)	Length cored (m)	Length recovered (m)	Recovery (%)
Hole 812A						
1H	20	1620	0–4.9	4.9	4.89	99.8
2H	20	1635	4.9–14.4	9.5	9.95	105.0
3H	20	1650	14.4–23.9	9.5	9.18	96.6
4H	20	1720	23.9–27.9	4.0	2.06	51.5
5X	20	1910	27.9–35.4	7.5	1.36	18.1
6X	20	1930	35.4–45.0	9.6	0.00	0.0
7X	20	1950	45.0–54.7	9.7	0.00	0.0
8X	20	2030	54.7–64.3	9.6	0.20	2.1
9V	20	2110	64.3–64.3	0.0	0.00	0.0
10X	20	2205	64.3–73.9	9.6	0.15	1.6
11X	20	2235	73.9–83.6	9.7	0.00	0.0
12X	20	2255	83.6–93.3	9.7	9.32	96.1
13X	20	2305	93.3–103.0	9.7	0.00	0.0
14X	20	2330	103.0–112.7	9.7	0.00	0.0
15X	21	0005	112.7–122.3	9.6	0.83	8.6
16X	21	0030	122.3–131.9	9.6	0.20	2.1
17X	21	0055	131.9–141.6	9.7	0.00	0.0
18X	21	0220	141.6–151.2	9.6	0.63	6.6
19X	21	0330	151.2–160.9	9.7	0.13	1.3
20X	21	0500	160.9–170.5	9.6	1.28	13.3
21X	21	0555	170.5–180.2	9.7	0.05	0.5
22X	21	0725	180.2–189.9	9.7	0.50	5.2
Coring totals				189.9	40.73	21.4
Hole 812B						
1W	22	0045	0–72.6	72.6	0.68	(wash core)
2W	22	0410	72.6–150.8	78.2	1.59	(wash core)
3R	22	0500	150.8–160.5	9.7	1.78	18.3
4R	22	0600	160.5–170.2	9.7	0.70	7.2
5R	22	0640	170.2–179.9	9.7	1.00	10.3
6R	22	0725	179.9–189.5	9.6	1.12	11.6
7R	22	0815	189.5–199.2	9.7	1.04	10.7
8R	22	0905	199.2–208.5	9.3	0.55	5.9
9R	22	0955	208.5–218.2	9.7	1.28	13.2
10R	22	1040	218.2–227.5	9.3	0.29	3.1
11R	22	1115	227.5–237.1	9.6	0.04	0.4
12R	22	1150	237.1–246.4	9.3	0.07	0.8
13R	22	1220	246.4–255.7	9.3	0.14	1.5
14R	22	1255	255.7–265.4	9.7	0.09	0.9
15R	22	1340	265.4–275.0	9.6	0.00	0.0
16R	22	1415	275.0–284.7	9.7	0.12	1.2
17R	22	1450	284.7–294.4	9.7	0.06	0.6
18R	22	1525	294.4–300.0	5.6	0.22	3.9
Coring totals				149.2	8.50	5.7
Washing totals				150.8	2.27	
Combined totals				300.0	10.77	
Hole 812C						
1H	26	1155	0–7.4	7.4	7.45	100.0
2H	26	1230	7.4–16.9	9.5	9.88	104.0
3H	26	1250	16.9–26.4	9.5	9.47	99.7
4X	26	1410	26.4–29.5	3.1	0.45	14.5
5H	26	1435	29.5–39.0	9.5	9.67	102.0
6H	26	1500	39.0–48.5	9.5	9.53	100.0
7H	26	1525	48.5–58.0	9.5	10.04	105.7
8H	26	1550	58.0–67.5	9.5	9.77	103.0
9H	26	1610	67.5–77.0	9.5	9.82	103.0
10H	26	1630	77.0–86.5	9.5	9.62	101.0
11H	26	1650	86.5–96.0	9.5	9.91	104.0
12H	26	1710	96.0–105.5	9.5	9.62	101.0
13H	26	1740	105.5–115.0	9.5	8.88	93.5
14X	26	1830	115.0–121.4	6.4	0.04	0.6
15X	26	1905	121.4–131.1	9.7	0.00	0.0
16X	26	1940	131.1–137.8	6.7	0.00	0.0
Coring totals				137.8	114.15	82.8

Note: Times are reported in Universal Time Coordinated (UTC), which is 10 hr later than local time (L).

tailed information on the factors controlling carbonate platform development on the Queensland Plateau. The site area was originally recognized as a potential ODP drilling target on a 1972 BMR sparker line (Fig. 2, line 13/071). In 1987 the BMR vessel *Rig Seismic* was used to conduct a site survey at this location (Symonds and Davies, 1988; Feary et al., 1990) and about 90 km of 24 channel, 80-in^3 water gun, magnetic, and bathymetric data were collected on a grid of north-south and east-west lines (Figs. 2 and 3). Although Sites 812, 813, and 814 all lie within this network, only Site 812 was on a line intersection. Initially this was to be the only site in the area; however, a westerly extension of the site survey lines (Fig. 3) crossed progradative and onlapping platform slope sequences thought to contain a record of Miocene sea-level change, and resulted in two further sites being proposed to examine this possibility. Site 814 (proposed site NEA-10A/2) was suggested immediately following the *Rig Seismic* site survey cruise and is included in the Leg 133 Safety Package (Feary et al., 1990) and Scientific Prospectus (ODP, 1990); however, Site 813 (proposed site NEA-10A/3) was only suggested and approved just prior to the start of Leg 133.

An important requirement of the Leg 133 site location surveys was that the seismic records obtained on the *JOIDES Resolution* be as close as possible in appearance to those collected during the 1987 site surveys by BMR's *Rig Seismic*, thus reducing ambiguity in site definition and in the comparison of the seismic stratigraphy between the two data sets. Accordingly, some modifications were made to the *JOIDES Resolution* seismic deployment systems (see "Site 811" chapter, this volume). The excellent correlation at Site 811 between the *JOIDES Resolution* single channel seismic data and the *Rig Seismic* multichannel seismic profile, as well as the vessels' respective GPS positions, indicated that it would be possible to reliably confirm the seismic characteristics and positions of other Leg 133 sites.

As Sites 812–814 all lie within the same site survey grid and are <13 km apart, it was decided to conduct their site location surveys at one time. The survey was designed to confirm their proposed positions on *JOIDES Resolution* seismic data collected along a *Rig Seismic* track; to obtain intersecting seismic lines at Sites 813 and 814; to obtain a seismic line directly connecting all three sites; and attempt to gain a better understanding of the distribution of the progradative "slope" unit. Following the survey, we intended to progressively located the sites by using the confirmed global positioning system (GPS) coordinates; therefore, the beacon was dropped as the ship was maneuvered into the site location using the dynamic positioning system of the *JOIDES Resolution*. We expected that this method would allow the vessel's moonpool to be positioned accurately over the site. It was favored over the more "hit-and-miss" approach where the beacon is dropped while collecting seismic data, which is used in an attempt to predict the site location more than 200 m ahead of the displayed seismic record.

The distribution of regional seismic data in the area around the sites is shown in Figure 2, and the tracks of the original *Rig Seismic* site survey and the *JOIDES Resolution* site location survey are shown in Figure 3. Following a reduction in ship speed to 5 kt, the *JOIDES Resolution*'s single channel seismic profiling system was deployed and seismic recording commenced at JD 232/0640 UTC on 20 August 1990 in calm seas (Beaufort Scale force 2). The *JOIDES Resolution* initially sailed south across Site 813, and then north across Site 814; she then headed west to look for the prograding unit and then east along a *Rig Seismic* line to confirm the locations of Sites 813 and 814; finally she sailed to the northeast, and then east along another *Rig Seismic* line to confirm the location of Site 812 and complete the tie between all sites (Fig. 3). Seismic acquisition was stopped and the equipment retrieved at JD 232/1027 UTC on 20 August 1990. About 37 km of data was collected during the survey. The signals from four GPS satellites were received throughout the survey and the ship's track is considered to be accurately positioned. The seismic equipment operated well and good quality shipboard analog records were obtained (Fig. 5). There was excellent correlation at all sites between the *Rig Seismic* and *JOIDES Resolution* seismic profiles (Fig. 6, this chapter; Fig. 3 "Site 813" chapter, this volume; and Fig. 3 "Site 814" chapter, this volume), as well as the vessels' respective GPS positions.

Site 812

Following the site location survey *JOIDES Resolution* returned to the confirmed GPS position of Site 812 at JD 232/1100 UTC on 20 August 1990. The thrusters were lowered and the final positioning of the ship over the site was achieved using dynamic positioning. The beacon was dropped at JD 232/1149 UTC, and the final coordinates of Hole 812A were 17°48.841′S and 149°36.313′E, with a water depth of 461.6 m.

Site 812 is the most easterly site of the group of three sites (Sites 812, 813, and 814) positioned to examine the factors controlling carbonate platform development on the Queensland Plateau. Site 812 represents an intra-platform or "lagoonal" setting about 6 km east of the subsurface platform margin. There was good correlation at the site between the *JOIDES Resolution* single channel seismic data and the intersecting *Rig Seismic* multichannel seismic profiles (Fig. 6). Basement is not visible on the water-gun data across the site, but other seismic data in the area indicates that it is about 1 s TWT (two-way traveltime) below seafloor. Seven major seismic sequences can be identified above the top of a strong band of reflectors about 0.45 s TWT below seafloor on both the *Rig Seismic* and *JOIDES Resolution* seismic profiles (Fig. 7). The pre-drilling prognosis of the age, lithology, and depositional environment of these sequences, as defined by Feary et al. (1991), is shown in Figure 7. The basal sequence (S7), which lies just below TD, consists of a unit with low-amplitude, subparallel reflectors about 0.13 s TWT thick. It is overlain by a 0.06 s TWT thick, possibly offlapping sequence (S6), which is in turn onlapped by 0.03 s TWT thick sequence S5. The next sequence, S4, has a flat base and a gently mounded top, and ranges from about 0.04 s TWT thick at the site up to 0.07 s TWT thick in a broad mound just west of the site. The overlying sequence S3 (0.07 s TWT thick) also contains gently mounded features, and is generally composed of low-amplitude reflectors. It is draped, and in some places onlapped, by sequence S2 (about 0.03 s TWT thick), which is itself onlapped by upper sequence S1. At the site, S1 lies within the wave train of the seafloor reflection. The pre-drilling interpretation (Fig. 7), which was based on regional considerations, including the results of DSDP Site 209, suggested that S1 and S2 are Quaternary to Pliocene or uppermost Miocene carbonate sand and mud of periplatform origin; S3 to S4 were expected to be upper Miocene carbonate gravel, sand, and mud deposited in a back-reef or lagoonal environment; and S5 and S6 were thought to be upper lower Miocene lagoonal grainstone, packstone, and wackestone, which had possibly undergone freshwater diagenesis.

To provide some predictive capability during the drilling at Site 812, an estimate of the two-way traveltime (TWT)/depth relationship below the seafloor was made using stacking-derived interval velocities from the BMR seismic lines across the site (Fig. 8). At depths greater than 150 mbsf the velocities of the sediments at Site 812 are higher than those for Site 811

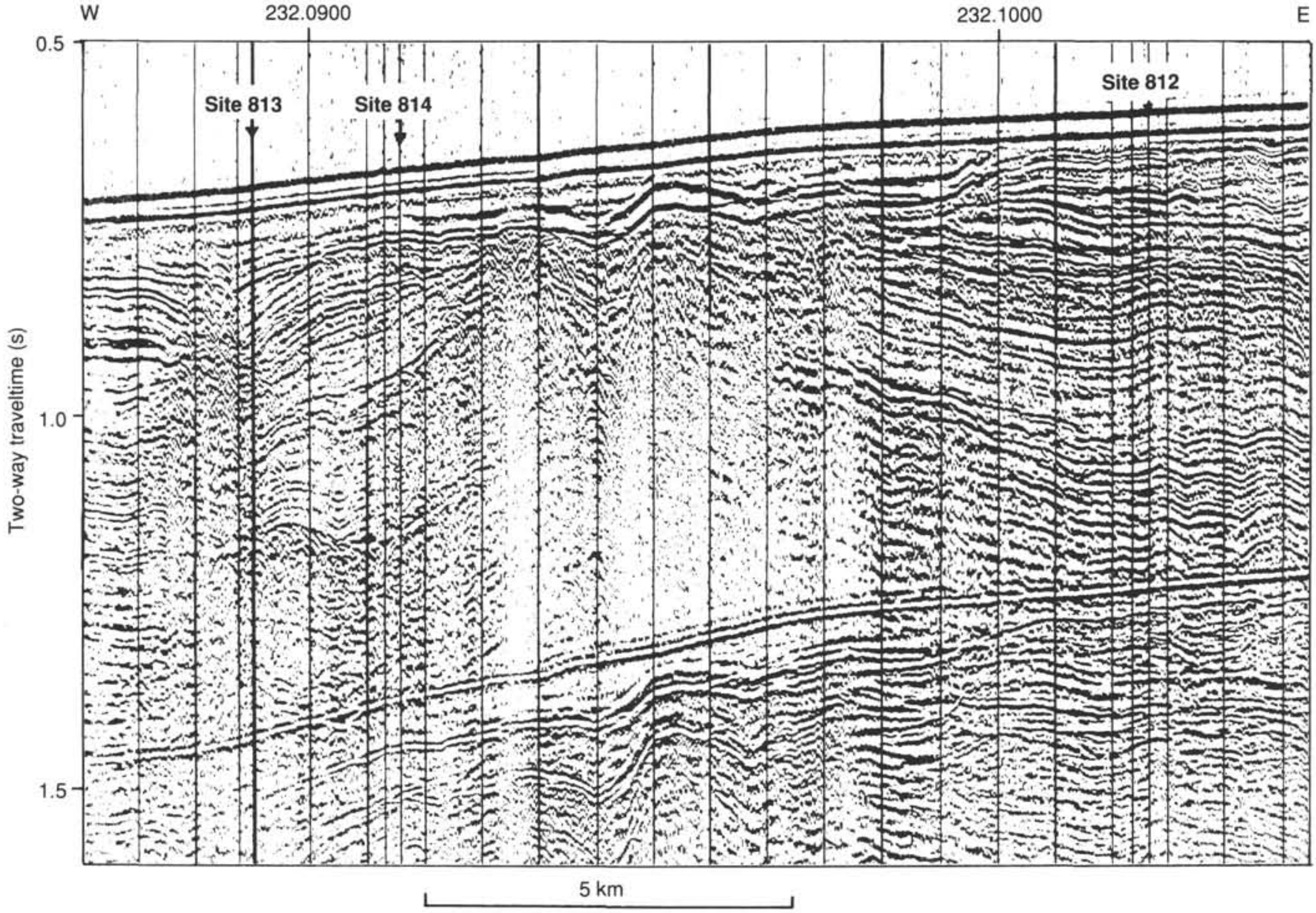

Figure 5. *JOIDES Resolution* shipboard analog single-channel seismic profile collected during the Site 812-813-814 site location survey using two 80-in.^{3} water guns. The seismic tie between all sites is shown.

and DSDP Site 209 (Andrews, 1973), and probably reflect the carbonate platform setting of Site 812.

LITHOSTRATIGRAPHY

Introduction

Site 812 was drilled in 462 m water depth on the southwestern margin of the Queensland Plateau. The overall lithology of the 300-m-thick sequence, extending from middle to upper Miocene through Pliocene and Pleistocene, consists of pelagic and deeper neritic carbonate oozes and/or chalks overlying shallower neritic packstone to floatstone in the upper and middle parts of the sequence; and reef-derived, skeletal grainstones to floatstones in the lower part of the sequence. The three holes drilled at Site 812 provide complementary information, whereby intervals cored in Hole 812A were recored in Holes 812B and 812C.

In Hole 812A, APC cores to 27.9 mbsf had almost 100% recovery and moderate disturbance; XCB cores to 189.9 mbsf had intense disturbance and poor recovery (generally <13%), except in some mixed, chalk/packstone horizons. Hole 812B was washed to 150.8 mbsf. The poorly recovered bottom interval of Hole 812A (151.2–189.9 mbsf) was recored in Hole 812B with the RCB to provide an overlapping record. Disturbance was moderate to intense and recovery was low, ranging from 18.3% to 0% (average value: 5.7%). Throughout most of the 137.8 m cored at Hole 812C (using APC/XCB), disturbance was slight and recovery was good, except for the hardground interval between 26.4 and 29.5 mbsf and the section below 115.0 mbsf (0%–5%). Despite poor recovery, the holes showed good overlap of cored sections, with less than a 2-m depth discrepancy.

Lithology Summary

The sedimentary succession is subdivided into three lithologic units on the basis of visual core, smear slide, thin section, and hand-specimen descriptions (Fig. 9). Unit I consists of foraminifer-nannofossil oozes with abundant pteropods. The boundary with Unit II occurs at the sharp contact with a phosphate-encrusted, dolomitized hardground. Unit II is divided into four subunits which consist successively of micritic nannofossil chalk, underlain by micritic foraminifer chalk with an intercalation of bryozoan-mollusk packstone to floatstone at the base, underlain by a foraminifer dolostone. Unit III is distinguished from the rest of the section on the basis of the transition from the distinct, sedimentary characteristics of overlying units passing downward into intensively dolomitized, reef-related deposits. This bottom unit is divided into three subunits whose major lithologies are respectively: (1) algal, mollusk, foraminifer rudstone/wackestone with rhodoliths; (2) coralgal floatstone/packstone with elements of coral boundstone; and (3) bioclastic peloid foraminifer packstone/rudstone.

Figure 9 provides a summary of lithology together with core recovery, depths, ages, lithologic units, and the main sedimentary features.

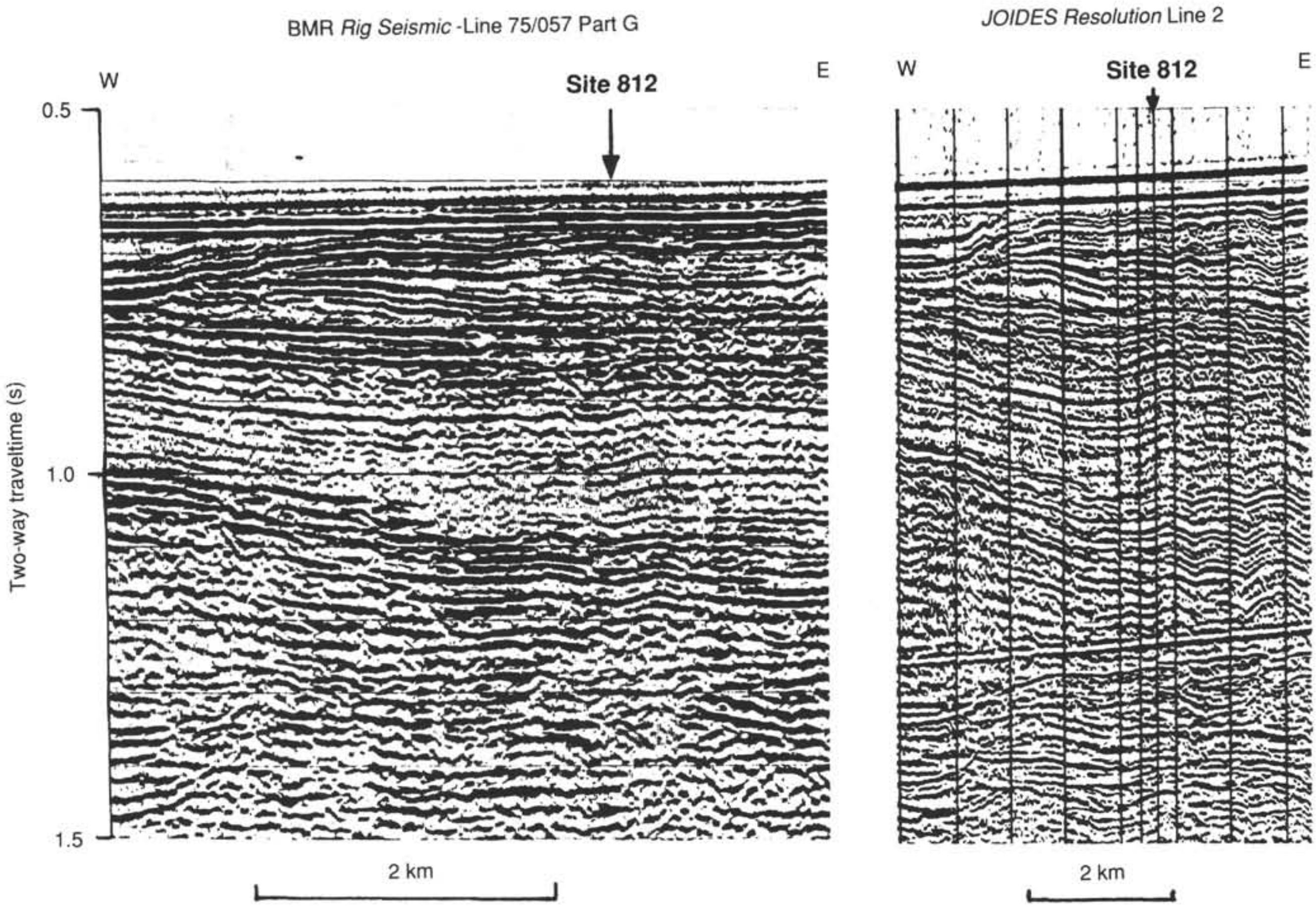

Figure 6. Comparison of *JOIDES Resolution* and *Rig Seismic* 80-in.^{3} water-gun seismic profiles across Site 812.

Lithologic Units

Unit I (Core 133-812A-1H through Section 133-812A-5X-1, 15 cm, and Core 133-812C-1H through Section 133-812C-3H-CC; depth, 0–27.9 mbsf; age, Pleistocene to late Pliocene

Unit I is mainly composed of planktonic foraminifer ooze with varying proportions of pelagic and benthic organisms. Foraminifer abundance varies from 40% to 85% with <5% being benthic forms. Nannofossils rarely exceed 20% of the whole sediment (Sections 133-812A-1H-2 and -1H-3). Pteropods in low amounts (5%) seem to be restricted to Cores 133-812A-1H and -2H (Sections 2, 3, and 4). The other main component is biodetritus (from 10% to 40% of the sediment), predominantly consisting of fine-grained, planktonic foraminifer debris and coarse-grained foraminifer and bryozoan particles. The silt-sized, skeletal fraction ("micrite") ranges from 0% to 10% in amount. The rest consists of spicules (0%–5%), calcareous needles (0%–10%) and, in Section 133-812A-3H-1, fish teeth (0%–1%).

Oozes are predominantly homogeneous and white. Color mottling appears to reflect bioturbation. However, partly lithified lumps were recorded in Sections 133-812A-2H-1 and -3H-1. Grain size is homogeneous throughout Unit I; the amount of sand fraction varies from 57% to 68%, whereas silt plus clay is present in amounts up to 35%. The only noticeable change in grain size results from the occurrence of a layered wackestone, which is an accumulation of foraminifer tests between 90 and 150 cm, in Section 133-812A-1H-1.

Unit II (Sections 133-812A-5X-1, 5 cm, through Core 133-812A-17X, and Cores 133-812C-4X through -16X; depth, 27.9–141.6 mbsf; age, late Pliocene to middle or early late Miocene)

Subunit IIA (Sections 133-812A-4H-1 through -8X-CC, and Core 133-812C-4X through Section 133-812C-8H-3; depth, 27.9–64.3 mbsf; age, late Miocene to early Pliocene)

A distinctive feature at the top of the unit is a thick hardground in Sections 133-812A-5X-1 at 5–9 cm, 133-812B-1W-1 at 5–8 cm, and 133-812C-4X-1 at 0–25 cm. This defines an abrupt contact with Unit I (Fig. 10). The uppermost 1 cm has a very sharp base, grading up to an irregular, laminated top with 0.5 cm of finely laminated, light reddish-brown and brownish crusts showing thin, translucent lamellae. These are tentatively identified as phosphatic at the base and goethite at the top. The hardground-capped section is a porous, white to light gray, bioclastic sediment. Compared with the whole sedimentary column of Subunit IIA, grain-size increases mirror a greater foraminifer abundance. Induration decreases downward, corresponding to increasing mud content; the sediment grades from a firmly lithified to a partially lithified grainstone, then to an unlithified packstone, within Section 133-812A-5X-1 at 9–123 cm. These sediments are mainly calcite, with dolomite occurring as poorly to well-preserved primary fabric. Porosity is usually moldic, with minor interparticle voids. Infilled large borings (3 cm in maximum diameter) penetrate the hardground layer. They are infilled with either foraminifer nannofossil chalk from Unit I, or multiple phases of goethite coatings.

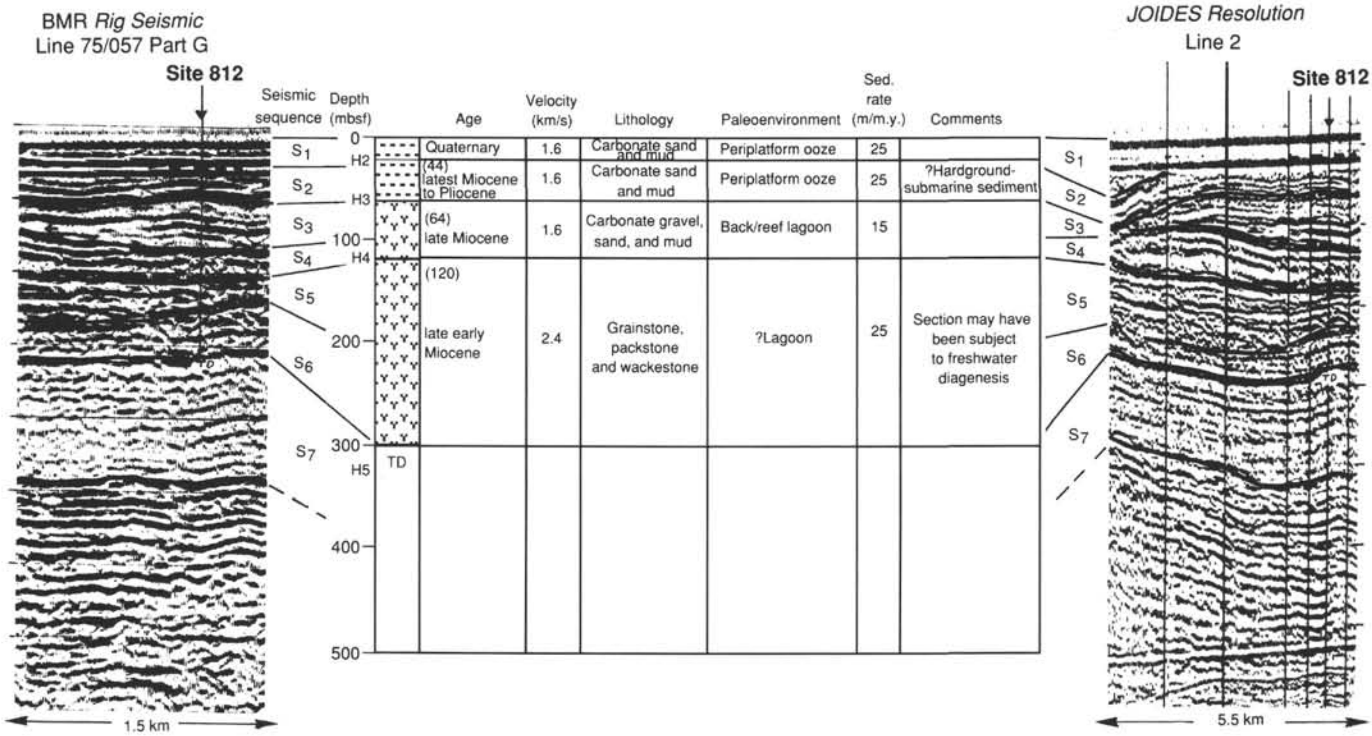

Figure 7. Seismic sequence characteristics on *JOIDES Resolution* and *Rig Seismic* water-gun seismic profiles across Site 812. Also shown is the pre-drilling prognosis.

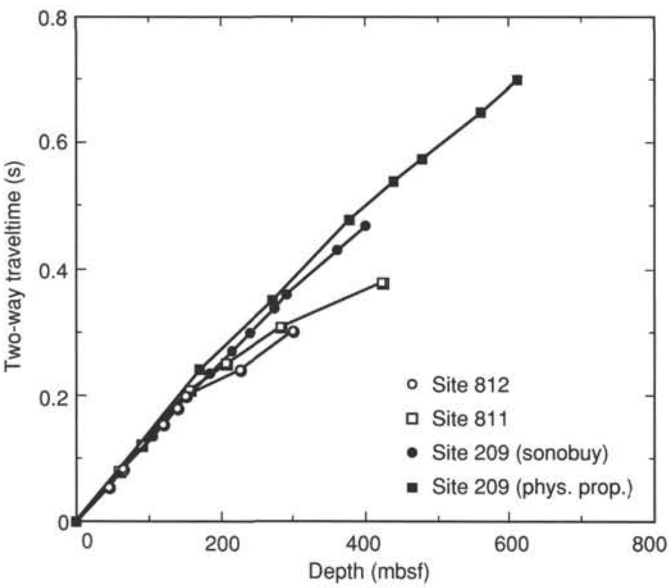

Figure 8. Comparison of TWT-depth curve estimated for Site 812 with those for Site 811 and DSDP Site 209 on the Queensland Plateau.

Subunit IIA at its base is fairly uniform, consisting of a mixture of white, partly lithified, micritic chalk (70%–80% of the total sediment) and white ooze (20%–30% of the sediment). Components include micrite composed of silt-sized bioclasts (25%–60% to 95%), planktonic foraminifers (5%–20%), benthic foraminifers (<3%), and nannofossils (5%–15% to 45%). There are few visible structures, except for some bioturbated zones and gray streaks. Examination of smear slides reveals well-crystallized dolomite rhombs (<1%) scattered within the matrix or overgrowing on foraminifer tests.

Subunit IIB (Section 133-812A-10X-CC through Core 133-812A-13X, and Sections 133-812C-8H-4 through -11H-1; depth, 64.3–86.5 mbsf; age, late Miocene)

Subunit IIB is a mainly uniform, white, micritic chalk. The distinction between Subunits IIA and IIB is based on a marked decrease in nannofossil concentration (0%–10%) and an increase in the amount of foraminifers (20%–30%) and dolomite crystals. The micrite matrix contains noticeable amounts of dolomite rhombs (2%–10%). Below 67.5 mbsf, the planktonic/benthic foraminifer ratio is <1.

Subunit IIC (Sections 133-812C-11H-2, 30 cm, through -12H-6, 150 cm; depth, 86.5–105.5 mbsf; age, late Miocene)

This subunit is distinguished on the basis of high concentrations of molluscan shells mixed with homogeneous chalk. The shelly accumulations contain a variety of bivalve tests (oysters, pectinids) whose large angular fragments are encrusted by bryozoans (Fig. 11). In the upper part of the mollusk-rich deposit (Sections 133-812C-11H-2 through -11H-CC), the matrix consists of a micritic chalk; by contrast, the bulk of the sediment varies in texture, and includes packstone, wackestone, and floatstone in Sections 133-812C-12H-1 through -12H-6. Throughout the subunit, large benthic foraminifers (amphisteginids, nummulitids) are the dominant components in the sand-sized fractions.

The lower boundary of Subunit IIC is apparently gradational into the underlying Subunit IID. It coincides with changes in sediment texture and composition, represented by a coarsening of particle size, an increase in dolomitic content, the disappearance of nannofossils, and the predominance of large foraminifers as sediment producers. The sediments at the base of Subunit IIC range from packstone/wackestone to floatstone. These sediments are white, partly lithified, and contain from 25% to more than 50% clear, well-crystallized

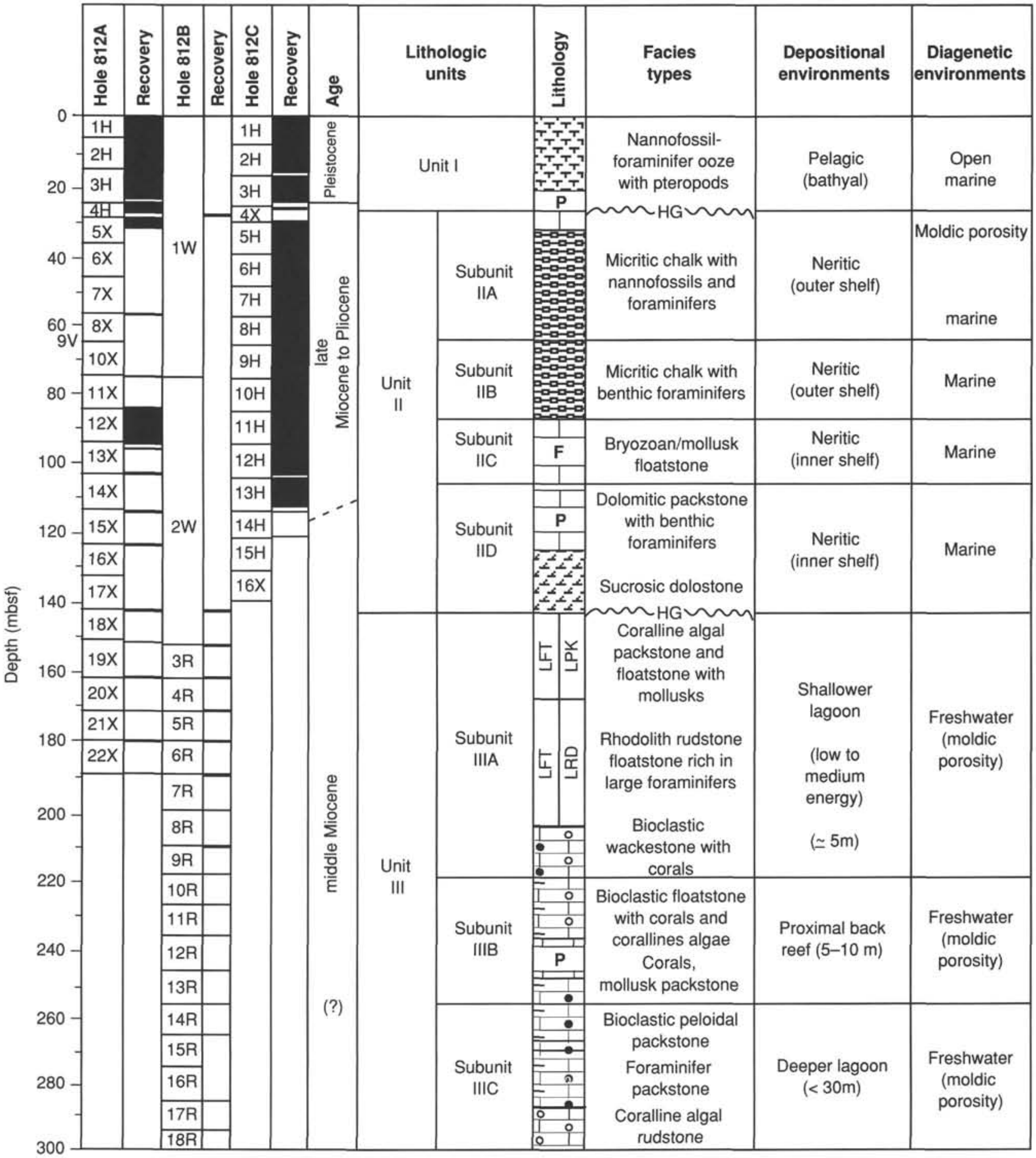

Figure 9. Lithostratigraphy of Site 812, on the southwestern margin of the Queensland Plateau. Recovered intervals are indicated by shading in the recovery column; HG = hardground. For a key to lithological symbols, see the "Explanatory Notes" chapter (this volume).

dolomite in the sand-sized fraction and up to 70% in the silt-sized fraction.

Subunit IID (Cores 133-812A-14X through -17X and Section 133-812C-2H-7 through Core 133-812C-16X; depth, 105.5–141.6 mbsf; age, late middle to early late Miocene)

Below Section 133-812C-13H-1, 107 cm, the rock type changes abruptly to a pure, indurated, sucrosic dolostone (100% dolomite), composed of sand-sized rhombs in which no biological constituent is still identifiable except a small, completely preserved, plate-shaped echinoid test (Section 133-812C-13H-1, 3–5 cm). Locally, the dolostone section shows 1- to 1.5-cm-thick, irregular layers (Fig. 12).

Unit III (Sections 133-812A-18X-1 through -22X-1, 58 cm, and 133-812B-2W-2, 42 cm, through -18R-1, 27 cm; depth, 141.6–300.0 mbsf; age, middle Miocene[?])

The contact with Unit II is considered to be sharp, since marked changes in sediment facies, induration, and porosity occur below 141.6 mbsf. The lithologic data are consistent

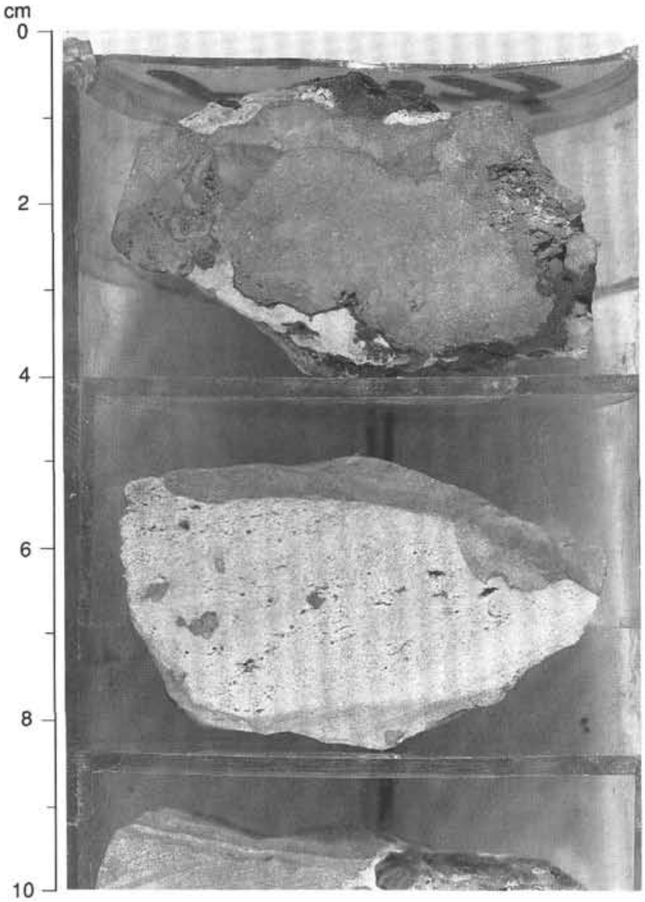

Figure 10. Phosphatic-goethitic hardground at the top of Subunit IIA (Section 133-812C-4X-1, 0–10 cm). Note the sharp contact between the dark, irregularly laminated crusts and the underlying white, lithified bioclastic grainstone showing reworked phosphatic gravels and burrow infillings.

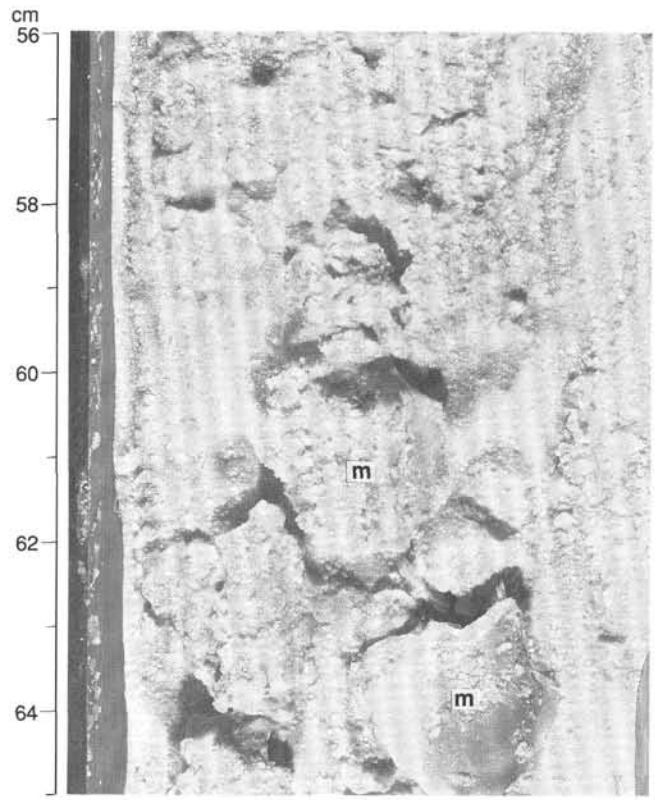

Figure 11. Molluscan floatstone, Subunit IIC (Section 133-812C-12H-1, 56–65 cm). Large, angular, bryozoan-encrusted oyster fragments within a partially dolomitized foraminifer floatstone; m = mollusk (oyster) fragments.

with the downhole logging data, indicating a distinct increase in resistivity, velocity, and uranium content at depths of 141–145 mbsf (see "Downhole Measurements" section, this chapter). Unit III is mainly coarse-grained, bioclastic sediment, varying from packstone/wackestone to rudstone/floatstone. Major biogenic components include branching red coralline algae, and rhodoliths, scleractinian corals, bivalves, gastropods, large foraminifers (mainly disc-shaped), bryozoans, and echinoderms. Throughout the sequence, the sediment is intensely recrystallized and lithified except for the possible occurrence of soft sediment at 218–255 mbsf (Cores 133-812B-10R through -13R), as indicated by an increased drilling rate. Dolomite is presumably the dominant mineral component, except for an occasional occurrence of low-magnesian calcite. Porosity is high (from 30% to as much as 60%), mainly resulting from selective leaching of skeletal particles (i.e., moldic porosity). Preservation of skeletal material therefore varies widely, as a function of initial mineralogy. Calcite-secreting coralline algae, bryozoans, large foraminifers, and echinoids are fairly well preserved, whereas initially aragonitic coral and molluscan debris have been dissolved or leave casts. The resulting cavities may be infilled by dolomite cements, forming molds (Fig. 13). Subdivision of Unit III into three subunits was based on appreciable changes in component composition within fossil assemblages and on visual petrographic characteristics (i.e., mud content, lithification rate).

Subunit IIIA (Sections 133-812A-18X-1 through -22X-1, 58 cm, and 133-812B-2W-2; depth, 141.6–218.2 mbsf; age, middle Miocene[?])

Material recovered from Hole 812A (Cores 133-812A-18X through -22X) and the washed portion of Hole 812B (Core 133-812B-2W) consists of moderately sorted, dolomitized, bioclastic packstones. The packstones exhibit white to very pale brown colors, a sucrosic fabric, and a moderate (20%–40%) porosity, either as vuggy (average diameter: 1–2 mm) or as moldic porosity mainly after shell fragments. White branching coralline algae debris, 1–4 mm in diameter, frequently occurs (Fig. 14), with the result that the algal content comprises 30%–40% of the rock. Additional constituents include corals, larger foraminifers (*Marginopora*), gastropods, bryozoans, and presumably, fragments of the green alga *Halimeda*. Although these rocks are mainly structureless, the deposits display subhorizontal bands of light/dark mottling in the interval 133-812B-9R-1, 23–33 cm; these features possibly represent trace fossils (Fig. 15) referred to *Astemosoma* or *Scoyema* ichnofacies types. Siliciclastic grains occur locally in minor quantities. These sediments alternate occasionally with rudstone (in Section 133-812A-22X-1), with the appearance of subspherical, massive rhodoliths, up to 2 cm in maximum diameter, contained within a bioclastic packstone matrix (Fig. 16). These macroids are composed of mammillate, laminar, encrusting algae which have formed concentric crusts over either coral or algal fragment nuclei.

From the rotary-cored part of Hole 812B (Cores 133-812B-3R through -9R), the sediment recovered exhibits changes in grain size and texture. It is a light brownish gray, poorly sorted rudstone/wackestone, containing rhodoliths,

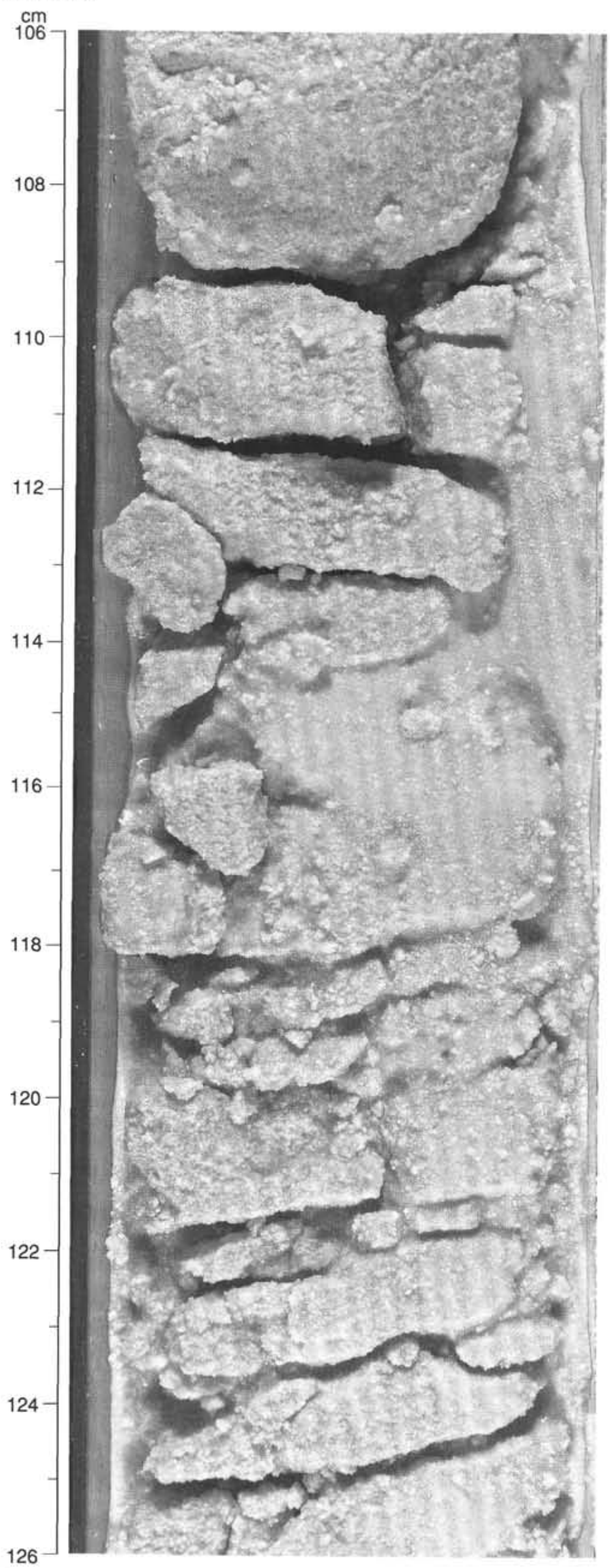

Figure 12. Irregularly bedded, sucrosic dolostone, Subunit IID (Section 133-812C-13H-2, 106–126 cm).

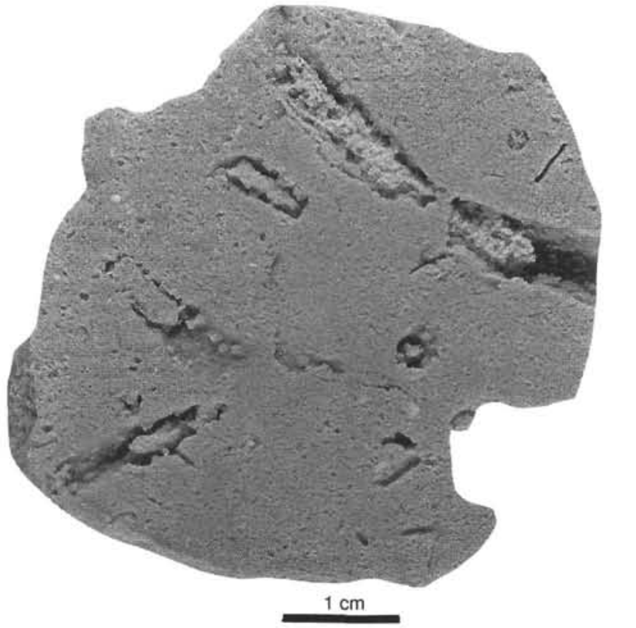

Figure 13. Solution features affecting a coral-bearing packstone, Subunit IIA (Section 133-812B-9R-1, 56–61 cm). Note the occurrence of large, elongated molds resulting from freshwater diagenesis of former fragments of branching scleractinian corals (presumably *Acropora*).

2–4 cm in size. Porosity is lower (10%–15%), and is mainly mold-related.

Minor fluctuations in texture recorded between holes, which reflect small coring offsets, may correlate with the sharp fluctuations in velocity and resistivity logs seen throughout Subunit IIIA, and particularly in the lower section between 180 and 220 mbsf (see "Downhole Measurements" section, this chapter).

Subunit IIIB. Sections 133-812B-10R-1 through -13R-1, 18 cm; depth, 218.2–255.7 mbsf; age, middle Miocene(?).

Although not substantiated by coring results because of the very poor recovery of pebbles (1.5% on average), the boundary between Subunits IIIA and IIIB is assumed to be gradational. It is placed at the uppermost abruptly increasing occurrence of scleractinian corals, which coincides with the uppermost occurrence of associated soft sediments. Downhole logging measurements clearly delineate the Subunit IIIA/Subunit IIIB boundary, at a depth of 220–222 mbsf, based on a sudden baseline shift in the resistivity, velocity, and bulk density signals.

Subunit IIIB predominantly consists of severely dolomitized skeletal floatstone, in which large fragments of coral colonies (Fig. 17), bivalve molds, and coralline algal debris are embedded within a peloidal packstone and wackestone matrix. The pebbles recovered presumably come from indurated layers which alternate with weakly consolidated or unconsolidated sediments. Rocks are white, pale brown, light gray, or light greenish-gray in color. Subordinate bioclastic constituents include large foraminifers and echinoids. Porosity, principally moldic (bivalve shells), is moderate (<20%).

Subunit IIIC (Core 133-812B-14R through Section 133-812B-18R-1, 23 cm; depth, 255.7–300.0 mbsf; age, middle Miocene[?])

Based upon the relative textural and compositional homogeneity of Unit III, the contact between Subunits IIIB and

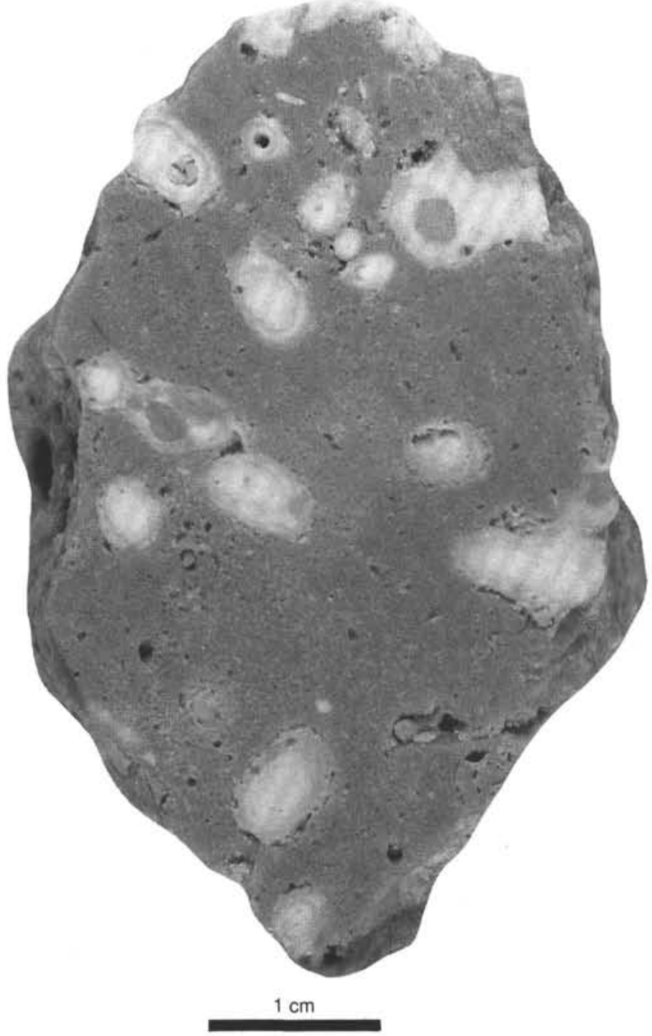

Figure 14. Coralline algal floatstone, Subunit IIIA (Section 133-812B-8R-1, 26–30 cm). Note the occurrence of white fragments of massive, branching, coralline algae within a packstone-type matrix. Moldic pores occur throughout the specimen.

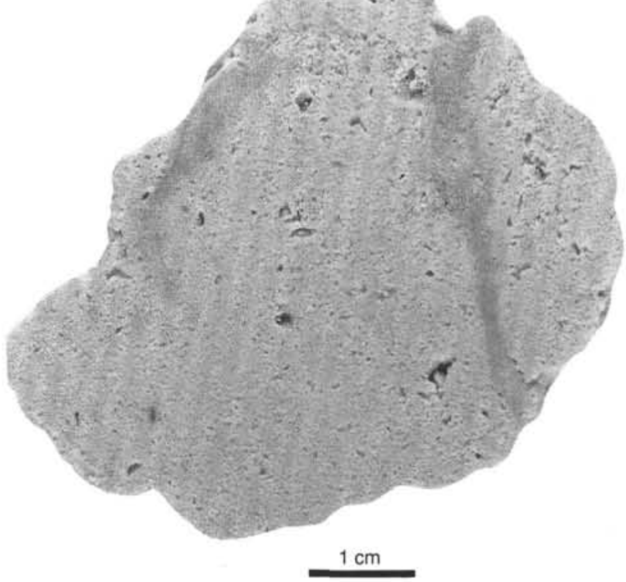

Figure 15. Subhorizontal trace fossils in a bioclastic packstone, Subunit IIIA (Section 133-812B-9R-1, 130–136 cm). These traces are tentatively referred to *Astemosoma* or *Scoyema* ichnofacies types. Note the abundance of moldic pores throughout the specimen.

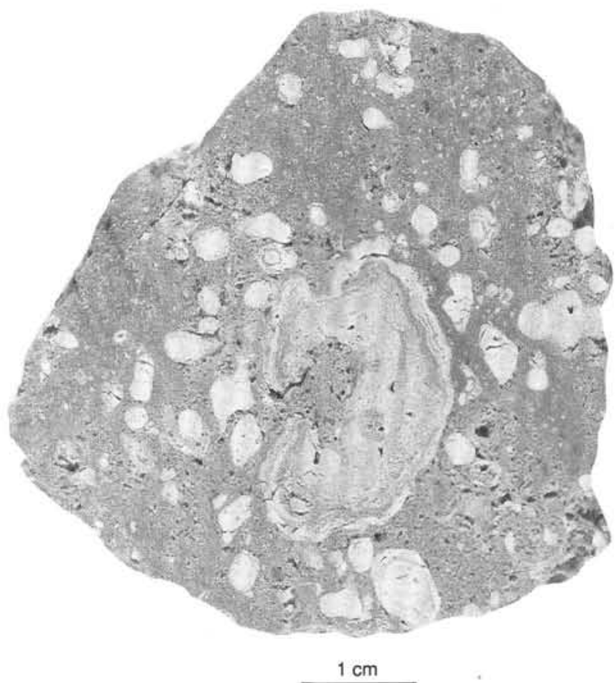

Figure 16. Massive, subspherical rhodolith composed of laminar to globular, coralline algal thalli encrusting a coral fragment nucleus in Subunit IIIA (Section 133-812B-3R-1, 110–116 cm). Rock matrix is a coral/coralline algal floatstone.

IIIC is thought to be gradational. It is marked by an enrichment in large benthic foraminifers and, to a lesser extent, in peloidal grains. The major lithology, therefore, is a poorly sorted, white to very pale brown, foraminifer packstone.

Subordinate rock types are peloidal, bioclastic packstones and rudstones. Although intensively dolomitized, both well-preserved skeletal grains and recognizable organic molds occur, including abundant disc-shaped foraminifer tests (*Lepidocyclina*), molluscan fragments, and minor coralline algal detritus. The lowermost layers of Subunit IIIC (133-812B-18R-1, 0-28 cm) contain rhodoliths. Porosity is moderate (<25%). Rare nannofossils were found in Section 133-812B-16R-CC.

Reconstruction of Depositional and Diagenetic Environments

Unit III at Site 812 is thought to be middle Miocene in age, and consists of skeletal packstone/wackestone to rudstone/floatstone, containing coralline algae, corals, mollusks, large benthic foraminifers and, to a lesser extent, echinoderms, bryozoans, and the green alga *Halimeda*. Despite limited recovery, there are components suggesting that this unit was deposited in a shallow-water, tropical, reef-related environment. The scarcity of open-marine fossils, restricted within Subunit IIIC to a few individual nannofossils, may indicate limited exchange with the open ocean when the Unit III carbonate platform developed. The depositional sequence of Unit III can be interpreted as follows:

Figure 17. Mold of a piece of faviid scleractinian coral colony, (presumably *Platygyra*) in Subunit IIIB (Section 133-812B-13R-1, 0–8 cm).

1. In Subunit IIIC the *Lepidocyclina*-dominated assemblages are indicative of a sheltered subtidal area (e.g., a lagoon) with bottom depths less than 30 m. Alternatively, the occurrence of rhodoliths at the base of the section may suggest shallower water depths (<10 m). Assuming that massive rhodoliths are more typical of a medium to high energy environment, possible scenarios include (1) reworking of algal nodules from a reef edge and redeposition in a back-reef setting; or (2) deepening of the depositional environment as Subunit IIIC developed, favoring the settlement of *Lepidocyclina*.
2. The nature of the Subunit IIIC/IIIB boundary at Site 812 is not actually clear because recovery was discontinuous. Nevertheless, it is presumed that it is gradual, since no drastic change in sediment composition occurs between recovered sections. The presence of coral colonies associated with mollusks and coralline algae in a muddy, fine-grained sandy depositional zone strongly suggests a protected back reef, situated just behind a reef edge (i.e., the proximal zone of coral patches); the bottom depth is thought not to have exceeded 10 m.
3. The uppermost section of Unit III is characterized by an association of massive rhodoliths, free-branching coralline algae, gastropods, large foraminifers (?*Marginopora*), and presumably green algae (*Halimeda*), inhabiting fine- to medium-sand-covered sandy bottoms. Although no information on the actual occurrence of corals throughout Subunit IIIA is available from shipboard studies, except in the lowermost part of the subunit, opinion is that the entire Subunit IIIA sequence might be related to a very shallow, back-reef zone rather than a subtropical, inner platform. This zone probably was subjected to medium-energy conditions (i.e., a tidally influenced environment).

The facies sequence from the entire Unit III apparently records an upward-shoaling sequence that may reflect the upward development of a carbonate reef platform in a regime of stillstand or falling sea level. This may be related to middle Miocene sea-level fluctuations. The Unit III sequence appears to be truncated by a major unconformity. Despite the lack of a biostratigraphically resolvable hiatus between Units II and III, the contact is assumed to be sharp and unconformable. Evidence for this assumption includes abrupt changes in sediment facies (shallow to deep-water conditions), intense recrystallization and dolomitization, and the well-developed porosity throughout Unit III. This suggests a long-term subaerial exposure. This emergence affecting the Queensland Plateau is tentatively ascribed to the major sea-level drop close to the middle/late Miocene boundary.

Compared with Unit III, the deposition of Unit II records a major environmental change, reflected by the sharp reef/nonreef contact. The demise of the reef tract developed over the Queensland Plateau may be explained by detrimental environmental change (e.g., enhanced ocean fertility) caused by the global cooling period which occurred during the late Miocene. These detrimental factors may presumably have been strengthened by basement subsidence. Unit II appears to reflect the reflooding of the reefal platform during late Miocene to late Pliocene time, with every subunit corresponding to a deepening step of the depositional environment. The occurrence of abundant shallow-water mollusks (oysters, pectinids) in Subunit IIC, together with the proliferation of large foraminifers in Subunit IID, provides evidence of a neritic, inner-shelf environment at depths not exceeding 50 m. Based on seismic profiles (see "Seismic Stratigraphy" section, this chapter) that indicate a submarine bank-shaped relief at the depth of shelf accumulation, we think that molluscan bioherms typified the early stages of recolonization across the Queensland Plateau. Moreover, the total lack of tropical marine organisms (e.g., corals) within these biological assemblages suggests a subtropical/temperate environment, possibly controlled by a late Miocene cooling event. The overlying section (Subunit IIB) contains micritic chalk, rich in benthic foraminifers, with subordinate planktonic foraminifers and rare nannofossils. This association suggests restricted open-ocean input to a neritic, outer-shelf environment. Subunit IIA is predominantly nannofossil-rich, micritic chalk with planktonic and benthic foraminifers, typifying a neritic outer-shelf area about 150–200 m deep (e.g., the upper boundary of the bathyal zone). Throughout Unit II, and more particularly in the lower part of the section of Subunit IID, well-crystallized dolomite rhombs occur, suggesting an *in-situ* postdepositional origin that still remains to be explained. The succession of sedimentary facies in Unit II reflects an upward-deepening sequence perhaps attributable to the major eustatic rise from early late Miocene to late Pliocene. The uppermost part of Unit II is marked by a phosphatic-encrusted hardground, which caps a 1-m-thick, firmly indurated, outer-shelf deposit with boring and solution features (i.e., moldic pores). This hardground was produced probably by submarine cementation/non-deposition/erosion, controlled by drastic changes in the water circulation regime perhaps attributable to rapid sea-level change. According to the available biostratigraphic data (see "Biostratigraphy" section, this chapter), the duration of the condensed sedimentation phase was at least 3 m.y., occurring between 5.2–8.2 Ma and 1.88–2.25 Ma. Strong currents may have swept across the drowned shelf-like plateau, precluding deposition and favoring the formation of a condensed sequence. Later, the hardground and lithified sediments were affected by dissolution, producing moldic porosity. This probably developed at the contact between sediment interstitial water and marine waters undersaturated with respect to metastable carbonates, possibly resulting from a decrease in the aragonite compensation depth (ACD) as sea level rose in the early Pliocene, rather than as a result of freshwater alteration.

During the Pleistocene, pelagic carbonates with foraminifers and nannofossils were deposited over the Queensland Plateau at depths of between 200 and 600 m (Unit I). Consequently, the Unit II to Unit I transition represents an overall upward-deepening succession reflecting subsidence, which dominates sedimentation in spite of sea-level fluctuations throughout the Pleistocene.

BIOSTRATIGRAPHY

Biostratigraphy and Paleoenvironment Summary

Calcareous nannofossils and planktonic, benthic, and larger benthic foraminifers were extracted from core-catcher samples, mainly from Hole 812A, but also from Holes 812B and 812C for the larger benthics. An overview of the biostratigraphic results is given on Figure 18. Planktonic fossils are abundant in the uppermost part of the cored section and preservation is generally good, but both the abundance and quality of fossils deteriorate rapidly downward. Datable planktonic fossils were recovered downward to the core catcher of Core 133-812A-13X which refer to the late Miocene. The benthic foraminifers indicate progressive deepening of the depositional environment from a neritic setting (0–200 m) at 35 mbsf and below to a bathyal environment (200–600 m) for sediments above 30 mbsf.

Calcareous Nannofossils

Hole 812A was drilled to 189.9 mbsf, and 23 cores were attempted over this interval. Biostratigraphic determinations were made principally using core-catcher samples. Calcareous nannofossils are common to abundant in Cores 133-812A-1H through -13X (0–103 mbsf), and indicate this interval to be upper Pleistocene to upper Miocene. Preservation of the nannofossils is moderate to poor. Species diversity is low and discoasters are scarce in the lower Pliocene and upper Miocene. The nannofossil assemblages thus are different from those recovered at nearby Site 811, which is probably an accident of sample spacing. Sediments from Core 133-812A-14X downward are barren of calcareous nannofossils.

Sample 133-812A-1H-CC contains very abundant *Gephyrocapsa caribbeanica* and a few *Calcidiscus leptoporus* but no *Emiliania huxleyi* or *Pseudoemiliania lacunosa*. This sample is, therefore, assigned to Zone CN14b (0.275–0.465 Ma). Sample 133-812A-2H-CC yielded *P. lacunosa* and is placed in Zone CN14a. *Calcidiscus tropicus* is present in Sample 133-812A-3H-CC but discoasters are lacking in this sample. An early Pleistocene age (about Zone CN13a) is assigned to this sample.

Sample 133-812A-4H-CC contains *Discoaster brouweri* and *Discoaster pentaradiatus* but no *Discoaster surculus*, and is placed in Zone CN12c (upper Pliocene). Sample 133-812A-5X-CC yielded *Sphenolithus abies* and *Reticulofenestra pseudoumbilica* and, therefore, is assigned to Zone CN11 (lower Pliocene), but may be older. No sediment was recovered in Cores 133-812A-6X and -7X. Samples 133-812A-8X-CC and -10X-CC yielded the upper Miocene marker species *Discoaster quinqueramus*, which constrains this interval to an age range from 5.26 to 8.2 Ma. *D. quinqueramus* was also found in Sample 133-812A-13X-CC and that sample also is assigned this same age range.

Three samples from Hole 812B contain nannofossils, but these assemblages are very sparse. Sample 133-812B-14R-CC yielded *Reticulofenestra minuta* and *Reticulofenestra pseudoumbilica*. These two species were also recorded in Sample 133-812B-16R-CC. In addition, *Coccolithus eopelagicus*, ?*Calcidiscus premacintyrei*, ?*Sphenolithus* sp., and a specimen of *Pseudoemiliania lacunosa* (apparently contamination) were found in this sample. Two specimens of *Reticulofenestra* sp. (~4 μm) were found in Sample 133-812B-18R-CC. For additional biostratigraphic information, see the Hole 812C barrel sheets (this volume).

Planktonic Foraminifers

The upper part of Hole 812A (Samples 133-812A-1H-CC through -4H-CC) contains abundant planktonic foraminifers; the preservation of the specimens is moderate and most specimens have thick-walled tests. This interval is assigned to Zone N22–N23 on the basis of the presence of *G. truncatulinoides*. One sample above the lowest occurrence of *G. truncatulinoides* is the highest occurrences of *G. obliquus* and *G. fistulosus*, which indicates the lowermost Pleistocene.

Below N22–N23 the abundance of planktonic foraminifers decreases. In Sample 133-812A-5X-CC *G. sacculifer, G. ruber, G. menardii, G. obliquus*, and *G. tumida plesiotumida* are all represented by small specimens, which points to a shallow-marine environment in the late Pliocene. In Sample 133-812A-12H-CC, small specimens of *N. acostaensis, G. altispira*, and *G. dehiscens* indicate the lowest part of Zone N16–N17.

Benthic Foraminifers

Benthic foraminiferal assemblages from Holes 812A and 812C show a paleobathymetric deepening from neritic (0–200 m) to upper bathyal (200–600 m) in the late Pliocene. Preservation is poor in and below Core 133-812A-8X, where recrystallization sometimes obscures test morphology. Species diversity increased upward in the section. Additional core-catcher samples were examined from Hole 812C. Preservation is poor in and below Sample 133-812C-5H-CC.

Benthic foraminifers in Samples 133-812A-12X-CC, -14X-CC, and -16X-CC are very poorly preserved and faunas show low species diversity. The dominant taxon in these three samples is *Elphidium* spp.; *Uvigerina auberiana* is also common. In addition, these core-catcher samples contain large (>250 μm) reefal foraminifer tests dominated by *Amphistegina* spp. Low species diversity, high species predominance, and high numbers of large reefal benthic foraminifer tests indicate that sediments from Samples 133-812A-12X-CC through -16X-CC were deposited in a shallow neritic setting near a reefal environment.

Samples 133-812A-5X-CC, -8X-CC, and -10X-CC show higher benthic foraminifer species abundance than assemblages lower in Hole 812A. Preservation shows moderate improvement above Sample 133-812A-10X-CC. *Elphidium* spp. and *Hyalinea balthica* are predominant species in these samples; *U. auberiana* is common. Other common depth-diagnostic species in these samples include *Cibicidoides dutemplei, Cibicidoides matanzasensis, Cibicidoides subhaidingerii, Plectofrondicularia parri, Nonionella turgidus*, and *Uvigerina laviculata* (van Markhoven et al., 1986). This species association indicates a middle to outer neritic paleodepth (30–200 m) for Samples 133-812A-5X-CC, -8X-CC, and -10X-CC. Large reefal benthic foraminifer tests also are present in these core-catcher samples.

Samples 133-812A-1H-CC through -4H-CC contain benthic foraminifer assemblages with high diversity. Species that indicate an upper bathyal paleodepth (200–600 m) for these samples include *Bulimina marginata, Bulimina mexicana, Cibicidoides grosseperforatus, Cibicidoides mundulus, Cibicidoides pachyderma, Hanzawaia mantaensis, Hoeglundina elegans, Planulina ariminensis, Sigmoilopsis schlumbergeri,*

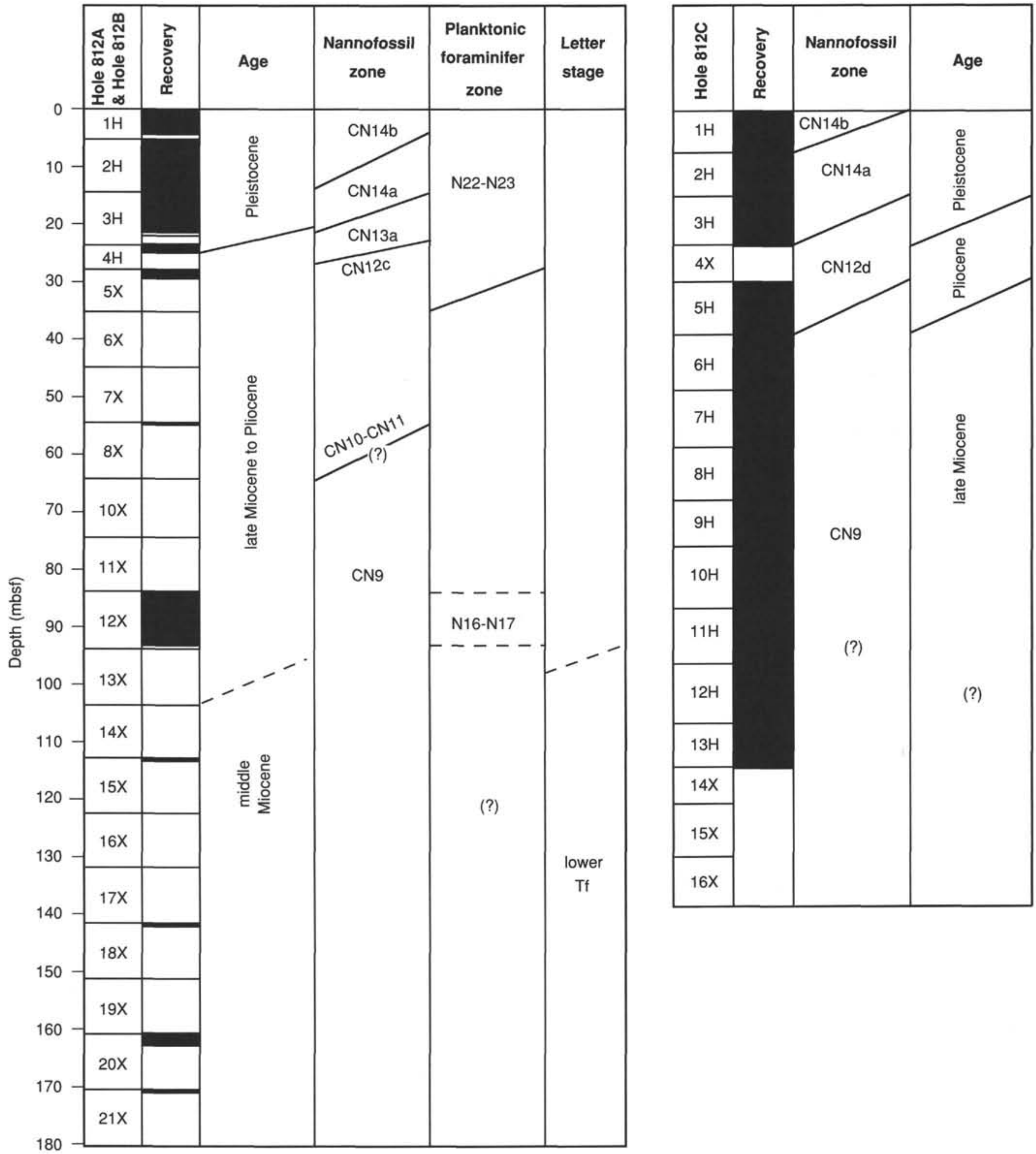

Figure 18. Overview of preliminary biostratigraphy for Site 812.

Sphaeroidina bulloides, and *Uvigerina carapitana* (van Markhoven et al., 1986).

Sample 133-812C-3H-CC contains an upper bathyal benthic foraminferal assemblage that includes *Bulimina marginata, Cibicidoides dutemplei, C. mundulus, C. subhaidingerii, Hanzawaia mantaensis*, and *Uvigerina pigmaea*. Core-catcher samples in and below Core 133-812C-5H contain neritic benthic foraminiferal assemblages dominated by *Elphidium* spp. and *Hyalinea balthica*. They also contain reefal benthic foraminifers. The lack of species that can be found in outer neritic assemblages indicates that these benthic foraminiferal faunas may represent paleodepths that are no deeper than middle neritic. Sample 133-812C-11H-CC is strongly recrystallized and contains foraminifers with a sugary texture. *Elphidium* spp. is the dominant taxon in this sample, suggesting a shallow neritic paleodepth for Sample 133-812C-11H-CC. Foraminifers are extremely rare in Sample 133-812C-13H-CC. Two specimens of *Elphidium* spp. and one of *Amphistegina* sp. were identified.

Larger Benthic Foraminifers

Core-catcher samples from Hole 812A and 812B were examined for larger foraminifers. Frequent to abundant larger foraminifers occur in Samples 133-812A-13X-CC and 133-812A-14X-CC. In the first sample rare *Cycloclypeus* sp. and rare to frequent *Lepidocyclina* (*Nephrolepidina martini* and *Nephrolepidina* sp.) occur. The fauna is moderately preserved. The value of parameter dc (O'Herne and van der Vlerk, 1971) of one specimen of *Nephrolepidina* sp. is 64.3%, pointing to a late middle Miocene to early late Miocene age of the sample. Palmieri (1973) has recorded *N. martini* from middle Miocene deposits of the Sandy Cape drill hole (Queensland, Australia). The second sample is characterized by the occurrence of rare to frequent *Operculina* sp., rare *Lepidocyclina*, and rare *Cycloclypeus*. This fauna is moderately preserved. In both samples we found well-preserved, conoidal, larger benthic foraminifers showing the characteristics of *Chapmanina* sp. The larger benthic foraminifers are accompanied by bryozoans, pelecypod shell debris, coral debris, and rare gastropods.

In Hole 812B, larger foraminifers from Samples 133-812B-3R-CC through -6R-CC have been dissolved and appear as vugs (i.e., moldic porosity). Only rare, recrystallized small miliolids can be recognized in these samples. Other bioclasts include red algal debris. In Samples 133-812B-8R-CC through -10R-CC *Marginopora* sp. and coral debris occur, and in Sample 133-812B-8R-CC one recrystallized specimen of *Cycloclypeus* sp. was observed. Sample 133-812B-16R-CC is characterized by frequent lepidocyclinas.

PALEOMAGNETISM

Shipboard paleomagnetics measurements conducted at Holes 812A and 812C yielded several magnetic polarity reversals that, with the aid of biostratigraphic tie-points, were correlated with the geomagnetic polarity time scale (GPTS). After shipboard measurements, these reversal boundaries were poorly defined and are in need of confirmation by shore-based study. Archive-half cores were analyzed continuously at NRM and AF 15 mT levels in the pass-through cryogenic system. In the upper part of Hole 812A, the pervasive drill-pipe related contamination that was recorded in Hole 811A was reduced considerably.

A composite section of Hole 812A and 812C produced an identical polarity reversal stratigraphy, with <1-m offset difference in boundary depths between the two holes (Table 2). In Hole 812A, on the basis of inclination changes after AF 15 mT demagnetization, three reversal boundaries have been tentatively identified. It appears that slightly higher AF demagnetization levels are necessary to further refine the preliminary boundaries. The Brunhes/Matuyama boundary at 0.73 Ma occurs at 13.0 mbsf. The top and bottom (0.92 and 0.97 Ma) of the Jaramillo subchron are placed at 15.2 and 16.6 mbsf, respectively. From the base of the Jaramillo to the base of the hole at 23.9 mbsf, a reversed polarity was measured, which is correlated to the upper part of the Matuyama (Chron 1r). The section did not penetrate the Olduvai normal event (top at 1.66 Ma) so it must be younger than this boundary age. At the base of Core 133-812A-3H (23.9 mbsf), a biostratigraphic age of 1.48–1.66 Ma occurs, confirming an early Pleistocene age. Pieces of cemented limestone in Core 133-812A-5X yielded predominantly reversed polarity, but this will have to be confirmed by shore-based studies since the sample orientation is questionable and a large scatter in inclination occurs. Magnetostratigraphy in the remaining core sections was not attempted because of the low and intermittent recovery. Recoring at Hole 812C recovered an additional section not recovered in Hole 812A above the cemented hardground, and also had excellent recovery below the cemented unit to about 115 mbsf. Thus, we extended the reversal stratigraphy down into the uppermost upper Pliocene above the unconformity(?) and found it to be consistent with the biostratigraphic markers in the core-catcher samples. At Hole 812C, the Brunhes/Matuyama boundary is placed at about 12.1 mbsf. The top and bottom of the Jaramillo subchron are preliminarily placed at 15.0 and 17.1 mbsf, respectively. The Pliocene/Pleistocene boundary lies immediately above the top of the Olduvai subchron at 23.7 mbsf. The base of Core 133-812C-3H (26.4 mbsf) is in the lower part of the Olduvai subchron, less than 1.88 Ma. Magnetostratigraphic and biostratigraphic dating above the cemented hardground constrain the onset of post-unconformity(?) deposition to the latest late Pliocene. Below the cemented unit in Core 133-812C-4R, the inclination record is dominated by scattered normal values, and is in need of additional demagnetization on discrete samples to resolve the magnetozones.

Interestingly, in both holes at this site, a possible magnetic excursion is recorded in the lower part of the Brunhes normal chron. In Hole 812A, between 9.5 and 11.0 mbsf, the inclination angles decrease progressively to values near 0°, after the 15 mT demagnetization step. In addition, although unoriented, the declination also shows a similar reversal trend, further supporting an excursion event. In Hole 812C, a similar inclination and declination event was also measured.

Generalized magnetic characteristics of the carbonate sediments can be assessed from the whole-core magnetic intensity data and their response to AF demagnetization. The Pliocene-Pleistocene carbonates decrease uniformly with alternating-field demagnetization, suggesting a magnetic component with moderate coercivity. The NRM magnetic intensity is weak and decreases progressively from 1–2 mA/m to 10^{-1} mA/m between 0 and about 13 mbsf. Below 13 mbsf, the intensity seems to remain fairly constant at about the 10^{-1} mA/m level. Intermittent archive-half analyses on the deeper sections (e.g., Core 133-812A-12X) indicate that rust contamination is still occurring, as strong intensity excursions were recorded at the top of several cores.

A total of 187 oriented discrete samples (7 cm^3) each, were collected from a composite of Holes 812A and 812C, from the 109-m-thick section. Based on the low intensities measured under shipboard time constraints, these samples will be analyzed in a field-free space at a shore-based laboratory. In addition, six 7-cm^3 soft sediment samples and four minicore plugs (2.54 cm diameter × 2.54 cm long) were collected for rock-magnetic analyses from Cores 133-812A-1H to -3H and the cemented limestones in Core 133-812A-5X. The rock-

Table 2. Preliminary determination of polarity reversal boundaries, Holes 812A and 812C.

Reversal boundary	Boundary age (Ma)	Cores 812A/812C	Sections 812A/812C	Depth (mbsf) 812A/812C
Brunhes/ Matuyama	0.73	2H/2H	6/4	13.0/12.1
Top of Jaramillo	0.92	3H/2H	1/6	15.2/15.0
Base of Jaramillo	0.97	3H/3H	2/1	16.6/17.1
Matuyama/ Olduvai	1.66	/3H	/5	/23.7

Note: Boundaries are derived from plots of inclination angles after 15-mT AF demagnetization step.

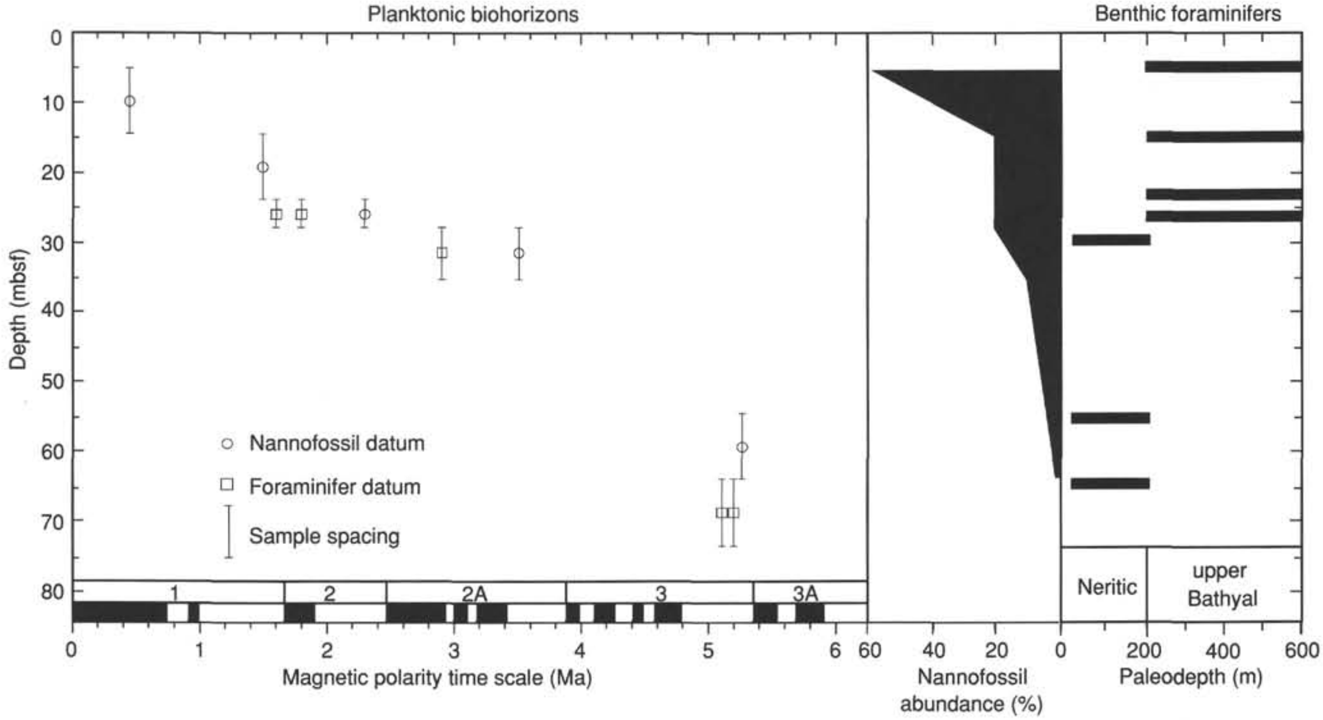

Figure 19. Age vs. depth plot for Hole 812A. All biohorizons are derived from calcareous nannofossils and planktonic foraminifers. Benthic foraminifer paleobathymetric estimates are from qualitative core-catcher picks.

magnetic work will consist of separation and identification of the magnetic minerals by transmission electron microscopy and coercivity spectral analysis to assess the nature of magnetization.

Whole-core volume susceptibility measurements were collected on the multisensor track (MST) for Holes 812A and 812C. The susceptibility record suggests that the concentration of ferrimagnetic minerals (mainly magnetite) is very small. In general the susceptibility is less than zero, indicating that mainly calcium carbonate and water are present in the cores. A few sharp but fairly weak susceptibility highs occur between 50 and 70 mbsf in Hole 812C, which are correlated with slight intensity peaks in NRM intensity. The origin of the positive susceptibility is unknown, but may be a result of contamination.

SEDIMENTATION RATES

Discussion of the sediment accumulation rate for Site 812 is restricted to Hole 812A, and principally to the upper 65 m, for which interval datable plankton microfossils were recovered. An age vs. depth plot for this site is given in Figure 19, using calcareous nannofossil and planktonic foraminifer biohorizons, with ages for the biohorizons taken from Berggren et al. (1985). Unfortunately, large sample spacing, poor recovery, and the subsidence history make interpretation of this interval difficult, and only the blandest generalizations can be made with any confidence. For the Pleistocene and latest Pliocene the sedimentation rate is just slightly more than 1 cm/k.y. based on calcareous nannofossils, with the highest rate in the latest Pleistocene. Planktonic foraminifers suggest a slightly greater sedimentation rate for this interval. In the middle part of the Pliocene, the sedimentation rate is reduced to about 0.5 cm/k.y. (and less if calculated with planktonic foraminifer biohorizons). For the earliest part of the Pliocene both calcareous nannofossils and planktonic foraminifers indicate an increase in sediment accumulation to about 1.5 cm/k.y. A middle Pliocene hiatus is a distinct possibility but cannot be resolved with the available sample spacing.

Nannofossil abundance in the sediment indicates predominantly pelagic sedimentation for the late Pleistocene, with pelagic influence diminishing in the early Pleistocene and late Pliocene, and further in the early Pliocene and latest Miocene. Benthic foraminifers indicate that the environment of deposition changed from an upper bathyal setting in the Pleistocene and late Pliocene to a neritic setting in the early Pliocene and late Miocene. Larger benthic foraminifers below this level indicate strong reefal influence.

INORGANIC GEOCHEMISTRY

Interstitial Waters

Calcium, Magnesium, and Strontium

Interstitial water samples were taken from Cores 133-812A-1H, -2H, -3H, -12H, and Cores 133-812C-1H, -2H, -3H, -5H, -6H, -7H, -8H, -9H, -10H, and -13H. Samples were squeezed and analyzed according to the methods outlined in the "Explanatory Notes" chapter (this volume).

Values for calcium show a small increase with depth from 10.54 mM in Core 133-812A-1H to 11.42 mM in Core 133-812C-13H (Table 3 and Fig. 20). Calcium is more or less constant from the sediment surface to a sub-bottom depth of 75 mbsf. From this depth there is a steady increase from 10.5 to 11.5 mM at 133 mbsf. Magnesium concentrations show a small decrease with increasing depth (53.4–52.4 mM). Therefore, magnesium and calcium concentrations are inversely correlated to some degree deeper in the hole. Strontium concentrations are nearly constant with depth at 100 μM, a value slightly higher than modern day seawater (~98 μM). An increase in strontium occurs between 20 and 25 m to a concentration of 110 μM. This is coincident with the point at

Table 3. Interstitial water data, Site 812.

Core, section, interval (cm)	Depth (mbsf)	pH	Alkalinity (mM)	Salinity (g/kg)	Calcium (mM)	Magnesium (mM)	Chloride (mM)	Phosphate (μM)	Silica (μM)	Strontium (μM)	Sulfate (mM)
Seawater	0.00	7.99	2.455	36.2	10.46	54.46	544.84	0.58	6	96	29.89
133-812A-											
1H-1, 145–150	1.45	7.72	3.176	35.8	10.54	52.70	540.01	0.70	55	110	29.62
2H-5, 145–150	12.35	7.42	3.212	35.8	10.43	53.13	544.81	1.12	70	114	29.32
3H-5, 145–150	21.85	7.28	3.189	35.8	10.34	54.24	555.38	0.58	76	118	30.74
12X-5, 145–150	91.05	7.27	3.107	35.8	10.99	52.41	545.77	0.85	60	112	30.02
133-812C-											
1H-3, 145–150	4.45	7.56	2.904	35.0	10.35	53.38	542.90		50	103	28.72
2H-5, 145–150	14.80	7.42	2.886	35.0	10.32	53.16	539.07		58	114	29.62
3H-5, 145–150	24.37	7.31	2.871	35.0	10.46	53.01	541.94		63	114	29.85
5H-5, 145–150	36.97	7.43	2.701	35.2	10.32	52.85	541.94		54	103	29.62
6H-5, 145–150	46.47	7.37	2.834	35.0	10.62	52.79	540.99		56	103	29.06
7H-5, 145–150	55.97	7.27	2.900	35.0	10.51	52.50	542.90		54	103	29.70
8H-5, 145–150	65.47	7.35	2.902	35.2	10.79	52.62	542.90		56	103	29.19
9H-5, 145–150	74.97	7.34	2.863	35.2	10.62	52.86	534.28		58	103	29.66
10H-5, 145–150	84.47	7.30	2.908	35.2	10.84	52.09	542.90		58	103	36.01
13H-5, 145–150	112.97	7.45	2.910	35.2	11.42	52.38	540.99		54	103	29.03

which aragonite disappears from the top sections of the core (Figs. 20 and 21).

Chloride

Chloride concentrations remain nearly constant with depth at ~540 mM, only slightly lower than modern seawater values (Table 3 and Fig. 20).

Alkalinity, Sulfate, pH, and Phosphate

Phosphate concentrations at Site 812 were below detectable limits. As a result, we did not analyze ammonia. The concentrations of alkalinity and sulfate remain nearly constant with depth, indicating negligible sulfate reduction and organic-matter diagenesis (Table 3 and Fig. 20). The lack of organic carbon remineralization in the sediments is evidenced by the low concentrations of organic carbon present (see "Organic Geochemistry" section, this chapter).

Silica

Silica concentrations were nearly constant at 55 μM throughout all of the samples (Table 3 and Fig. 20). Silica concentrations are low as a result of the small amount of biogenic silica and quartz in the sediments, as shown by X-ray diffraction and micropaleontological analysis.

Carbonate Content and X-ray Diffraction Data

Samples for X-ray diffraction (XRD) analyses were taken from IW squeeze cakes and physical properties samples (Table 4). X-ray analysis at Site 812 indicates that the sediments in the top 25 m are a mixture of calcite and aragonite. Aragonite concentrations relative to calcite reach values of ~50% near the top of the section and decrease with depth. Below 25 m, aragonite is absent. As discussed previously, the disappearance of aragonite coincides with an increase in pore-water strontium concentrations indicative of carbonate dissolution and remineralization. Quartz concentrations are nearly undetectable at Site 812, indicating low terrestrial inputs of sediment from the continent, most of which was probably trapped in the Queensland Trough to the west.

The main fluctuations in mineralogy are between calcite and dolomite. Calcite dominates the top 130 m and the lower 100 m of the cored sediments. Dolomite is most abundant between 130 and 275 m. The decrease in magnesium and the increase in calcium near this interval may be related to dolomite formation.

The stoichiometry of the dolomite in Sample 133-812A-21-1, 1–2 cm, was calculated using the equation of Lumsden and Chimahusky (1980):

$$N_{CaCO_3} = Md + B \quad (1)$$

where N_{CaCO_3} = the mol% of $CaCO_3$,

d = the D-spacing of the 104 crystal plane,

M and B = constants with values of 333.33 and −911.99, respectively.

D-spacings were calibrated to a sylvite (KCl) internal standard. The dolomite sample has a calculated formula of $Ca_{0.57}Mg_{0.43}CO_3$.

Carbonate values were measured on interstitial water and physical properties samples. Data in the dolomite layer was corrected for the difference in molecular weight between calcite and dolomite using the formula:

$$\frac{\text{measured \% carbon value}}{(\text{\%calcite} * 12) + (\text{\%dolomite} * 13)} \quad (2)$$

Percentages of calcite and dolomite were taken from X-ray data. Values for carbonate range from 95% to 99% increasing slightly with depth (Table 5 and Fig. 22). The insoluble fraction in these samples is probably a mixture of clays and quartz.

ORGANIC GEOCHEMISTRY

In addition to safety monitoring for hydrocarbons, the main purpose of the shipboard organic geochemistry studies at Site 812 was to assess the amount and type of organic matter preserved in the Pleistocene to middle Miocene sediments of the Queensland Plateau. We determined the total nitrogen, sulfur, carbon, and the organic carbon contents of nine additional samples collected for chromatographic analyses of the volatile hydrocarbons (headspace samples) using a NA 1500 Carlo Erba NCS analyzer. Detailed descriptions of methods are outlined in our "Explanatory Notes" chapter (this volume).

Volatile Hydrocarbons

Light hydrocarbon gases (C_1–C_3) in sediments were analyzed routinely as part of the safety and pollution-prevention

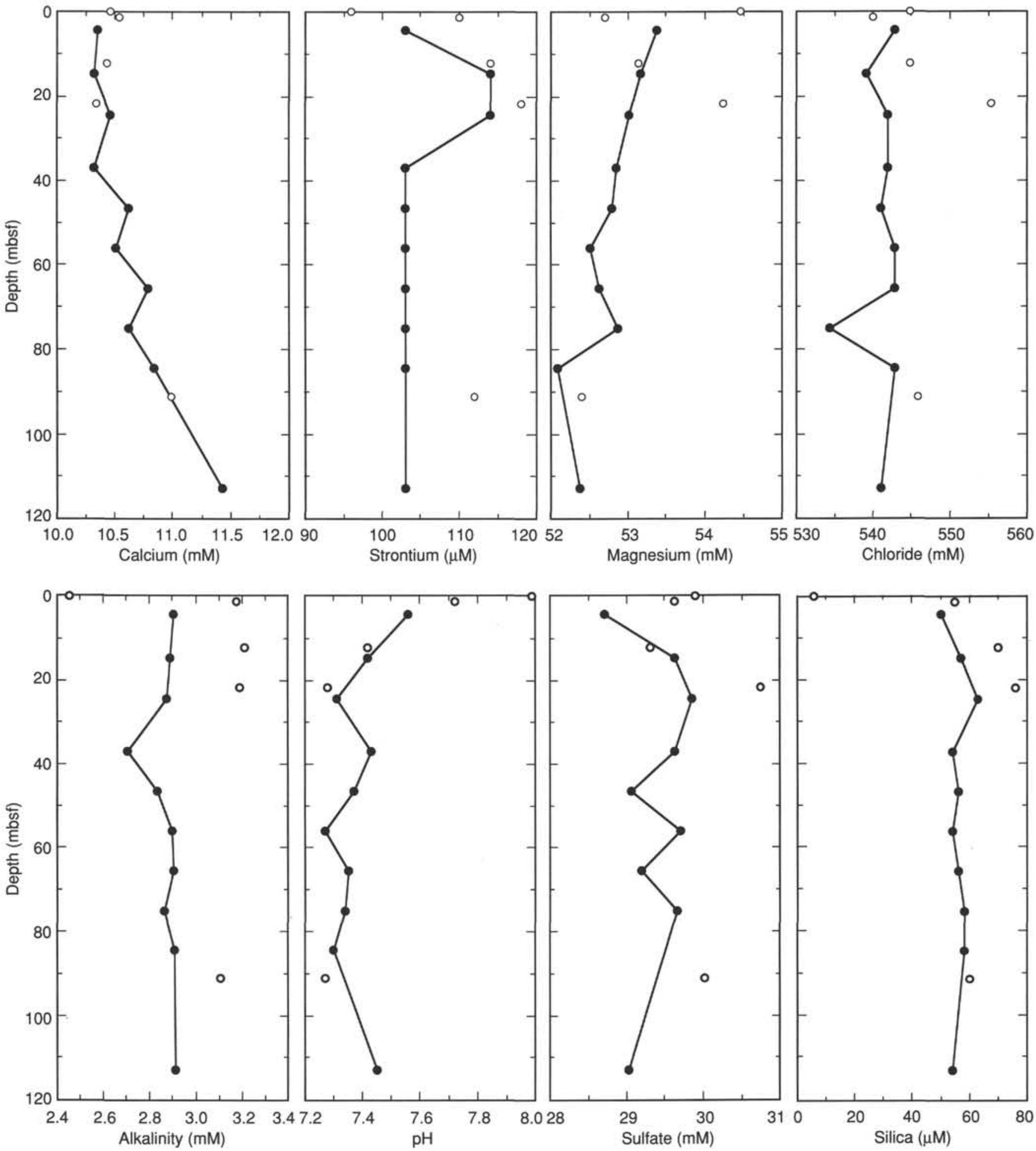

Figure 20. Composition of interstitial waters as a function of depth for Site 812. Open circles indicate data from Hole 812A. Closed circles indicate data from Hole 812C.

monitoring program, using the headspace technique and the Carle gas chromatograph. The results of 15 analyses from Holes 812A, 812B, and 812C are presented in Table 6. Sediments from Site 812 contained very low concentrations of hydrocarbon gases. Concentrations of methane in the headspace gas were ~2 ppm, whereas ethane and propane were not detected.

Organic Carbon Contents

The total organic carbon (TOC) contents recorded in Holes 812A, 812B, and 812C are presented in Table 7. We observed very low TOC values in the calcium-carbonate-rich or dolomite-rich sediments encountered at Site 812. These values averaged <0.15%, whereas total nitrogen and sulfur concen-

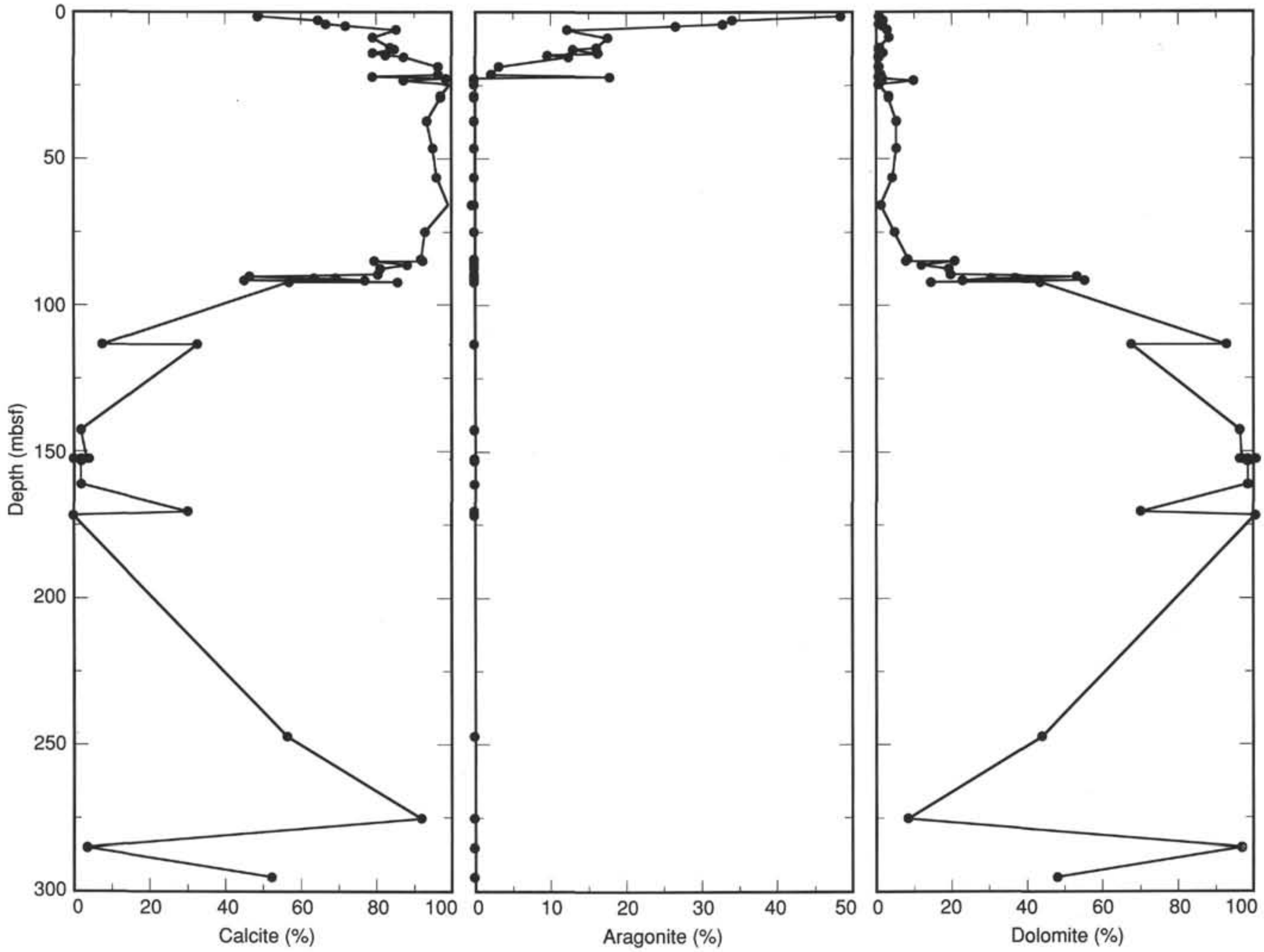

Figure 21. X-ray diffraction data (relative concentrations) as a function of depth for Site 812.

trations were below the detection limits of the NCS analyzer. As a consequence of the low organic contents, we were unable to conduct detailed geochemical characterization of kerogen types using the Rock-Eval pyrolysis method, as originally planned.

PHYSICAL PROPERTIES

Physical properties analyzed in cores from this site include bulk density, *P*-wave velocity, and magnetic susceptibility on unsplit cores and *P*-wave velocity, electrical resistivity formation factor, shear strength, and index properties (including bulk density, grain density, water content, porosity, and void ratio) on split cores. The methods used are described in detail in the "Explanatory Notes" chapter of this volume.

Bulk Density

Bulk densities for Site 812 were determined from volume and mass measurements on discrete core samples, from gamma-ray absorption on whole round cores, and from Schlumberger logging of Hole 812C (Table 8; Figs. 23, 24A, and 25). The data indicate intervals having high bulk density values centered on about 25, 105, 150, and 200 mbsf. The first three intervals correspond with lithologic changes. Unconformities were recognized at ~25 and 150 mbsf (see "Lithostratigraphy" section, this chapter).

P-Wave Velocity

P-wave velocities were measured on whole-round cores using the multisensor track (MST) and on discrete core samples using the Hamilton frame. Schlumberger sonic logs also provided velocity data (Table 9; Figs. 23, 24B, and 25). Intervals with velocity values were centered at 105, 150, and 200 mbsf. These intervals coincide approximately with the zones of high bulk density noted previously, although the high density interval at 25 mbsf does not seem to have a counterpart in the velocity profile.

Porosity

Porosity was one of the index properties determined from discrete core samples using the mass balance and the pycnometer. A graph of porosity vs. depth is shown in Figure 24C. Water content values derived from the same set of index property measurements, is plotted in Figure 24D. Water content plotted against porosity is depicted in Figure 26. Given high-precision measurements, one would expect a high degree of correlation between calculations of porosity and of

Table 4. X-ray diffraction data, Site 812.

Core, section, interval (cm)	Depth (mbsf)	Calcite (%)	Aragonite (%)	Quartz (%)	Dolomite (%)
133-812A-					
1H-1, 103–104	1.03	49.10	48.80	2.10	0.00
1H-2, 145–150	2.95	65.00	34.20	0.00	0.80
1H-3, 103–104	4.03	66.90	33.10	0.00	0.00
2H-1, 100–102	5.90	85.60	12.40	0.00	2.00
2H-3, 100–102	8.90	79.20	17.90	0.00	2.80
2H-5, 100–102	11.90	83.80	16.20	0.00	0.00
2H-5, 145–150	12.35	85.30	13.20	1.50	0.00
2H-7, 21–22	14.11	79.50	16.40	3.00	1.10
3H-1, 85–87	15.25	87.40	12.60	0.00	0.00
3H-3, 85–87	18.25	96.70	3.30	0.00	0.00
3H-5, 145–150	21.85	79.20	18.00	2.60	0.20
3H-5, 85–87	21.25	96.80	2.40	0.00	0.70
3H-6, 85–87	22.75	98.90	0.00	0.00	1.10
4H-1, 50–51	23.45	87.50	0.00	3.40	9.10
5X-1, 88–89	28.70	97.60	0.00	0.00	2.40
5X-1, 113–114	28.90	97.50	0.00	0.00	2.50
12X-1, 100–102	84.60	80.10	0.00	0.00	19.90
12X-1, 49–50	84.00	92.10	0.00	0.00	7.90
12X-2, 101–102	86.11	88.70	0.00	0.00	11.30
12X-3, 101–102	87.61	81.50	0.00	0.00	18.50
12X-4, 100–102	89.11	81.10	0.00	0.00	18.90
12X-5, 50–52	90.05	46.90	0.00	0.60	52.50
12X-5, 101–101	91.05	69.60	0.00	0.70	29.70
12X-5, 145–150	91.50	45.40	0.00	0.00	54.60
12X-5, 100–102	91.05	64.10	0.00	0.00	35.90
12X-6, 101–102	92.10	86.20	0.00	0.00	13.80
12X-6, 49–50	91.10	77.20	0.00	0.40	22.40
12X-6, 100–102	92.11	57.10	0.00	0.00	42.90
15X-1, 66–67	113.36	33.10	0.00	0.00	66.90
19X-1, 15–16	142.21	2.30	0.00	1.60	96.10
20X-1, 126–127	152.02	0.00	0.00	0.00	100.00
20X-1, 124–125	152.02	2.30	0.00	0.00	97.70
20X-1, 117–118	152.01	3.80	0.00	0.00	96.20
20X-1, 126–127	152.02	3.90	0.00	0.00	96.10
21X-1, 1–2	160.60	2.30	0.00	0.00	97.70
22X-1, 1–1	171.20	0.00	0.00	0.00	100.00
133-812B-					
3X-2, 48–49	153.00	2.00	0.00	0.00	98.00
5X-1, 10–11	170.30	30.60	0.00	0.00	69.40
13X-1, 33–34	246.73	56.50	0.00	0.00	43.50
16X-1, 1–2	275.02	92.30	0.00	0.00	7.70
17X-1, 1–2	284.70	3.70	0.00	0.00	96.30
18X-1, 1–2	294.40	52.50	0.00	0.00	47.50
133-812C-					
1H-3, 145–150	4.45	72.40	26.80	0.00	0.80
2H-5, 145–150	14.80	83.10	9.70	7.10	0.00
3H-5, 145–150	24.37	100.00	0.00	0.00	0.00
5H-5, 145–150	36.97	93.90	0.00	1.70	4.40
6H-5, 145–150	46.47	95.40	0.00	0.00	4.60
7H-5, 145–150	55.97	96.50	0.00	0.00	3.50
8H-5, 145–150	65.47	99.50	0.00	0.00	0.50
9H-5, 145–150	74.97	93.20	0.00	2.90	3.90
10H-5, 145–150	84.47	93.00	0.00	0.00	7.00
13H-5, 145–150	112.97	7.60	0.00	0.00	92.40

water content. The high scatter seen in Figure 26 may be a result of water loss before wet volume measurement and possibly to helium solution in pore water during the pycnometer volume measurement. A better correlation observed at later sites may be attributable to larger sample size and to conducting wet-sample measurements immediately after sampling the cores.

Electrical Resistivity Formation Factor

We measured the formation factor (FF) at three intervals in sections from Hole 812A (see Table 10 and Fig. 24E). The high permeability of the section recovered at Hole 812A permitted the rapid escape of pore water, so that we could not make reasonable resistivity measurements.

In addition to the FF experiments that are normally conducted on ODP cores, a special experiment was conducted to obtain an electrical core image of an interval from 74.9 to 99.0 cm in Section 133-812A-12X-6 (Fig. 27). Details of the method are given in the "Explanatory Notes" chapter (this volume). The variability in the display in Figure 27 has been optimized to suit the data range and the shipboard graphics facilities. Measurements are in terms of electrical resistance and have been converted into apparent resistivities and FFs:

Apparent resistivity = (geometrical factor)*(voltage/current) and
Formation factor = (app. resistivity)/(pore water resistivity).

The FF can be related to porosity by a number of relationships, of which Archie's law is probably the most suitable in unconsolidated sediments:

$$FF = (\text{porosity})m, \quad (3)$$

where m has been shown to be dependent on the particle shape, being 1.2 for spheres, 1.4 for rounded sands, 1.6 for platy sands, 1.8 for shell fragments, and 1.8–2.0 for deep-sea clays. More complex relationships are used in cemented oil-bearing formations where pore waters have low salinities and conductive clays may be present. The image from 74.4 to 99.0 cm in Section 133-812A-12X-3 indicates an FF range of 1.8–2.5, which is likely to represent a corresponding porosity range from 0.69 to 0.56, assuming a shape factor m of 1.6. There was no visual evidence in the core of any internal variability, but discussions suggested that this may be expected in response to changes in depositional environment such as may be caused by climatic fluctuations. The resistivity structure of the above core section suggests that there is fine-scale layering within the apparently uniform lithology that can only be detected by very high-resolution methods. The only downhole method capable of evaluating this during Leg 133 was the FMS.

Shear Strength

We obtained few shear strength measurements at this site because most of the material recovered in the cores was extremely sandy (Table 11 and Fig. 24F). Permeability was so high that pore water quickly drained from the split sections. Most of the cores were too friable to make meaningful measurements.

DOWNHOLE MEASUREMENTS

Log Reliability

Hole size is the most important control on accuracy of logs from Hole 812B. Three types of caliper logs were obtained: an apparent caliper calculated from the sonic log (see "Explanatory Notes" chapter, this volume), a two-axis caliper from the formation microscanner (FMS), and a one-axis caliper from the lithodensity tool. The caliper log obtained by the lithodensity tool shows broad swings in hole size, and even the minimum diameter of 12 in. (30 cm) is significantly larger than bit diameter of 9.9 in. (25 cm). In the intervals 68–128, 160–170, and 222–250 mbsf the hole size was larger than the 18-in. (46-cm) maximum opening of the caliper arm, resulting in inadequate pad contact of the lithodensity tool against the borehole wall. As a result, logs of density and photoelectric effect show swings to unreliably low values; the density compensation factor, which attempts to correct for inadequate pad contact, is applying corrections so large that the compensation is only approximate. Although the fully open caliper makes us dubious of the reliability of the density log in the

Table 5. Carbonate data, Site 812.

Core, section, interval (cm)	Depth (mbsf)	Sample	Carbon (%)	Calcium carbonate (%)	Corrected carbonate (%)
133-812A-					
1H-1, 103–105	1.03	PP	11.57	96.40	96.40
1H-2, 145–146	1.45	HS	11.57	96.42	96.42
1H-3, 103–105	4.03	PP	11.52	96.00	96.00
2H-1, 100–102	5.90	PP	11.41	95.00	95.00
2H-3, 100–102	8.90	PP	11.65	97.00	97.00
2H-5, 100–102	11.90	PP	11.65	97.00	97.00
2H-5, 145–146	12.35	HS	11.69	97.34	97.34
2H-7, 21–23	14.11	PP	11.53	96.00	96.00
3H-1, 85–87	15.25	PP	11.59	96.50	96.50
3H-3, 85–87	18.25	PP	11.68	97.30	97.30
3H-5, 85–87	21.25	HS	11.58	96.50	96.50
3H-5, 145–146	21.85	HS	11.68	97.25	97.25
3H-6, 85–87	22.75	PP	11.52	96.00	96.00
5X-1, 0–2	27.90	HS	12.00	99.96	94.56
12X-1, 100–111	84.60	PP	11.86	98.80	97.21
12X-2, 101–102	86.11	PP	11.94	99.50	98.60
12X-3, 101–102	87.61	PP	11.86	98.80	97.37
12X-4, 101–102	89.11	PP	11.89	99.00	97.54
12X-5, 101–102	90.61	PP	12.02	100.10	97.72
12X-5, 145–146	91.05	HS	12.06	100.46	96.10
12X-6, 101–102	92.11	PP	11.98	99.80	98.68
15X-1, 66–67	113.36	PP	12.29	102.75	97.00
16X-1, 19–20	122.49	HS	12.31	102.54	
133-812B-					
3R-1, 0–2	150.80	HS	12.63	105.20	
3R-1, 70–71	151.50	PP	11.51	95.90	
4R-1, 27–28	160.77	PP	12.70	105.80	
5R-1, 5–6	170.25	HS	12.69	105.70	
5R-1, 40–41	170.65	PP	12.73	106.00	
6R-1, 5–6	180.40	HS	12.75	106.20	
6R-1, 54–55	179.95	PP	12.80	106.60	
7R-1, 90–91	190.40	PP	12.71	105.90	
8R-1, 40–42	199.60	PP	12.81	106.70	
9R-1, 25–27	208.75	PP	12.82	106.80	
16R-1, 2–3	275.02	PP	11.99	99.54	
133-812C-					
5H-1, 101–104	30.51	PP	12.00	100.00	
5H-2, 101–104	32.01	PP	11.85	99.04	
5H-4, 101–104	35.01	PP	11.89	99.00	
5H-5, 67–70	36.17	PP	12.01	100.00	
5H-6, 101–104	38.01	PP	12.00	100.00	
6H-1, 102–105	40.02	PP	11.88	99.00	
6H-2, 102–105	41.52	PP	11.86	98.80	
6H-3, 102–105	43.02	PP	12.02	100.10	
6H-4, 102–105	44.52	PP	12.01	100.00	
6H-5, 96–99	45.96	PP	12.02	100.10	
6H-5, 149–150	46.49	HS	11.87	98.79	
6H-6, 98–101	47.48	PP	11.92	99.30	
7H-1, 102–106	49.52	PP	11.55	96.20	
7H-2, 103–106	51.03	PP	11.92	98.79	
7H-3, 103–106	52.53	PP	11.98	99.80	
7H-4, 100–103	54.00	PP	11.99	99.90	
7H-5, 93–96	55.43	PP	11.96	99.60	
7H-6, 101–104	57.01	PP	12.02	100.10	
8H-1, 105–107	59.05	PP	11.68	97.30	
8H-2, 105–107	60.55	PP	11.99	99.90	
8H-3, 105–107	62.05	PP	11.92	99.30	
8H-4, 105–107	63.55	PP	11.82	98.50	
8H-5, 105–107	65.05	PP	11.98	99.80	
8H-5, 149–150	65.49	HS	11.90	100.29	
8H-6, 105–107	66.55	PP	11.87	98.90	
8H-7, 42–45	67.42	PP	11.90	99.10	
9H-1, 92–94	68.42	PP	11.93	99.40	
9H-2, 92–94	69.92	PP	11.17	98.96	
9H-3, 92–94	71.42	PP	11.85	98.70	
9H-4, 92–94	72.92	PP	12.01	100.00	
9H-5, 92–94	74.42	PP	11.99	99.90	
9H-7, 92–94	76.92	PP	11.87	98.90	
10H-1, 101–103	78.01	PP	11.95	99.50	
10H-2, 101–103	79.51	PP	11.95	99.50	
10H-3, 101–103	81.01	PP	12.06	100.50	
10H-4, 101–103	82.51	PP	12.08	100.60	
10H-5, 101–103	84.01	PP	11.79	98.20	

Table 5 (continued).

Core, section, interval (cm)	Depth (mbsf)	Sample	Carbon (%)	Calcium carbonate (%)	Corrected carbonate (%)
10H-5, 149–150	84.49	HS	11.82	98.96	
10H-6, 101–103	85.51	PP	11.96	99.60	
11H-1, 103–106	87.53	PP	12.04	100.30	
11H-2, 103–106	89.03	PP	11.94	100.37	
11H-3, 103–106	90.53	PP	12.10	100.80	
11H-4, 103–106	92.03	PP	12.19	101.50	
11H-5, 103–106	93.53	PP	12.11	100.90	
11H-6, 103–106	95.03	PP	11.99	99.90	
13H-1, 102–104	106.52	PP	12.59	104.90	
13H-2, 121–123	108.21	PP	12.86	106.96	
13H-3, 102–104	109.52	PP	12.87	107.20	
13H-4, 102–104	111.02	PP	12.81	106.70	
13H-5, 36–38	111.86	PP	12.77	106.40	
13H-6, 36–38	113.36	PP	12.56	104.60	

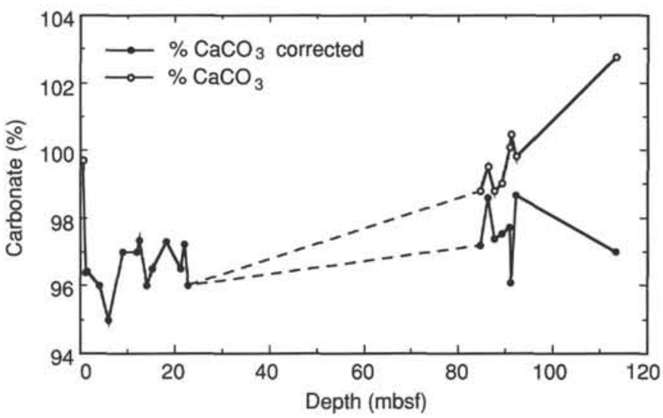

Figure 22. Carbonate and carbonate values corrected for differences in molecular weight between calcite and dolomite as a function of depth for Site 812.

Table 6. Volatile hydrocarbon data from headspace analysis, Site 812.

Core, section, interval (cm)	Depth (mbsf)	Sample	Volume (mL)	Gas chromato.	C_1 (ppm)
133-812A-1H-2, 145–146	2.95	HS	5	CARLE 132	2
812A-2H-5, 145–146	12.35	HS	5	CARLE 132	2
812A-3H-5, 145–146	21.85	HS	5	CARLE 132	2
812A-5X-1, 0–2	27.9	HS	5	CARLE 132	2
812C-6H-5, 149–150	46.49	HS	5	CARLE 132	2
812C-8H-5, 149–150	65.49	HS	5	CARLE 132	2
812C-10H-5, 149–150	84.49	HS	5	CARLE 132	2
812A-12X-5, 145–146	91.05	HS	5	CARLE 132	2
812C-12H-1, 0–1	96	HS	5	CARLE 132	2
812A-16X-1, 19–20	122.49	HS	5	CARLE 132	2
812B-3R-1, 0–2	150.8	HS	5	CARLE 132	2
812A-20X-1, 125–126	162.15	HS	5	CARLE 132	2
812B-5R-1, 5–6	170.25	HS	5	CARLE 132	2
812B-6R-1, 5–6	179.95	HS	5	CARLE 132	2
812A-22X-1, 34–35	180.54	HS	5	CARLE 132	2

Note: HS = headspace sample.

intervals 68–128 and 222–250 mbsf, interlog relationships discussed later suggest that the log may be accurate throughout almost all of both intervals.

Most other logs do not require pad contact and therefore are rather insensitive to the changes in borehole size. Two minor exceptions are the gamma ray and resistivity logs, which are likely to be changed slightly by post-cruise borehole correction. A major exception is the formation microscanner, which uses four measurement pads that open to only 15 in. (38

Table 7. Concentrations of organic carbon, inorganic carbon, and total carbon in sediments, Site 812.

Core, section, interval (cm)	Depth (mbsf)	Sample	Total organic carbon (%)	Total inorganic carbon (%)	Total carbon (%)
133-812A-1H-2, 145–146	2.95	HS	0.1	11.5	11.6
812A-2H-5, 145–146	12.35	HS	0.1	11.6	11.7
812A-3H-5, 145–146	21.85	HS	0.1	11.6	11.7
812A-5X-1, 0–2	27.9	HS	0.1	11.9	12
812C-6H-5, 149–150	46.49	HS	0	11.9	11.9
812C-7H-2, 103–106	51.03	PP	0	11.9	11.9
812A-12X-5, 145–146	91.05	HS	0.1	12	12.1
812C-13H-2, 121–123	108.21	PP	0	12.8	12.8
812B-6R-1, 2–3	179.95	HS	0	12	12

Note: HS = headspace sample and PP = physical properties sample.

cm). We ran this tool throughout the open-hole interval, anticipating that the 1° hole deviation would cause two pads to maintain pad contact; this anticipation was correct.

As is often the case with ODP holes, the initial sonic logs from Hole 812B exhibited several zones in which cycle skipping caused unreliable swings in apparent velocity. Reprocessing (see "Explanatory Notes" chapter, this volume) removed virtually all unreliable data. Only in the interval 211–220 mbsf are residual problems likely (Fig. 28).

The spectral gamma-ray tool is the only tool in the seismic stratigraphic combination that can provide useful formation data even through pipe. At Hole 812B through-pipe spectral gamma-ray logs were obtained for the interval 12.0–68.7 mbsf, but all values for uranium, thorium, and potassium are either at or below the resolving power of the tool. For the open-hole interval (67.8–137.0 mbsf), replicate spectral gamma-ray logs show modest agreement for uranium and almost no agreement for both potassium and thorium. The latter two elements are present in such low quantities at Hole 812B that their logs fluctuate about zero, and the total gamma log is almost entirely attributable to uranium.

Velocity, Resistivity, and Density

Velocity, resistivity, and density are strongly correlated throughout the logged interval at Hole 812B (Fig. 28). Because lithologic changes here are minor and confined to variations in relative proportions of the geophysically rather similar minerals dolomite and calcite, log responses are controlled almost entirely by porosity. The increases in velocity and density with depth do not follow a simple compaction profile, suggesting that diagenesis and grain-size fluctuations affect porosity much more than does mechanical compaction. Both velocity and density increase more rapidly with depth than is commonly observed in pelagic carbonates (Hamilton, 1976, 1979); comparable data for near-reef carbonates are rare.

The reprocessed sonic log has been converted to an integrated traveltime log (Fig. 29), to facilitate depth-to-time conversion for comparison of Hole 812B data with seismic facies. For the unlogged interval between the seafloor and 68.7 mbsf, we used two simplified models: the empirical traveltime/depth relation of Hamilton (1979) for calcareous sediments, and a simple linear interpolation between water velocity at the seafloor and the first log value at 68.7 mbsf. We consider the latter to be more appropriate, but display of both results in Figure 29 illustrates the subtle difference of only 4 ms associated with uncertainties of velocities in the top 68.7 mbsf. For the short interval 281.1–295.8 mbsf at the bottom of the hole, resistivity logs but not sonic logs are available, because the resistivity tool is much lower on the tool string. A pseudosonic log was generated and used in Figure 29 for this interval, based on regression of sonic transit time on logarithm of

Table 8. Index property data, Site 812.

Core, section, interval (cm)	Depth (mbsf)	Bulk density (g/cm^3)	Grain density (g/cm^3)	Porosity (%)	Water content (%)	Void ratio
133-812A-						
1H-1, 103–104	1.03	1.56	2.69	61.7	67.8	1.61
1H-3, 100–103	4.00	1.82	2.75	68.9	63.4	2.22
2H-1, 100–103	5.90	1.81	2.62	71.3	67.6	2.49
2H-3, 100–103	8.90	1.78	2.80	65.1	60.1	1.87
2H-5, 100–103	11.90	1.87	2.88	65.5	55.9	1.90
2H-7, 21–24	14.11	1.83	2.76	67.5	60.8	2.08
3H-1, 101–104	15.41	1.79	2.82	65.2	59.7	1.87
3H-3, 101–104	18.41	1.96	2.77	67.3	54.2	2.06
3H-5, 101–104	21.41	1.83	2.83	66.2	58.8	1.96
3H-6, 101–104	22.91	1.97	2.80	68.0	54.6	2.13
5X-1, 88–90	28.78	2.11	2.82	64.2	45.2	1.79
5X-1, 113–115	29.03	2.10	2.79	56.3	37.8	1.29
12X-1, 101–103	84.61	1.98	2.75	59.9	44.8	1.49
12X-2, 101–103	86.11	2.00	2.70	61.9	46.3	1.62
12X-3, 101–103	87.61	1.98	2.86	60.1	45.3	1.51
12X-4, 101–103	89.11	1.88	2.78	65.2	55.2	1.88
12X-5, 101–103	90.61	2.07	2.85	52.8	35.3	1.12
12X-6, 101–103	92.11	2.06	2.76	61.1	43.7	1.57
15X-1, 66–67	113.36	2.26	2.70	47.0	27.0	0.89
20X-1, 117–118	162.07	2.24	2.77	63.1	40.4	1.71
133-812C-						
3H-1, 101–104	17.91	1.74	2.88	63.3	59.4	1.72
3H-2, 101–104	19.41	1.97	2.51	68.2	54.8	2.15
3H-3, 101–104	20.91	1.91	2.72	66.2	55.0	1.96
3H-4, 101–104	22.41	1.72	2.68	55.7	49.7	1.26
3H-5, 101–104	23.91	1.79	2.61	58.4	50.2	1.40
5H-2, 101–104	32.01	1.82	2.65	61.5	52.9	1.60
5H-3, 101–104	33.51	1.83	2.62	57.0	47.0	1.33
5H-4, 101–104	35.01	1.73	2.43	61.0	56.4	1.56
5H-5, 67–70	36.17	1.76	2.72	61.6	56.1	1.60
5H-6, 101–104	38.01	1.77	2.66	63.0	57.4	1.70
6H-1, 101–104	40.01	1.72	2.86	62.6	59.5	1.67
6H-2, 102–105	41.52	1.70	2.48	62.5	60.5	1.67
6H-3, 102–105	43.02	1.78	2.48	58.5	50.6	1.41
6H-4, 102–105	44.52	1.83	2.44	60.3	51.1	1.52
6H-5, 96–99	45.96	1.88	2.71	56.3	44.4	1.29
6H-6, 98–101	47.48	1.70	2.47	59.8	56.3	1.49
7H-1, 102–106	49.52	1.71	2.71	63.6	61.4	1.75
7H-2, 103–106	51.03	1.77	2.66	63.7	58.7	1.76
7H-3, 103–106	52.53	1.77	2.50	58.7	51.7	1.42
7H-4, 100–103	54.00	1.70	2.48	62.3	60.2	1.65
7H-5, 93–96	55.43	1.73	2.72	61.3	56.9	1.58
7H-6, 101–104	57.01	1.80	2.65	58.0	49.3	1.38
8H-1, 101–104	59.01	1.75	2.63	59.2	52.9	1.45
8H-2, 101–104	60.51	1.68	2.49	63.2	62.7	1.72
8H-3, 104–107	62.04	1.78	2.71	58.4	50.9	1.41
8H-4, 104–107	63.54	1.82	2.69	59.1	49.7	1.44
8H-5, 104–107	65.04	1.86	2.64	54.8	43.2	1.21
8H-6, 104–107	66.54	1.79	2.51	57.6	49.2	1.36
8H-7, 51–54	67.51	1.83	2.74	57.5	47.6	1.35
9H-1, 91–94	68.41	1.77	2.65	62.5	56.7	1.67
9H-2, 91–94	69.91	1.79	2.56	58.1	49.7	1.38
9H-3, 91–94	71.41	1.80	2.44	58.3	49.8	1.40
9H-4, 91–94	72.91	1.93	2.74	50.4	36.4	1.02
9H-5, 91–94	74.41	1.86	2.69	56.2	44.6	1.28
9H-7, 41–44	76.91	1.86	2.61	52.7	40.8	1.12
10H-1, 101–104	78.01	1.73	2.51	60.1	55.1	1.51
10H-2, 101–104	79.51	1.71	2.70	62.0	59.4	1.64
10H-3, 101–104	81.01	1.76	2.66	59.8	53.6	1.49
10H-4, 101–104	82.51	1.80	2.72	60.6	52.5	1.54
10H-5, 101–104	84.01	1.58	2.48	49.1	46.5	0.97
10H-6, 101–104	85.51	1.67	2.39	63.6	63.7	1.75
11H-1, 103–106	87.53	1.76	2.52	60.3	54.2	1.52
11H-2, 103–106	89.03	1.80	2.73	56.5	47.5	1.30
11H-3, 103–106	90.53	1.75	2.67	59.6	53.4	1.48
11H-4, 103–106	92.03	1.82	2.64	59.6	50.5	1.47
11H-5, 103–106	93.53	1.73	2.35	59.8	55.1	1.49
11H-6, 103–106	95.03	1.66	2.47	64.8	66.9	1.84
12H-1, 101–104	97.01	1.77	2.71	59.3	52.3	1.46
12H-2, 101–104	98.51	1.77	2.63	57.6	49.9	1.36
12H-3, 101–104	100.01	1.84	2.57	55.2	44.2	1.23
12H-4, 101–104	101.51	1.88	2.65	56.9	45.0	1.32
12H-5, 101–104	103.01	1.84	2.74	56.0	45.2	1.27
12H-6, 101–104	104.51	1.90	2.70	52.6	39.6	1.11
13H-1, 102–105	106.52	1.99	2.76	53.9	38.3	1.17
13H-2, 121–124	108.21	1.95	2.84	51.4	36.9	1.06
13H-3, 102–104	109.52	1.95	2.75	51.6	37.3	1.07
13H-4, 102–104	111.02	1.94	2.65	51.8	37.8	1.08
13H-5, 36–38	111.86	2.03	2.84	51.4	35.0	1.06
13H-6, 36–38	113.36	1.98	2.78	53.3	38.1	1.14

Table 9. Compressional-wave velocity data, Site 812.

Core, section, interval (cm)	Depth (mbsf)	Distance (mm)	Traveltime (μs)	Velocity (m/s)
133-812A-				
1H-1, 100–103	1.00	25.80	19.51	1484
1H-3, 100–103	4.00	25.61	18.11	1611
2H-1, 100–103	5.90	26.79	19.07	1589
2H-3, 100–103	8.90	27.06	18.88	1626
2H-5, 100–103	11.90	26.79	18.45	1654
2H-7, 21–24	14.11	26.23	18.34	1628
3H-1, 101–104	15.41	27.28	18.73	1656
3H-3, 101–104	18.41	27.55	19.05	1639
3H-5, 101–104	21.41	28.58	19.34	1675
3H-6, 101–104	22.91	27.54	18.69	1677
5X-1, 44–50	28.34	64.95	20.53	3697
5X-1, 44–50	28.34	29.13	8.51	4787
12X-1, 100–103	84.60	27.80	18.80	1682
12X-3, 100–103	87.60	28.80	19.90	1632
12X-5, 100–103	90.60	28.20	18.80	1708
15X-1, 66–67	113.36	29.90	19.80	1709
20X-1, 88–90	161.78	27.86	16.20	2018
133-812C-				
3H-1, 10.1–10.4	17.00	27.54	19.16	1673
3H-2, 101–104	19.41	27.05	18.69	1692
3H-3, 101–104	20.91	26.58	18.52	1679
3H-4, 101–104	22.41	27.83	21.68	1453
3H-5, 101–104	23.91	26.50	18.69	1655
3H-6, 101–104	25.41	26.79	18.86	1656
5H-1, 101–104	30.51	28.37	19.65	1674
5H-2, 101–104	32.01	28.36	21.89	1466
5H-3, 101–104	33.51	28.37	21.46	1503
5H-4, 101–104	35.01	29.17	20.14	1673
5H-5, 67–70	36.17	27.26	19.09	1662
5H-6, 101–104	38.01	27.85	19.21	1688
6H-1, 101–104	40.01	27.86	21.73	1451
6H-2, 102–105	41.52	28.67	20.29	1628
6H-3, 102–105	43.02	27.19	21.65	1420
6H-4, 102–105	44.52	28.20	19.45	1684
6H-5, 96–99	45.96	28.33	19.61	1676
6H-6, 98–101	47.48	27.58	19.54	1635
7H-1, 102–105	49.52	28.58	19.69	1683
7H-2, 103–106	51.03	28.85	19.82	1687
7H-3, 103–106	52.53	28.11	19.87	1635
7H-4, 100–103	54.00	28.64	20.00	1655
7H-5, 93–96	55.43	29.33	20.03	1695
7H-6, 101–104	57.01	28.51	22.14	1454
8H-1, 104–107	59.04	28.15	19.54	1672
8H-2, 104–107	60.54	28.36	22.05	1453
8H-3, 104–107	62.04	27.71	21.74	1442
8H-4, 104–107	63.54	28.86	22.49	1446
8H-5, 104–107	65.04	28.19	19.40	1689
8H-6, 104–107	66.54	27.58	21.15	1484
8H-7, 51–54	67.51	28.76	19.80	1683
9H-1, 91–94	68.41	27.67	20.81	1519
9H-2, 91–94	69.91	27.83	19.47	1659
9H-3, 91–94	71.41	28.15	21.39	1496
9H-4, 91–94	72.91	27.07	21.40	1433
9H-5, 91–94	74.41	28.54	19.86	1663
9H-7, 51–54	77.01	28.28	21.45	1498
11H-1, 103–106	87.53	27.89	19.76	1632
11H-2, 103–106	89.03	28.50	21.96	1468
11H-3, 103–106	90.53	28.54	19.79	1670
12H-1, 101–104	97.01	27.76	19.36	1666
12H-2, 101–104	98.51	28.94	20.02	1671
12H-3, 101–104	100.01	27.92	19.58	1653
12H-4, 101–104	101.51	27.88	21.70	1455
12H-5, 101–104	103.01	28.76	19.39	1727
12H-6, 101–104	104.51	27.95	19.36	1678
12H-7, 21–24	105.21	28.54	20.54	1596

shallow resistivity for the overlying interval 228.4–281.0 mbsf ($R = -0.38$).

The resistivity logs shown in Figure 28 define three log-based units:

1. Log Unit I, above 140 mbsf, has resistivity values of 0.6–0.8 ohm-m with only slight variability.

2. Log Unit II, between 140 and 222 mbsf, has a resistivity that varies rapidly, indicating alternating layers of high and low porosity. This is consistent with the heterogeneity identified for Subunit IIIA from the core analysis (see "Lithostratigraphy" section, this chapter), though the limited core recovery does not allow matching of individual beds between core and log.

3. Log Unit III, from 222 mbsf to the end of the logging run at 280 mbsf, has log values and character that are similar to Log Unit I.

A more detailed investigation of the data can be made when viewed at a more suitable scale as shown in Figure 30, where the shallowest penetrating sonde (spherically focused log, or SFL) can be seen to have the highest resolution but generally lower values than the medium and deep Phasor Induction resistivity sondes, which have greater depths of investigation. The differences between the three resistivity log types are attributable to the different responses of the three sondes. This effect is accentuated by the large hole diameter.

The general relative position of the three logs can be seen in Figures 28 and 30, where the deep induction provides the highest resistivities and the SFL the lowest, with the medium induction log providing intermediate values. Given that the formation water is of similar resistivity to seawater, this situation suggests resistivity that increases with distance away from the borehole sondes because of the large diameter of the borehole. Thus, we are in the position that the deepest penetrating devices will provide the most reliable data when the beds are thick, but all values are likely to be degraded in the presence of thin beds.

The situation in Log Unit II appears to fit the case above, where a large number of thin beds of high resistivity alternate with lower porosity zones. These lower resistivity zones coincide with lower velocities and larger hole diameters, suggesting weaker unlithified material that has been preferentially removed during the drilling process. It is likely that these beds are very thin and that the sondes do not have the resolving power to delineate them accurately; for example, in Figure 30 the "wavelength" of the anomalies can be seen to be no smaller than 2 m (SFL). The deeper penetrating devices exhibit proportionately less resolution.

The FMS has the highest resolution of any resistivity device currently available and is able to delineate these thin beds to a precision of 2–5 mm. This device has a penetration of 5–10 mm which is enough to provide reliable geological information concerning structure in addition to qualitative changes in borehole-wall resistivity.

Further interpretation of the resistivity is shown in Figure 31, where the electrical FF has been plotted using the deep induction log and pore-water resistivities that decrease from 0.25 ohm-m (11.4°C) at the seafloor to 0.20 ohm-m (20°C) at 300 mbsf. Porosity values derived from the density log have been used to calculate m in Equation 3 (above; Archie, 1942), which is probably the most applicable in the unlithified portion of the sediment column. The value of m has been shown to be controlled by particle shape for unconsolidated marine sands and clays, the pore spaces being in turn dependent on the grain shapes. Thus, m may be a useful indicator of changes in lithology where such changes are accompanied by a change in grain morphology. Some of the density values have been degraded by the large hole size, as this sonde requires contact with the borehole wall for accurate measurements. The values of m tend to accentuate these situations, providing an indicator of exactly which portions of the density log are unreliable. Based on the log of m, there appears to be a major change in

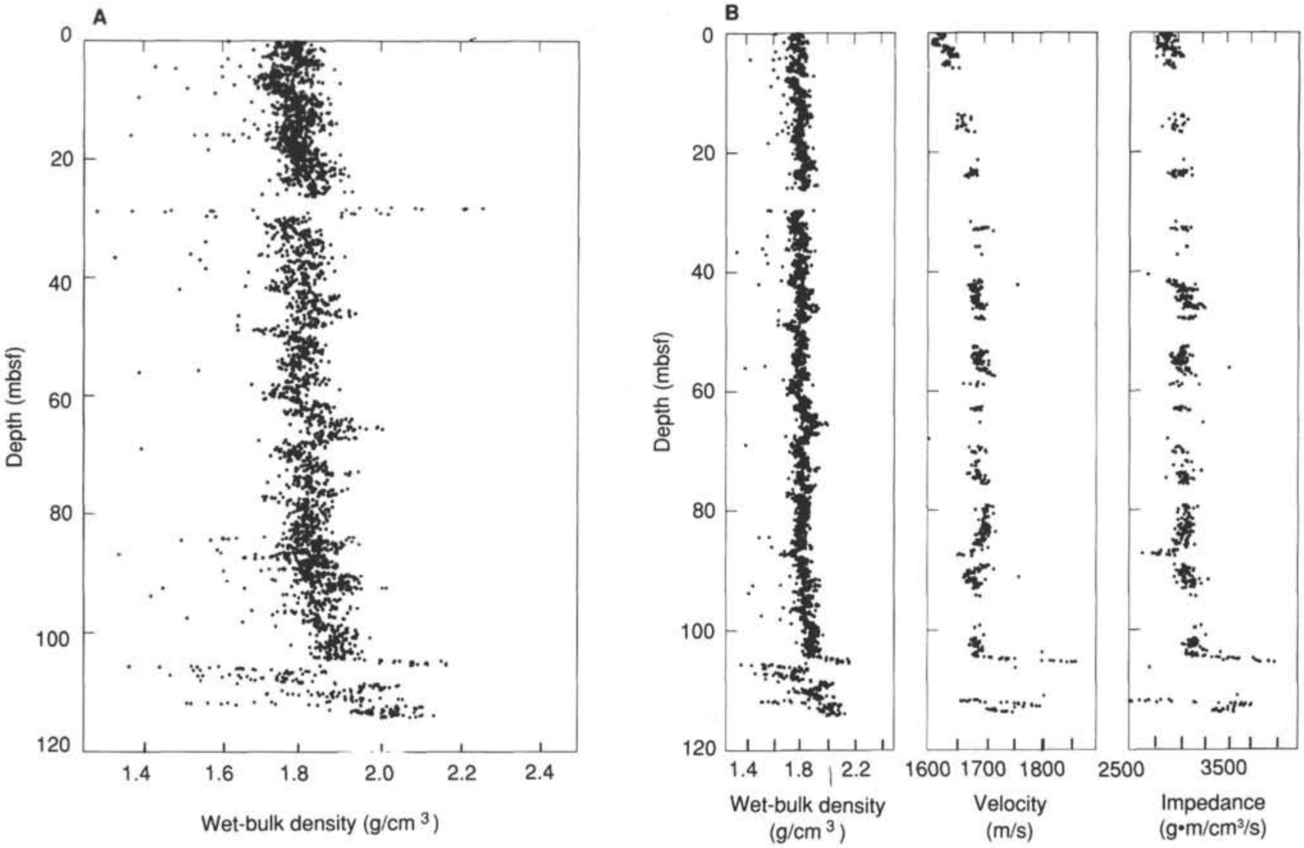

Figure 23. **A.** Unfiltered GRAPE bulk density measurements for Holes 812A (+) and 812C (•); because of the varying rate of motion of the core through the GRAPE system, there are often multiple measurements at the same position in the core. **B.** MST derived wet-bulk density, velocity, and calculated impedance from Hole 812C. All data points displayed are averages of all data in 5-cm blocks along the core.

pore/particle shape at 198 mbsf, within the second resistivity log unit identified above.

Log-based Units

Lithologic Subunits I and IIA (see "Lithostratigraphy" section, this chapter) were logged through the pipe with the spectral gamma-ray tool. A pipe attenuation with a factor of ~3, when combined with the already low proportions of uranium, potassium, and thorium, resulted in near-zero log responses for these three elements. We found no evidence of the 28-mbsf packstone layer on the uranium log, though this horizon should have been evident on through-pipe logs if it had uranium enrichment similar to the many hard layers of Subunit IIIA.

Lithologic Subunits IIB, IIC, and IID (~64–142 mbsf) are seen on logs to be uniform high-porosity ooze. The logs do not distinguish between the three subunits, although IIB is composed of outer-shelf micritic turbidites whereas IIC and IID are composed of inner-shelf floatstone and packstone (see "Lithostratigraphy" section, this chapter). Nor do the logs show any evidence of the zone of decreased lithification seen at 93–120 mbsf in the cores (see "Lithostratigraphy" section, this chapter); indeed, this interval includes a higher-lithification bed evident at 106–111 mbsf on both resistivity and velocity logs (Fig. 28). As resistivity and velocity are extremely sensitive to lithification, the apparent lithification decrease in the cores may be an artifact of XCB coring. The 106 mbsf top of the high-lithification bed probably corresponds to the Subunit IIB/IIC boundary, which was identified at 103 mbsf, based on the poor core recovery.

Lithologic Subunit IIIA, at about 142–220 mbsf in the cores (see "Lithostratigraphy" section, this chapter), is clearly defined by logs as 140–222 mbsf (Fig. 28). This unit is much higher in resistivity, velocity, and density than overlying and underlying units, implying much lower porosity. As even the overlying and underlying units are lower than typical pelagic carbonates in porosity, Subunit IIIA porosities imply substantial diagenetic cementation. This cementation must be quite variable with depth, as seen by the highly variable velocities, resistivities, and densities (Fig. 28).

Based on log responses, Subunit IIIA can be subdivided into three further subunits. The top interval, 140–156 mbsf, consists of very thin-bedded alternating porous and massive beds; as discussed in the previous section, these beds are below the resolving power of conventional logging tools but are well-delineated by the high-resolution formation microscanner. This top interval appears to be composed of two or three "upward coarsening" packets, but this term is less appropriate for the observed diagenetic porosity variations than for primary sedimentary porosity variations. The middle interval, 156–198 mbsf, is composed of four very similar packets whose origin is not known from the low core recovery. Each packet is about 10 m thick and is characterized by a baseline shift upward in porosity from the underlying packet; the pattern is most obvious on resistivity logs (Fig. 28). The bottom 50%–80% of each packet is fairly constant and has high porosity values, whereas the overlying portion has one or two thin beds of substantially lower porosity. The bottom interval, 198–222 mbsf, is very similar to the top interval, with alternation of porous and more cemented thin

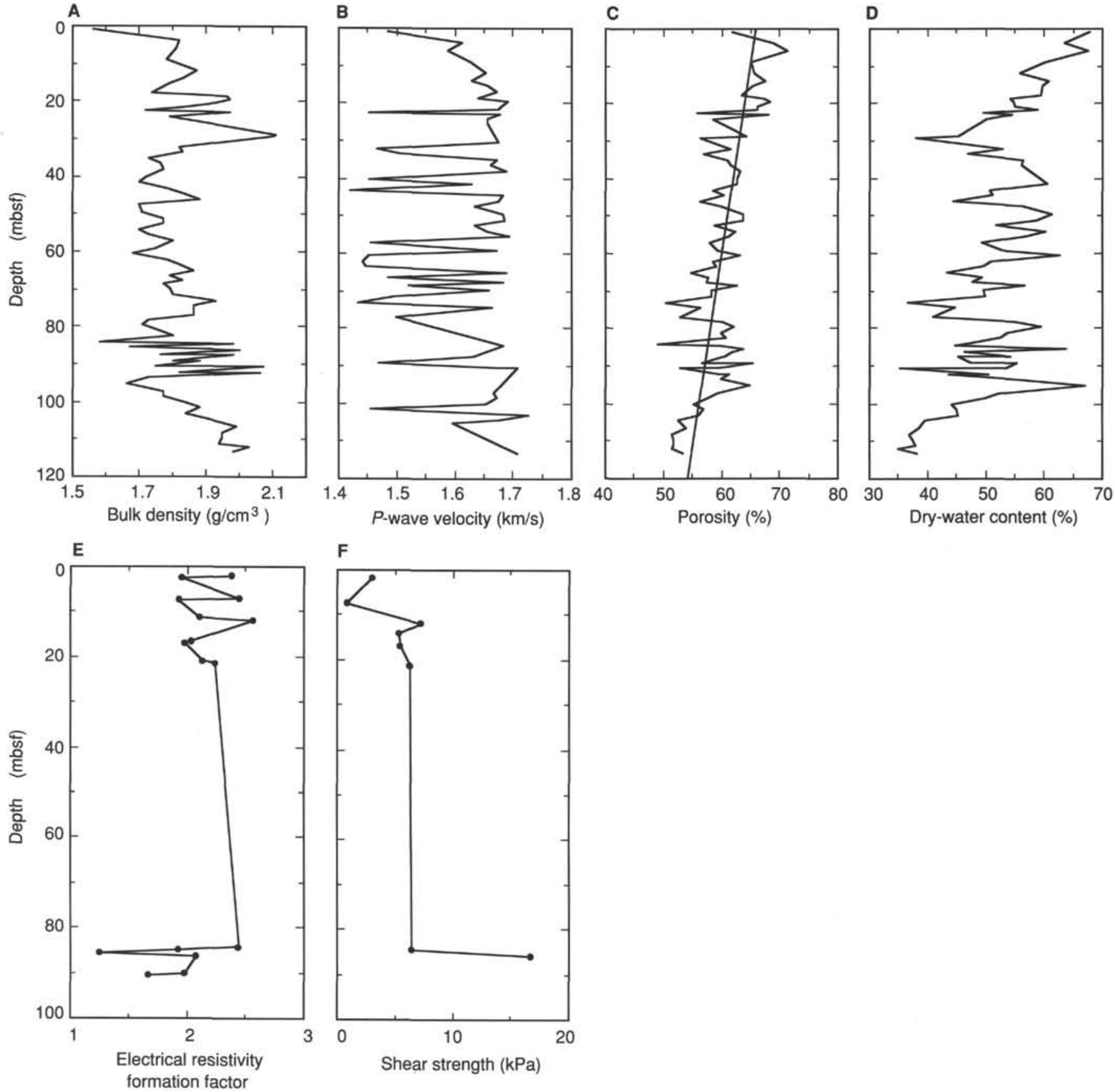

Figure 24. Physical properties data plotted vs. depth, Site 812. **A.** Wet-bulk density derived from mass and volume measurements on discrete core samples (pycnometer determinations). **B.** *P*-wave velocity; data from Holes 812A and 812C plotted together. Data derived from Hamilton Frame measurements for discrete core samples. Values < 1.5 km/s probably result from rapid draining of permeable sands. **C.** Porosity; data from Holes 812A and 812C plotted together. Data derived from mass and pycnometer volume measurements on discrete samples from cores. A linear regression was calculated for the porosity-depth function yielding: porosity = 65.843−0.097463 × depth, with a regression coefficient of 0.427. **D.** Dry-water content, which is water mass/dry sediment mass. Data from Holes 812A and 812C plotted together. Data derived from mass measurements on discrete samples from cores before and after drying. **E.** Electrical resistivity formation factor. **F.** Shear strength.

beds. In both the bottom and top intervals, strong uranium enrichment is evident in the more cemented beds.

The top boundary of the upper interval of Subunit IIIA is a solution unconformity, separating shallow lagoon sediments with freshwater moldic porosity from overlying inner-shelf sediments (see "Lithostratigraphy" section, this chapter). Shipboard formation microscanner images reveal the moldic porosity of the more resistive (lower porosity) parts of this interval. However, the grey-level scaling is not appropriate for imaging the contact at 140 mbsf because the overlying and underlying beds have fairly high porosity levels (Fig. 28).

In contrast, the bottom interval, which the logs suggest to be generally similar to the top interval, is capped by a very resistive thick bed. An expanded-scale plot of the top of this interval (Fig. 32) shows that porosity steadily increases upward over a 3-m interval, then drops suddenly at the contact to middle-interval values. Uranium and thorium mimic almost exactly the porosity pattern of the density and resistivity logs.

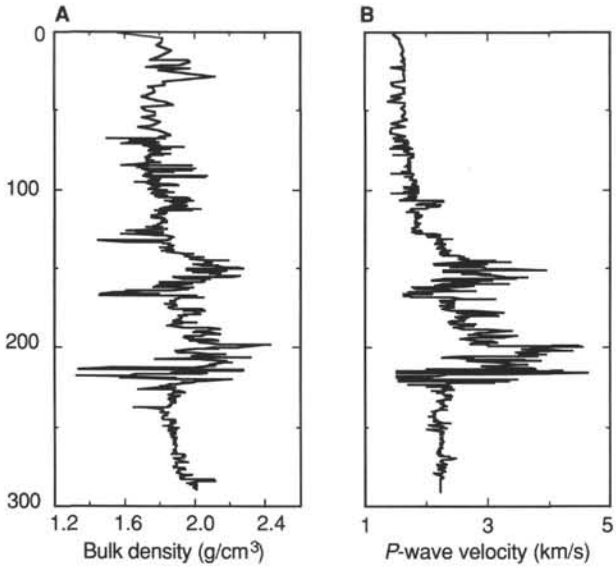

Figure 25. **A.** Wet-bulk density vs. depth for Site 812; the data from pycnometer measurements (Fig. 25) are plotted along with data from the Schlumberger logging (see "Downhole Measurements" section, this chapter) to form a continuous log for the site. Logging data extend from 68 to 290 m, and pycnometer data extend from 1 to 113 m. **B.** *P*-wave velocity for Site 812; data for depth range 1–162 mbsf derived from Hamilton Frame measurements of discrete core samples (see Fig. 25); data for depth range 67–290 mbsf derived from the Schlumberger sonic log.

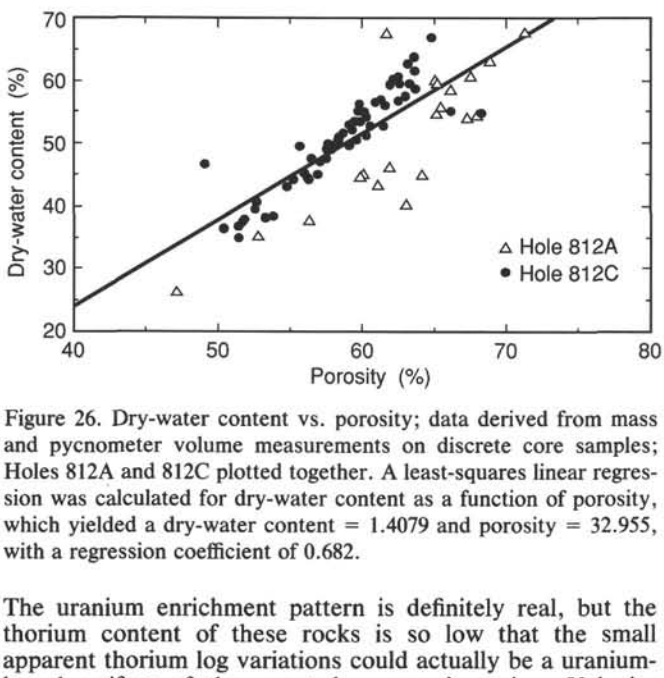

Figure 26. Dry-water content vs. porosity; data derived from mass and pycnometer volume measurements on discrete core samples; Holes 812A and 812C plotted together. A least-squares linear regression was calculated for dry-water content as a function of porosity, which yielded a dry-water content = 1.4079 and porosity = 32.955, with a regression coefficient of 0.682.

The uranium enrichment pattern is definitely real, but the thorium content of these rocks is so low that the small apparent thorium log variations could actually be a uranium-based artifact of the spectral gamma inversion. Velocity exhibits almost the same porosity-dependent pattern as density and resistivity, except for a peak at 200.7 mbsf that is confirmed to be real by examination of raw traveltimes.

The FMS provides a high-resolution picture of this 197.6 mbsf contact (Fig. 32) that strongly suggests an origin similar to the 140-mbsf unconformity recognized in the cores. The contact is sharp and separates highly conductive (shown as black on Fig. 32) sediments above from highly resistive (white) sediments below. This resistive interval has vugular

Table 10. Formation factor data, Hole 812A.

Core, section, interval (cm)	Depth (mbsf)	Seawater (ohms)	Sample (ohms)	Formation factor
133-812A-				
1H-2, 50	2.00	3.9	9.3	2.38
1H-2, 100	2.50	3.9	7.6	1.95
2H-2, 50	6.90	3.9	9.5	2.44
2H-2, 100	7.40	4.1	7.9	1.93
2H-5, 50	11.40	4.1	8.6	2.10
2H-5, 100	11.90	3.7	9.5	2.57
3H-2, 50	16.40	4.0	8.1	2.03
3H-2, 100	16.90	4.0	7.9	1.98
3H-5, 50	20.90	3.8	8.1	2.13
3H-5, 100	21.40	3.8	8.5	2.24
12X-1, 64	84.24	4.1	10.0	2.44
12X-1, 120	84.80	4.3	8.3	1.93
12X-2, 50	85.60	5.5	6.8	1.24
12X-2, 100	86.10	3.6	7.5	2.08
12X-5, 50	90.10	4.7	9.3	1.98
12X-5, 100	90.60	4.7	7.8	1.66

porosity with voids up to 10 cm in size in the top 2 m that gradually increase in abundance while decreasing in size with greater depth. The simplest explanation of this pattern is that the lower interval was exposed and underwent extensive subaerial(?) diagenetic solution, recrystallization, and cementation, followed by the dissolution that created its vugular porosity. Subsequent submergence allowed resumption of lagoonal sedimentation; the resulting sediments are much higher in porosity and less recrystallized than underlying sediments. This exposure and submergence might have been caused by changes in eustatic sea level or local uplift and subsidence; a small change in sea level seems most likely.

Lithologic Subunits IIIB (220–257 mbsf) and IIIC (257–300 mbsf) are from successively deeper depositional environments than IIIA (see "Lithostratigraphy" section, this chapter). Although the contact between IIIA and IIIB is well marked at 222 mbsf (Fig. 28), neither the IIIB/IIIC contact nor this downward deepening is evident in log responses. Indeed, log responses indicate a rather uniform lithology and porosity throughout both units. Small excursions to higher velocity and especially resistivity in Figure 28 at 222–226 mbsf and 247–251 mbsf are revealed by FMS images as several resistive beds only 10 cm or less thick, far below the resolving power of conventional velocity and resistivity logs.

The bottom of the seismic stratigraphic tool string reached within about 1 m of the bottom of Hole 812B. However, individual tools begin between 270 mbsf (spectral gamma-ray) and 299 mbsf (temperature), depending on the position of each tool on the string. Thus, Subunit IIIC was only partially logged by most tools.

Temperature

No heat flow measurements were conducted at Site 812, and thus the thermal gradient at the site is unknown. The Lamont-Doherty Geological Observatory (L-DGO) temperature tool was run at the bottom of the seismic stratigraphic tool string. Because the hole temperatures had been reduced by circulation during coring and by hole conditioning immediately before logging, we were unable to infer an equilibrium thermal profile from a single temperature logging run. Our recorded temperature of 17.6°C at 300 mbsf is therefore a minimum estimate of equilibrium temperature. The temperature tool was run to determine whether fluid flow was present. The possibility of active fluid circulation within periplatform carbonates has been investigated so seldom that the likelihood

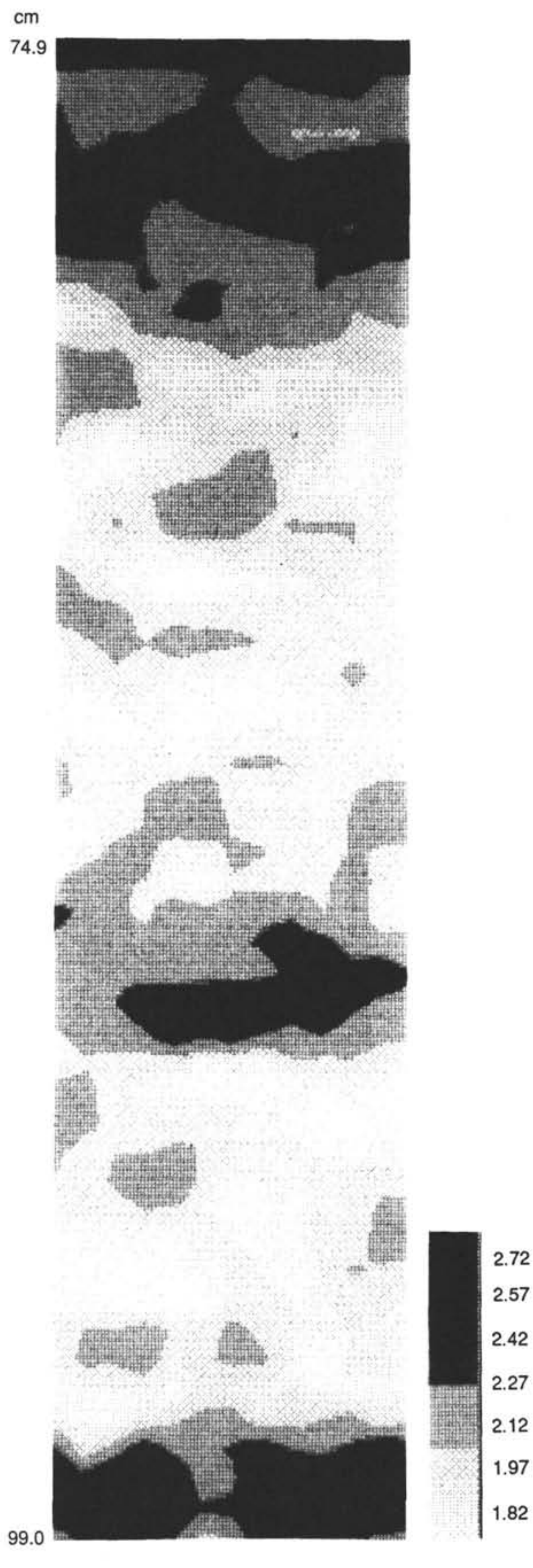

Figure 27. Electrical resistivity core image from Section 133-812A-12X-6 generated during a special experiment designed to test a prototype system (as described in the "Explanatory Notes" chapter, this volume).

Table 11. Vane shear strength at Hole 812A.

Core, section, interval (cm)	Depth (mbsf)	Torque (deg.)	Strain (deg.)	Shear strength (kPa)
133-812A-				
1H-2, 9–9.1	1.59	14	15	3.0
2H-2, 90–91	7.30	4	2	0.8
2H-5, 90–91	11.80	34	20	7.2
2H-7, 35–36	14.25	25	39	5.3
3H-2, 90–91	16.80	26	18	5.5
3H-5, 90–91	21.30	29	16	6.2
12X-1, 90–91	84.50	30	17	6.4
12X-2, 90–91	86.00	78	13	16.6

of detecting fluid flow at Site 812 was unknown. In Figure 33, measured temperatures are plotted as a function of pressure recorded simultaneously by the tool. Depths shown are approximate and may be revised by up to 5 m by post-cruise merging of the Schlumberger time/depth data with the temperature-tool time/pressure data.

The temperature pattern of Figure 33 is highly nonlinear and is difficult to account for as an artifact of the circulation history. Virtually the entire hole was swept with mud 3 hr prior to logging; much of this circulation occurred with the bit 30 m or less from the bottom of the hole. Thus, circulation probably would have suppressed temperatures for 0–270 mbsf with respect to 270–300 mbsf, but such a pattern was not observed. Instead, almost isothermal temperatures were seen from the seafloor to about 225 mbsf. These temperatures are approximately equal to bottom-water temperatures and seem to require major downflow of waters to 225 mbsf. Because no driller's circulation occurred with the pipe set at 225 mbsf, we can think of no plausible explanation for this pattern except that fluid flow down to a zone at 225 mbsf is sucking water into the formation. Probably the low-permeability beds of log Unit II (140–222 mbsf) prevented similar downward flow into the high-porosity log Unit III prior to drilling the hole. Below 225 mbsf, lowered circulation apparently permits temperatures to approach more closely to equilibrium.

SEISMIC STRATIGRAPHY

The seismic stratigraphic data for Site 812, obtained by comparison of the seismic analysis with the sedimentological data is defined below. The time-depth velocity plot (shown in Fig. 8) was calculated during the cruise to compare the seismic data with the drilling results and to predict lithologies ahead of the drilling. An interpretation of the seismic stratigraphy at Site 812 is shown in Figure 34. The seismic section defines the crossing for the originally proposed site. Six seismic reflectors were identified below the seafloor that can be tied around the site survey grid. These reflectors are numbered 1 through 6 and are used to define the seismic stratigraphic sequences shown in Figure 35. There is excellent agreement between the seismic sequences defined in the prognosis and the lithostratigraphic units seen in the cores.

Seismic sequence 1 is ~60 ms thick at the drill site and occurs between the seafloor and seismic reflector 1. Sequence 1 maintains a nearly constant thickness throughout the site survey area, i.e., it appears as a blanket over the sediments beneath. On the basis of the time-depth plot, the base of seismic sequence 1 was estimated at between 30 and 40 mbsf. The drilling results show that lithologic Unit I is composed of pelagic bioclastic foraminifer ooze that contains pteropods, with a hard dolomitized bioclastic packstone at its base, forming seismic horizon 1.

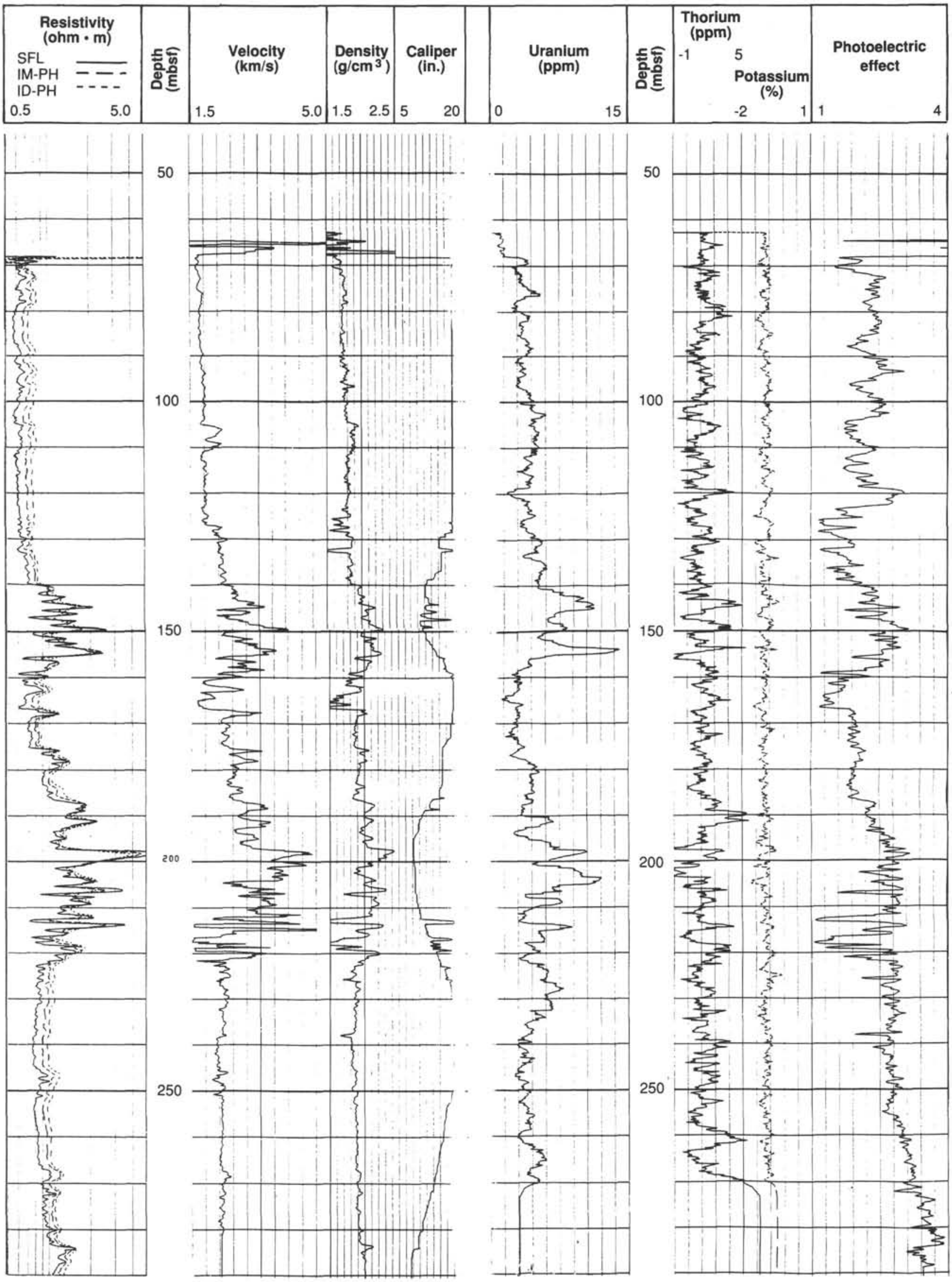

Figure 28. Primary logs obtained using the seismic stratigraphic tool string at Hole 812B.

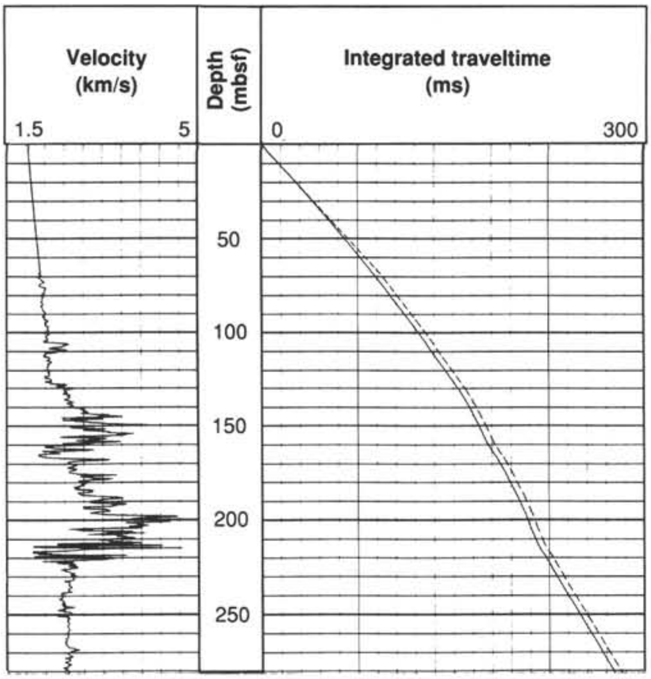

Figure 29. Velocity log, and integrated TWT function that it implies, for matching core-derived information from Site 812 with seismic section data across the site.

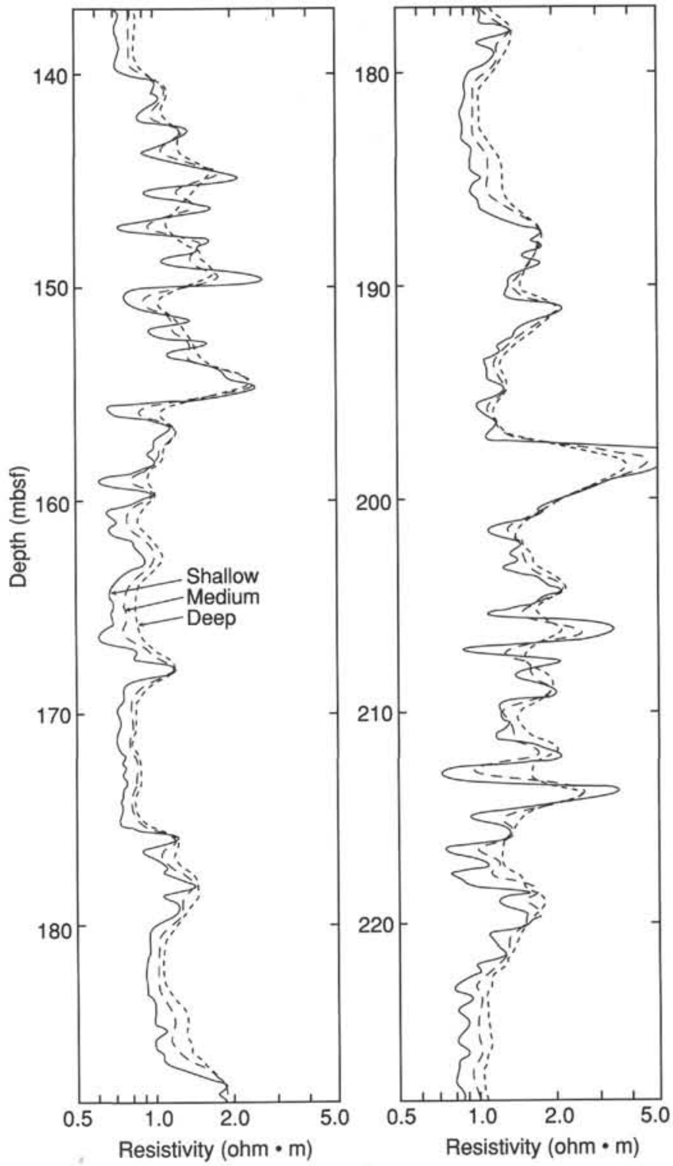

Figure 30. Expanded-scale plot of a portion of the three resistivity logs of Figure 29, showing their differing vertical resolutions and slight baseline shifts between them.

Seismic sequence 2 occurs between horizons 1 and 2 and comprises sinuous reflectors that appear to have been truncated by horizon 1. The thickness of sequence 2 at the site is <50 ms, but it thickens to more than 100 ms to the west of the drill site, where it also is more conformable with sequence 1. The lower boundary of sequence 2 is clearly an unconformity as seen to the w est of the drill site. Sequence 2 accords with lithologic Subunit IIA, which was defined as a micritic chalk with nannofossils and represents a change in depositional environment to outer shelf. The dolomitized bioclastic limestone between lithologic Unit I and Subunit IIA is identified as occurring within the lower part of seismic sequence 1. It separates shelf from pelagic sediments and therefore represents a major subsidence pulse and/or a change in sea level at about 2.2 Ma.

Seismic sequence 3 occurs between reflectors 2 and 3. Seismically, it is mounded and pinches out to the west at that same time that it maintains a uniform thickness of ~50 ms to the north and the east. The upper boundary of sequence 3 is an unconformity. It corresponds with most of lithologic Subunit IIB, defined as micritic chalk with foraminifers deposited in an outer-shelf environment. The lower boundary of sequence 3 is also an unconformity cutting out reflectors in the unit below and appears to correspond to a facies change about 10 m above the base of lithologic Subunit IIB, that is, at the level of the bioclastic rudstones with large foraminifers interpreted as being turbiditic.

Sequence 4 is bound by unconformities top and bottom and is ~60 ms thick at the drill hole. The sequence is cut out to the west by reflector 2. It maintains its integrity to the east, north, and south. Sequence 4 is equivalent to lithologic Subunit IIC, defined as dolomitic packstones changing upward into dolomitic ooze. The base of sequence 4 is clearly seen in the seismic data as an unconformity and is interpreted on the basis of the lithologies as also representing a solution unconformity.

Sequence 5 occurs between reflectors 4 and 5 and is ~30 ms thick at the drill site. It maintains this thickness throughout the site area, except to the west, where it is cut out by reflector 2. Sequence 5 equates with the upper part of lithologic Subunit IIIA, defined as coralline algal bioclastic packstone that was deposited in a shallow lagoon or inner shelf.

Sequence 6 occurs between reflectors 5 and 6 and is approximately as thick as the sequence above. It equates with the lower half of lithologic Subunit IIIA and is composed of bioclastic wackestones with coralline algae, similar in composition and depositional environment to the lithologic unit above. Seismic data, however, show that sequence 5 downlaps onto sequence 6.

Sequence 7 is 80 ms thick and is composed of a mounded unit overlying a bedded, almost prograding unit below. Sequence 7 is not cut by reflector 2. Sequence 7 equates with lithologic Subunits IIIB and IIIC, which are respectively coral-dominated boundstones overlying bioclastic packstones and rudstones of lagoonal facies. In seismic character and sedimentological facies, therefore, sequence 7 shows an upward-shallowing facies change from lagoonal to reefal.

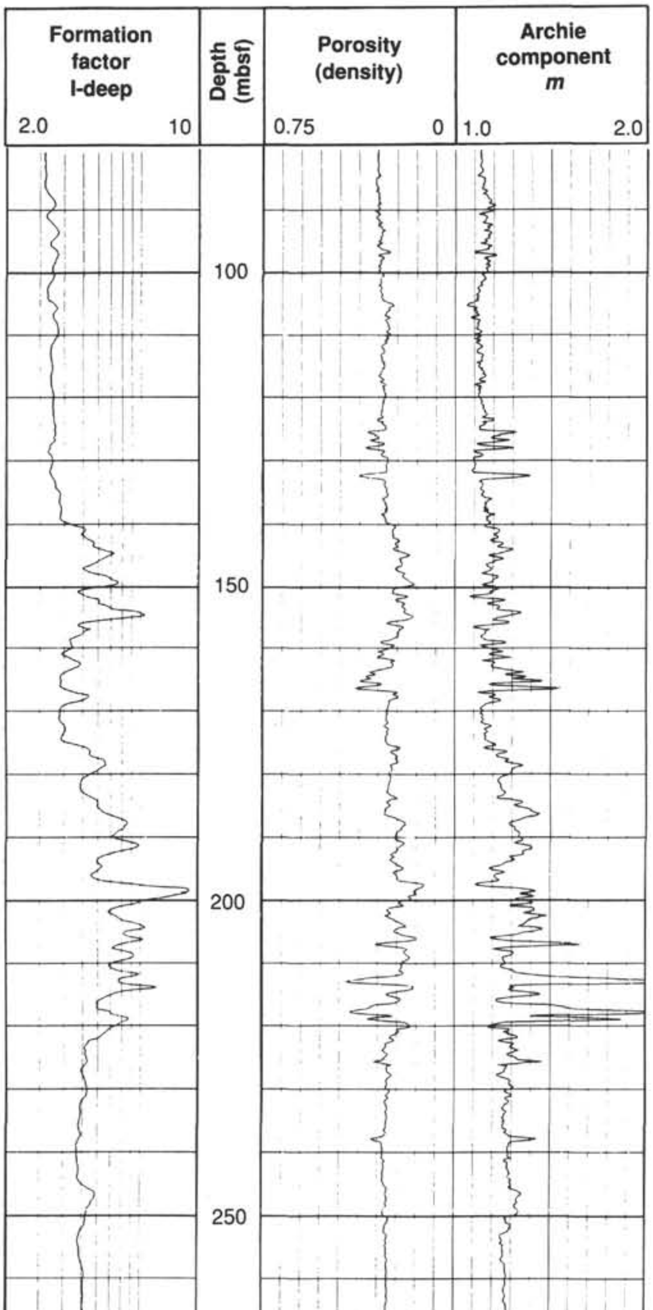

Figure 31. Hole 812B logs of FF (from ratio of formation resistivity to fluid resistivity), porosity (from density), and Archie's component *m* (1942) relating FF to porosity.

Substantial accord exists between the seismic interpretation and the lithologic units defined from the drill hole. In summary, the section may be divided into three parts:

1. a lower shallow-water and upward-shallowing series of facies changes from lagoonal through reefal to shallow water and coral dominated; this upward-shallowing cycle appears to have been interrupted by exposure and dolomitization at a depth of 140–150 mbsf;
2. a shelf sequence ~80-m-thick, divided into an inner-shelf dolomitized section and an outer-shelf undolomitized section above.
3. Above 30 mbsf, a pelagic sequence indicating substantial increase in water depth, probably related to subsidence of the margin.

The hardground separating the shelfal and pelagic sequences is problematic. It may represent an exposure unconformity or a shelf-edge condensed sequence. At an age of 2.2 Ma, it corresponds with previously identified low-sea-level condensed sections, which, although not the lowest sea-level drop, may have been sufficient to expose the outer shelf.

SUMMARY AND CONCLUSIONS

Overview

Sites 812, 813, and 814 are uniquely positioned along a northeast- to southwest-trending transect on the southern margin of the Queensland Plateau between Tregrosse and Flinders reefs to study facies relationships in a variety of depositional settings for evaluating the control of sea level, paleoenvironment, and tectonics on the development of carbonate platforms. Site 812, at a water depth of 462 m and the most easterly of the three sites, represents an intra-platform or "lagoonal" setting, whereas Site 814, about 11 km away at a water depth of 520 m, represents a proximal setting on the prograding platform margin system. Site 813 at a water depth of 539 m is the most westerly of the three sites and represents a more distal setting on the prograding platform margin about 2.5 km east of Site 814. The sedimentary geometry of the general depositional environment is well defined in seismic profiles, whereas correlation among the three sites is well constrained by seismic stratigraphy. Shore-based studies on the cored sediments and evaluation within the context of this seismic framework will undoubtedly provide a refined interpretation of factors that controlled the Neogene development of the Queensland Plateau.

However, a preliminary interpretation of drilling results from the three different depositional settings at Sites 812, 813, and 814 has already yielded a middle Miocene to Pleistocene sedimentation history of paleoenvironmental changes on the plateau margin. These changes resulted from a combination of sea-level and climatic/paleoceanographic fluctuations and varying subsidence rates. In addition, stratigraphic events interpreted from the plateau margin sites can be correlated with drilling results from Sites 817 and 818 on the nearby lower and upper slope of the southwestern margin of the Queensland Plateau. The sedimentary record at the latter two sites consists of redeposited carbonate sediments produced on the shallow-water banks and, in fact, is a record of processes that occurred on the plateau margin.

Drilling at the three plateau margin sites recovered intervals containing extensively dolomitized carbonates. Associated pore-water geochemistry and temperature profiles indicate the presence of distinctive fluid flow patterns within the platform, possibly pertinent to dolomitization (see "Inorganic Geochemistry" section, "Site 814" chapter, this volume). Shore-based studies of dolomite and interstitial fluids should provide insights into processes controlling massive dolomite formation in ancient carbonate platforms.

Sedimentation History

Based on shipboard studies, we have outlined a preliminary interpretation of carbonate facies development on the

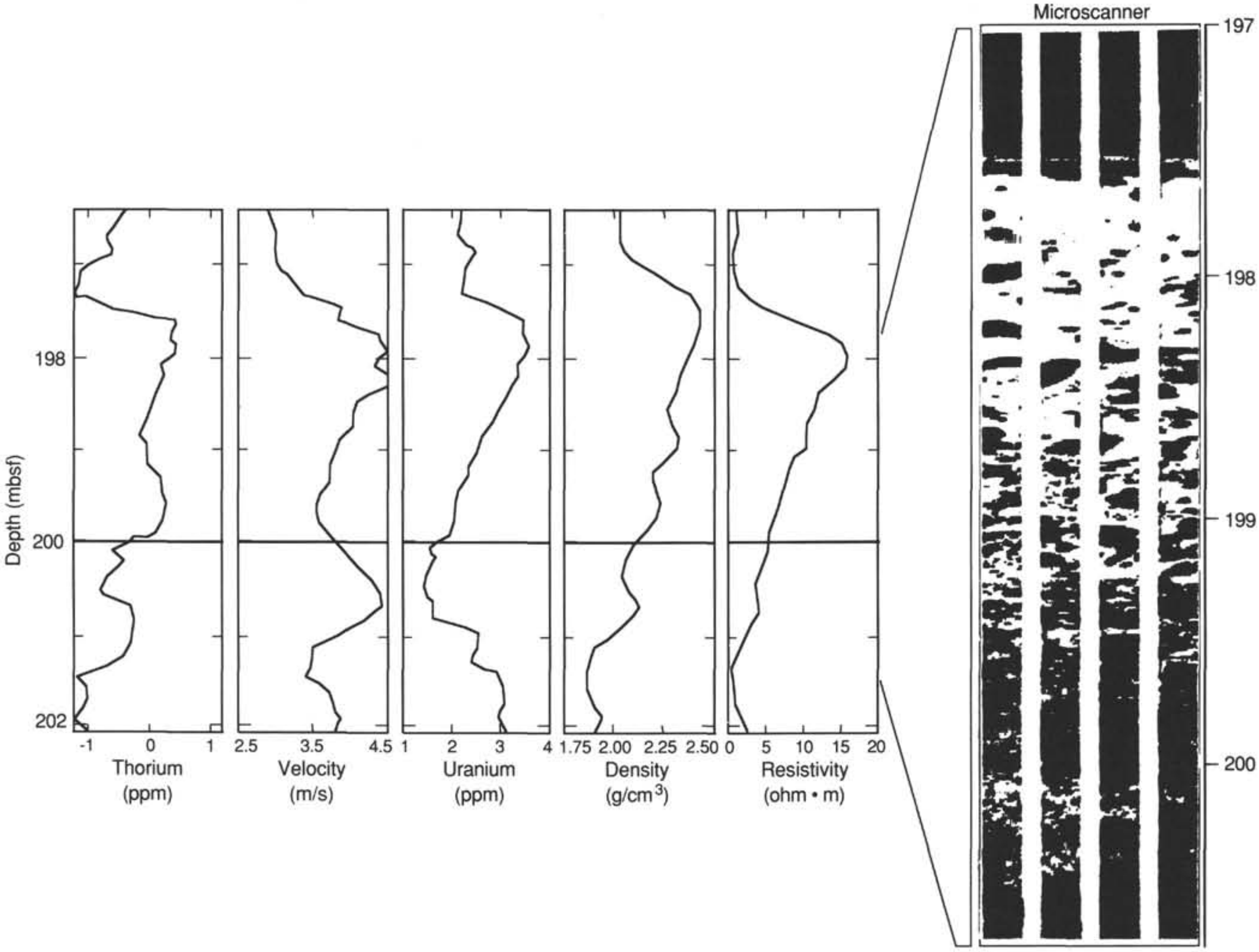

Figure 32. Expanded-scale plot of conventional logs in the interval 196–202 mbsf at Hole 812B, bracketing a possible unconformity, and FMS imaging of porosity variations within this zone.

margin of the Queensland Plateau since the middle Miocene. Correlation of the stratigraphic data from Sites 812, 813, and 814 subdivides the Neogene sedimentation history into three distinct periods, distinguished by a successive deepening of paleodepths at each site. Benthic foraminiferal assemblages indicate the following ranges of paleodepths across the three-site transect during these periods: (1) in the middle Miocene, inner neritic to outer neritic (<30–200 m); (2) in the late Miocene to early Pliocene, middle neritic to upper upper bathyal (30–400 m); and (3) in the late Pliocene to Pleistocene, upper bathyal (200–600 m). The sediments deposited within these periods exhibit characteristic variations at each site to provide a record of the influence of sea level, paleoenvironment, and tectonics on the evolution of carbonate facies.

Middle Miocene

The middle Miocene sequence at Site 812 records an initial shallowing, followed by a return to deeper waters at the top of the interval. Sedimentation began in the shallow neritic environment with the deposition of bioclastic peloidal packstone and coralline algal rudstone in a lagoonal environment at a <30 m water depth. The water shallowed with time to ~5–10 m, and bioclastic floatstone with corals and coralline algae and mollusk packstone, indicative of a near reefal setting, were deposited. Shallowing continued as subsequent deposition occurred in a more lagoonal low-to-medium energy environment at water depths of ~5 m. In contrast, the waters must have deepened afterward at the top of the middle Miocene section to between 10 and 50 m, with sedimentation occurring in a shallow neritic inner-shelf environment after deposition of a packstone with large benthic foraminifers.

At Site 814, sedimentation of calcareous ooze and mudstone in the early middle Miocene occurred in a middle neritic environment in water depths between 30 and 100 m. As at Site 812, water depth deepened with time to between 100 and 200 m with sedimentation in an outer neritic environment. A similar pattern of deepening water depths throughout the middle Miocene was recorded in the sediments at nearby Site 813 with earlier skeletal grainstone deposition in an inner-neritic environment adjacent to or on a carbonate bank, followed by deepening at the site with deposition of fine-grained micritic oozes and chalks in the middle to outer neritic zone (30–100 m).

In summation, by comparing the development of carbonate facies among the three sites, it is possible to evaluate relative changes in sea level during the middle Miocene on the margin of the Queensland Plateau. In general, relative sea level tended to rise during the middle Miocene, although reversals in this trend may have occurred intermittently. The deepening trend is in contrast to the overall decline in sea level recog-

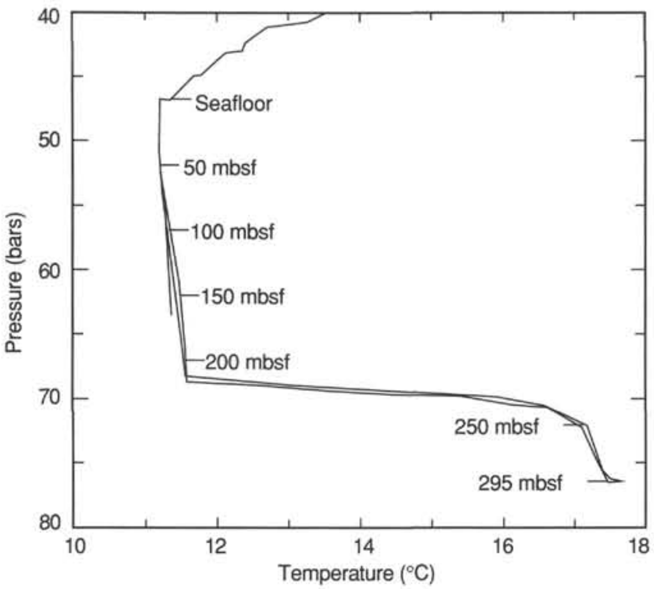

Figure 33. Temperature log as a function of pressure (or depth) at Hole 812B, showing a possible downward flux of seawater into a bed at about 225 mbsf.

nized worldwide during the middle Miocene and may represent a general subsidence of the plateau that occurred at that time. The inability of the reefs and carbonate banks to maintain growth in pace with the subsidence of the plateau, particularly during a period of decline in eustatic sea level, probably is the result of a multitude of factors. This interpretation is also consistent with our evaluation of the sedimentary record at Site 817, which indicates a period of gradual decline in carbonate productivity in the shallow-water system during the middle Miocene.

Integrating data from the margin and slope sites, we derive the following scenario. At the beginning of the middle Miocene, conditions promoted the growth of an extensive and robust shallow-water carbonate system that extended to the extremities of the plateau and facilitated the shedding of debris onto the slope. Approaching the late middle Miocene, the area covered by the shallow-water carbonate system shrank, withdrawing to a point that permitted only fine-grained suspended carbonate to be transported beyond the platform rim to settle on the slopes. This decline in productivity of the shallow-water system is consistent with a drowning of the banks as a result of subsidence; however, this interpretation does not explain why the bank growth could not keep pace with subsidence, particularly when one considers the steady middle Miocene decrease in eustatic sea level. Undoubtedly, other environmental factors related to change in paleoclimate or paleocirculation contributed to the general decline.

Environmental conditions contributing to the deterioration of the shallow-water carbonate system continued to dominate until the latest middle Miocene, when only minor amounts of bank-derived material reached the slopes and pelagic sedimentation prevailed. The change from bank-derived to pelagic carbonate sedimentation may reflect possible termination of shallow-water production as a result of bank exposure coincident with the late middle Miocene decline in sea level. The consequence of these combined environmental factors ultimately resulted in major changes in sedimentation on the margins during the following period.

Late Miocene–Early Pliocene

During the late Miocene, paleodepths at Site 812 were shallow neritic (<30 m), deepening to middle neritic (30–200 m) during the early Pliocene. At first, upper Miocene sediments were bryozoan molluscan floatstones, which were probably deposited as an oyster-encrusting bryozoan bank on the inner shelf, but later became a typical periplatform ooze with decreasing age. These latter sediments are micritic chalk with increasing amounts of nannofossils in the younger sediments. At Site 814, the upper Miocene micritic ooze was deposited in middle neritic paleodepths (30–100 m). The lower Pliocene sediments are probably confined entirely within an 8-m-thick hardground limestone unit that is capped by a condensed laminated surface, obviously representing a time of drastically reduced sedimentation at this location. At Site 813, upper Miocene to lower Pliocene sediments were deposited in outer neritic to upper upper bathyal paleodepths (100–400 m). The upper Miocene sediments are bioclastic foraminiferal ooze with micrite and nannofossils, whereas the lower Pliocene sediments are nannofossil foraminiferal ooze with micrite containing phosphatized reworked benthic foraminifers. Again, an increase in nannofossil content is seen in the younger sediments. The thickness of the lower Pliocene sequence is greatly reduced, compared with that of the upper Miocene. The phosphatized elements may be related to phosphatization processes associated with the upper surface of the hardground at nearby Site 814.

Sedimentation on the margin of the Queensland Plateau during the late Miocene to early Pliocene generally was reduced or condensed. Although fine-grained, bank-derived carbonate, present now as micrite, was produced, undoubtedly the quantities were not abundant. This interpretation is consistent with drilling results from Site 817, which showed that only minor amounts of this material reached the lower slope of the Queensland Plateau during this period. It is also consistent with the synchronous change from periplatform to pelagic sedimentation at Site 811 on the western margin of the Queensland Plateau. The upper Miocene oyster-bryozoan bioassemblage deposited at Site 812 suggests that the surface waters were probably cooler (i.e., temperate to subtropical) than during the middle Miocene, certainly not conducive for vigorous coralgal reefal productivity. Perhaps, cooler waters were brought into these tropical latitudes during the late Miocene, either by surface currents or with seasonal upwelling.

During the late Miocene to early Pliocene, relative sea level rose as the oyster-encrusting bryozoan bank was drowned and replaced by periplatform sediments. The carbonate banks apparently were drowned and unable to respond to climatic amelioration in the earliest Pliocene. A pulse of more rapid subsidence on the Queensland Plateau, in combination with rising eustatic sea level, may have essentially drowned the banks.

Late Pliocene–Pleistocene

At Site 813, periplatform sedimentation across the early/late Pliocene transition was apparently continuous, whereas at Sites 812 and 814 the transition is unconformable with passage from the condensed hardground sequence directly to the overlying upper Pliocene periplatform ooze. Magnetostratigraphic and biostratigraphic data indicate that the renewal of periplatform sedimentation above the hardground at Site 814 began no earlier than about 3.4 Ma. These lowermost upper Pliocene sediments contain foraminiferal packstone mixed with periplatform ooze, indicative of extensive current winnowing. Magnetostratigraphic and biostratigraphic data con-

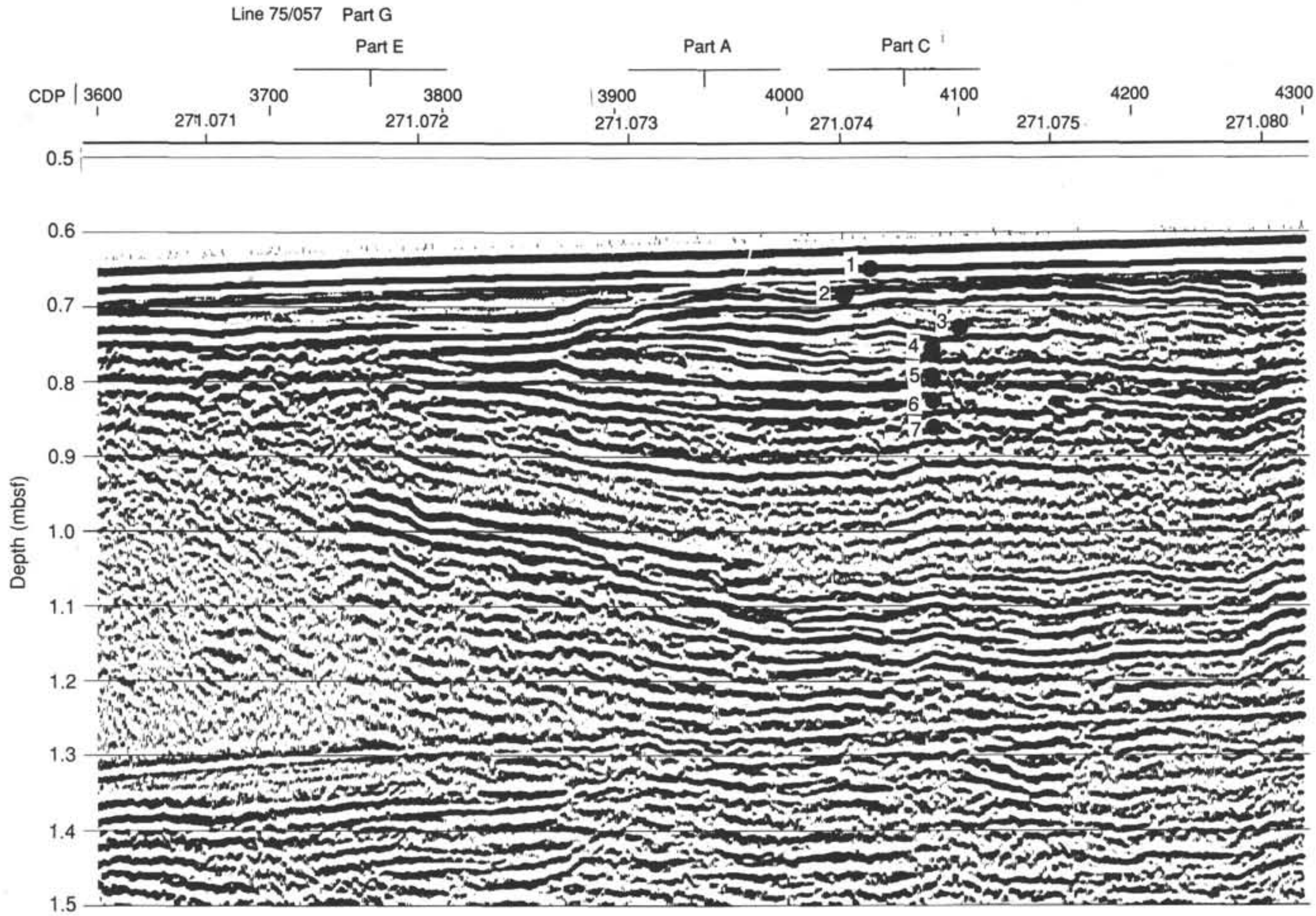

Figure 34. Interpreted seismic section through Site 812. Seven seismic sequences are identified.

strain the onset of post-hardground deposition at Site 812 to the latest late Pliocene (<1.88 Ma).

At Site 813, an apparent rapid deepening in paleodepth in the earliest late Pliocene from outer neritic/upper upper bathyal to upper bathyal environments may signify an accelerated pulse in the subsidence rate of the Queensland Plateau at that time. The lowermost upper Pliocene sediments at Site 813 contain iron-stained components, possible evidence for condensed sedimentation during the passage from shallower to deeper waters. A marked increase in paleodepth is also recorded at Site 812 with a more extreme change from middle/outer neritic to upper bathyal environments. This occurs within the upper Pliocene sediments; however, the change from shallower to deeper water sediments is separated by a 1.5-m-thick condensed hardground sequence. The transition from shallower to deeper waters may represent a time of reduced sedimentation. As most of the late Pliocene record is missing in the section cored at Site 812, conditions favoring nonreduced or drastically reduced sedimentation, such as strong currents, must have been focused at this location.

Based on benthic foraminiferal assemblages, deposition at all three sites was within an upper bathyal environment (200–600 m) throughout the remainder of the late Pliocene and Pleistocene. Throughout the late Pliocene–Pleistocene, the dominant sediment type along the transect was nannofossil foraminiferal ooze. The uppermost sediments contain aragonite mixed with nannofossils, a mixture characteristic of periplatform ooze. With depth aragonite is diagenetically altered to micrite, the presence of which denotes periplatform sedimentation throughout the late Pliocene–Pleistocene. Nannofossil concentration, however, increases upsection and indicates that the sediments became increasingly more pelagic in origin since the late Pliocene. Apparently, the supply of fine-grained, bank-derived carbonate to the plateau margin decreased with time, possibly in response to continued subsidence of the Queensland Plateau and sinking of large areas of carbonate production below the photic zone. High concentrations of foraminifers imply that the fine fraction was intensively winnowed by currents passing over the plateau margin. Obviously, current circulation patterns over the plateau margin were important for development of carbonate facies by winnowing and removing sediment, perhaps since the late Miocene.

In conclusion, this interpretation of the sedimentation history on the margin of the Queensland Plateau uses the combined data from a multitude of shipboard studies to estimate the timing of events. This interpretation will undoubtedly be greatly refined after shore-based studies have been completed, but initial results are promising. These results demonstrate that this record of environmental change can be used to differentiate among influences of fluctuation in sea level, tectonic subsidence, paleoclimate, and paleoceanography regarding the evolution of the Queensland Plateau.

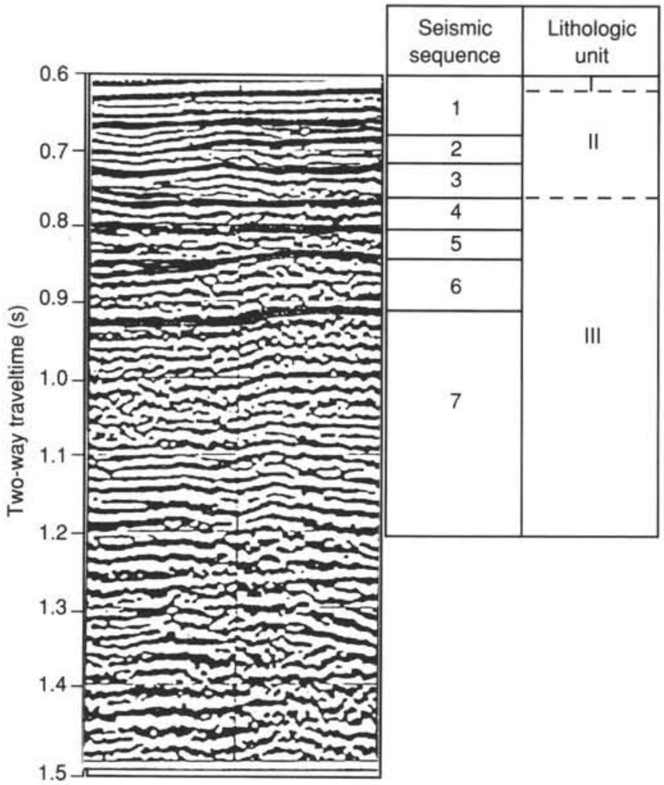

Figure 35. Seismic section at Site 812 and interpreted correlation with lithologic units.

REFERENCES

Andrews, J. E., 1973. Correlation of seismic reflectors. *In* Burns, R. E., Andrews, J. E., et al., *Init. Repts. DSDP,* 21: Washington (U.S. Govt. Printing Office), 459–479.

Archie, G. E., 1942. The electrical resistivity log as an aid in determining some reservoir characteristics. *J. Pet. Tech.,* 5:1–8.

Berggren, W. A., Kent, D. V., and Van Couvering, J. A., 1985. Neogene geochronology and chronostratigraphy. *In* Snelling, N. J. (Ed.), *The Chronology of the Geological Record.* Geol. Soc. London Mem., 10:211–260.

Davies, P. J., Symonds, P. A., Feary, D. A., and Pigram, C. J., 1987. Horizontal plate motion: a key allocyclic factor in the evolution of the Great Barrier Reef. *Science,* 238:1697–1700.

_______, 1989. The evolution of the carbonate platforms of northeast Australia. *Spec. Publ.–Soc. Econ. Paleontol. Mineral.,* 44:233–258.

Feary, D. A., Pigram, C. J., Davies, P. J., Symonds, P. A., Droxler, A. W., and Peerdeman, F., 1990. Ocean Drilling Program–Leg 133 safety package. *BMR Aust. Record,* 6.

Hamilton, E. L., 1976. Variation of density and porosity with depth in deep-sea sediments. *J. Sediment. Petrol.,* 46:280–300.

_______, 1979. Sound velocity gradients in marine sediments. *J. Acoust. Soc. Am.,* 65:909–922.

Lumsden, D. N., and Chimahusky J. S, 1980. Relationship between dolomite nonstoichiometry and carbonate facies parameters. *SEPM Spec. Publ., 28:* 123–137.

Mutter, J. C., 1977. The Queensland Plateau. *BMR Geol. Geophys. Bull.,* 179.

O' Herne, L., and van der Vlerk, I. M., 1971. Geological age determinations on a biometrical basis (comparison of eight parameters). *Boll. Soc. Paleontol. Ital.,* 10:3–18.

Palmieri, V., 1973. Comparison of correlation methods for planktonic and larger foraminifers in the Capricorn Basin, Queensland. *Govt. Mineral. J.,* 74:312–317.

Pinchin, J., and Hudspeth, J. W., 1975. The Queensland Trough: its petroleum potential based on some recent geophysical results. *APEA J.,* 15:21–31.

Symonds, P. A., and Davies, P. J., 1988. Structure, stratigraphy, evolution and regional framework of the Townsville trough and Marion Plateau region - research cruise proposal, project 9131.11. *BMR Aust. Record,* 48.

van Morkhoven, F.P.C.M., Berggren, W. A., Edwards, A. S., et al., 1986. Cenozoic cosmopolitan deep-water benthic foraminifera. *Bull. Cent. Rech. Explor.-Prod. Elf-Aquitaine,* Mem. 11.

Ms 133A-105

NOTE: All core description forms ("barrel sheets") and core photographs have been printed on coated paper and bound separately as Part 2 of this volume, beginning on page 813.

Formation microscanner images for this site are presented on microfiche in the back of Part 2.

Hole 812B: Resistivity-Sonic-Natural Gamma Ray Log Summary

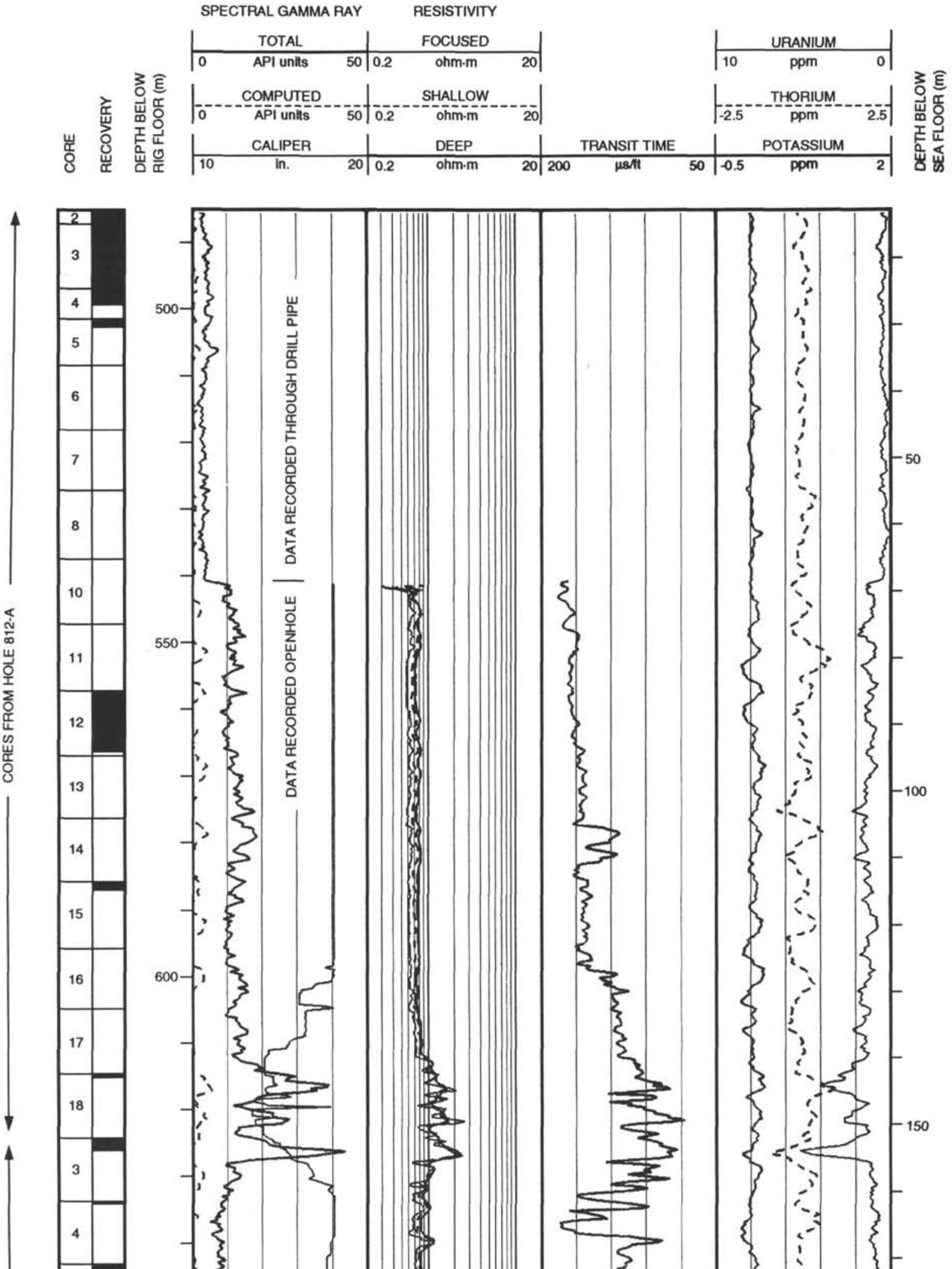

Hole 812B: Resistivity-Sonic-Natural Gamma Ray Log Summary (continued)

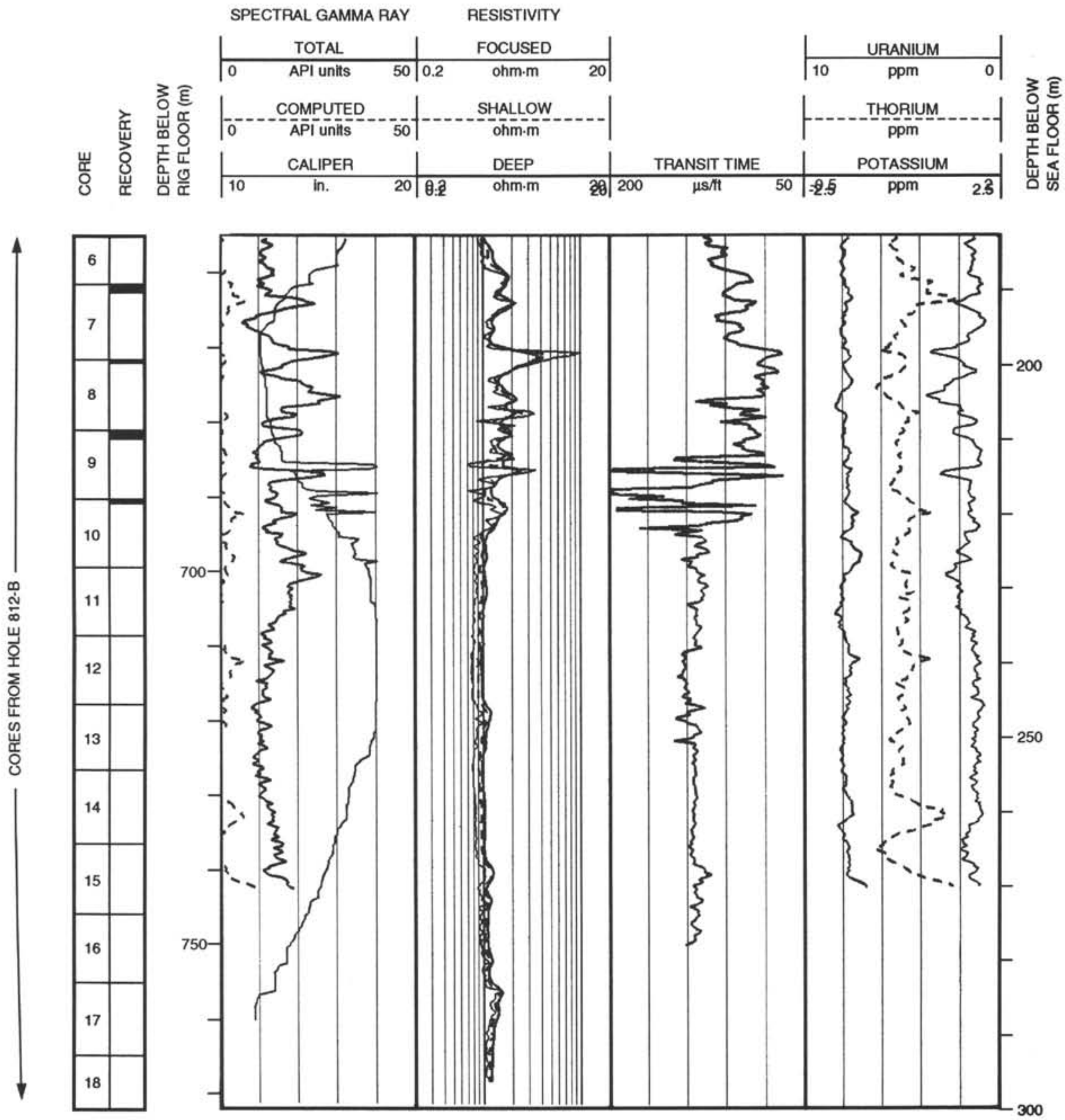

Hole 812B: Density-Natural Gamma Ray Log Summary

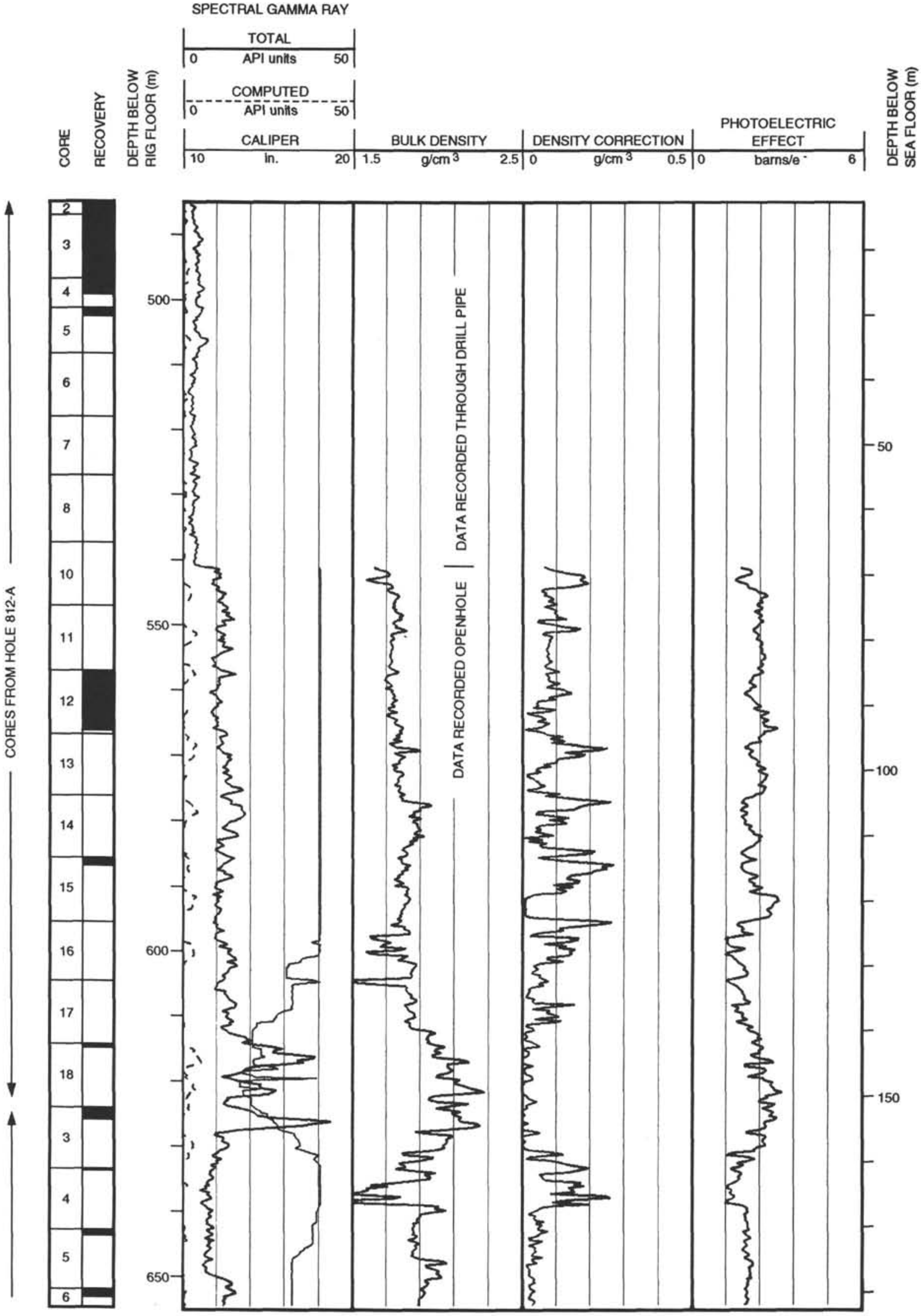

Hole 812B: Density-Natural Gamma Ray Log Summary (continued)